Mono- and Bimetallic Au-Cu dendrimer micelle encapsulated nanoparticles as catalysts in the oxidation of styrene.

By

Gerbrandt Kotzé

Thesis presented in partial fulfilment of the requirements for the degree

Master of Science in Chemistry at the University of Stellenbosch

Supervisor: Dr. R. Malgas-Enus

Co-supervisor: Dr. A. J. Swarts (NWU-Potchefstroom)

Faculty of Science

Department of Chemistry and Polymer Science

December 2018

DECLARATION

By submitting this thesis/dissertation electronically, I declare that the entirety of the work contained therein is my own, original work, that I am the sole author thereof (save to the extent explicitly otherwise stated), that reproduction and publication thereof by Stellenbosch University will not infringe any third party rights and that I have not previously in its entirety or in part submitted it for obtaining any qualification.

Gerbrandt Kotzé

December 2018

ACKNOWLEDGEMENTS

“I believe in God, the Father almighty,

Creator of heaven and earth.

I believe in Jesus Christ, God’s only Son, our Lord,

who was conceived by the Holy Spirit,

born of the Virgin Mary,

suffered under Pontius Pilate,

was crucified, died, and was buried;

he descended into hell.

On the third day he rose again from the dead;

he ascended into heaven,

and sits at the right hand of God the Father Almighty,

from whence he shall come to judge the living and the dead.

I believe in the Holy Spirit,

the holy catholic Church,

the communion of saints,

the forgiveness of sins,

the resurrection of the body,

and the life everlasting.

Amen.”

ACKNOWLEDGEMENTS

Dr. Rehana Malgas-Enus – my research supervisor,

for her continual support throughout the duration of my post-graduate research, her insight into this project, continuously sharing her wisdom and knowledge, and her help in my endeavors, both academic and personal. Also for her financial assistance which, in no small manner, contributed to me being able to do this research.

Dr. Andrew Swarts – my co-supervisor,

for his assistance in this project and his tremendous insights which he shared.

RME Nano Group and the other students at Inorganic Chemistry,

for their friendships, camaraderie, and helpful suggestions which helped me during the course of this project.

The staff and technical assistants of the Inorganic Chemistry Building,

for their continual assistance with all manner of tasks related to my experiments.

Dr. Jaco Brand and Elsa Malherbe,

For their help and attention to detail when I submitted samples for NMR analysis.

The National Research Foundation of South Africa, for financial assistance.

Tersia Crous, the Crous family, and Gateway City Church.

Dr. Lizelle Fourie, St. Stephen Health Care Centre and staff.

ACKNOWLEDGEMENTS

A Word of Thanks from Gerhard and Amanda Kotzé – Gebrandt's parents

What an honour and privilege to get involved at the Department of Chemistry and Polymer Science at the University of Stellenbosch. As Gerbrandt Kotzé enrolled as a student, we never thought that he would live out his dream and passion for Science in such a special way, doing a Masters degree in Nanotechnology.

We are grateful to Dr. Rehana Malgas-Enus who was Gerbrandt's research supervisor. Gerbrandt not only shared her passion for the academics, but also her passion for learners of underprivileged schools. He shared her dream - to create a love for science, but also to see them make better choices for future. With Dr. Rehana he could live his dream to the full… to touch the lives of the next generation. SUNCOI was the instrument used to reach this dream. Thank you Dr. Rehana that every student counts on you. That you saw the potential in Gerbrandt and made funding available so that he could become the scientist he dreamed of being.

Dr. Rehana, may the good work, not only for our son, Gerbrandt, but for all your students bear much fruit. May your enthusiasm for academia and for the lives of people, rub off on all the people you are connected to. Thank you for your involvement in Gerbrandt's life, and in the lives of us as a family. Thank you for your continuous support during Gerbrandt's sickness. You are a role model in the way you deal with people's lives.

Dr. Andrew Swarts from North-West University. Thank you for being Gerbrandt's co-supervisor. We appreciate your dedication to Gerbrandt's thesis.

Professor Selwyn Mapolie, thank you for the role you are fulfilling at the Department of Chemistry and Polymer Science, and that Gerbrandt's wellbeing was important to you, especially in his time of sickness.

To all the lecturers at the University of Stellenbosch, Thank You. Every one played a role to make Gerbrandt's studies a success.

To Gerbrandt's fellow students or his "Lab Mates" as he referred to you. You are such beautiful people with lots of potential. Thank you for the friendship each and every one of you showed towards Gerbrandt. Use your potential and make the best of every opportunity that cross your paths.

Our greatest desire is that Gerbrandt's research studies would become a building stone for future students. That Gerbrandt's passion for the next generation of students, and his passion for physics and science will ignite a flame in everyone who was touched by him.

ACKNOWLEDGEMENTS

Nelson Mandela once said:

"What counts in life is not the mere fact that we have lived. It is what difference we have made to the lives of others that will determine the significance of the life we lead"

SOLI DEO GLORIA

Gerhard and Amanda Kotzé and family

In this thesis, we report the synthesis and characterization of mono- and bimetallic gold and copper nanoparticles, stabilized by a dendrimer micelle. This was achieved by modifying commercially available DAB G3-PPI dendrimers by introducing alkyl chains to the dendrimers peripheries. This enabled the preparation of dendrimer micelles with the unique property of possessing a hydrophilic interior and hydrophobic exterior. This dual nature of the dendrimer micelles' solubility allowed us to exploit the advantage of solubility-driven encapsulation/stabilization of metallic NPs. Dendrimer micelles with varying alkyl chain lengths (**M1**-**M3**) were successfully synthesized, characterized and employed as both templates and stabilizers for the synthesis of monometallic Au, Cu and bimetallic Au_mCu_n NPs. HR-TEM analysis showed that the alkyl chain length on the periphery of the dendrimer micelle influences NP size, viz. the longer the chain, the higher the degree of stabilization and hence, the smaller and monodispersed the metal NPs.

Having identified M1, with the C_{15} alkyl chain, as the most effective dendrimer micelle for stabilizing the metal NPs, the long-term stability of the prepared DSNs was evaluated. It was found that the bimetallic DSNs are more stable over extended periods compared to the monometallic DSNs, which showed agglomeration. This was likely due to a stabilizing effect of the Cu NPs on the Au NPs and the nature of the bimetallic NPs.

After optimizing the synthetic method to give reproducible results, we set out to evaluate and compare the stabilities of these various DSNs. After keeping these mono- and bimetallic DSNs in solution for nine months, it was found that bimetallic DSNs were very stable and generally showed little change in size and dispersity over such an extended period of time. This showed that the composition of metallic NPs affects the stability of the NP clusters.

These mono and bimetallic DSN's were then evaluated as catalysts in the solvent-free oxidation of styrene. A general trend was observed throughout the course of testing five different mono- and bimetallic DSNs with varying metal composition. It was found that the DSNs with a greater proportion of Au exhibited slightly greater conversions. These conversions, however, was found to decrease slightly as the amount of Au in the NPs was gradually replaced with Cu. Hence, the Au DSNs generally converted the most of the substrate, followed by the Au_3Cu_1, Au_1Cu_1, Au_1Cu_3, and Cu DSNs, respectively. Since the Au NPs were the largest and the Cu NPs were the smallest, it was concluded that conversion of styrene was not dependent on the NP size, but

rather the metal content. The rationale behind this was that NP size-dependent catalysis would show the highest conversion for the smallest NPs, however, the results obtained showed the highest conversion for the larger Au NPs, whilst the small Cu NPs showed the lowest conversion. Additionally, the selectivity of the DSNs was found to vary depending on the oxidant employed. In the case of H_2O_2, benzaldehyde formation was favoured over the formation of styrene oxide, whilst the converse was true when TBHP was employed as the oxidant. Of the two oxidants, TBHP produced the highest activity and favoured formation of the desired product – styrene oxide.

Articles in Refereed/Peer-reviewed Journals

1. Effect of nanoparticle metal composition: mono and bimetallic gold/copper dendrimer stabilized nanoparticles as solvent-free styrene oxidation catalysts, A. Blanckenberg, G. Kotzé, A. J. Swarts, R. Malgas-Enus, *Journal of Nanoparticle Research* (2018) 20:44. https://doi.org/10.1007/s11051-018-4144-3

Refereed/Peer-reviewed Conference Outputs

Selected Conference Presentations:

1 Poster titled, "Mono- and bimetallic Au-Cu dendrimer micelle stabilized nanoparticles as catalysts in the solvent-free oxidation of styrene", Gerbrandt Kotzé, Andrew J. Swarts and Rehana Malgas-Enus*, Inorg2017, Hermanus, South Africa, 2017.

2 Poster titled, "Mono- and bimetallic Au-Cu dendrimer micelle stabilized nanoparticles as catalysts in the solvent-free oxidation of styrene", Gerbrandt Kotzé, Andrew J. Swarts and Rehana Malgas-Enus*, Catalysis South Africa (CATSA) Conference, Kleinmond, South Africa, 2015.

3 **International conference:** Poster titled, "Mono- and bimetallic Au-Cu dendrimer micelle stabilized nanoparticles as catalysts in the solvent-free oxidation of styrene", Gerbrandt Kotzé, Andrew J. Swarts and Rehana Malgas-Enus*, presented at OMCOS18, Sitges, Spain, June 2015.

Mono- and Bimetallic Au-Cu dendrimer micelle encapsulated nanoparticles as catalysts in the oxidation of styrene.

Contents

CHAPTER 3

CHAPTER 4

Au_mCu_n : $_m$ denotes the number of Au atoms and $_n$ denotes the number of Cu atoms

ATR : attenuated total reflectance

DAB-PPI : diaminobutane poly(propylene imine)

DENs : dendrimer encapsulated nanoparticles

DPA : phenylazomethine dendrimer

DSNs : dendrimer stabilized nanoparticles

EDX : energy-dispersive X-ray spectroscopy

ESCA : electron spectroscopy for chemical analysis

FT-IR : Fourier Transform infrared

GC : gas chromatography

LMCT : ligand-to-metal charge-transfer

MALDI-TOF : matrix-assisted laser desorption-ionization time of flight mass spectrometry

MS : mass spectrometry

NMR : nuclear magnetic resonance

NP(s) : nanoparticle(s)

PAMAM : poly(amidoamine)

SPR : surface plasmonic resonance

TBHP : *t*-butyl-hydroperoxide

TOF : turnover frequency

HR-TEM : high resolution - transmission electron microscopy

UV-Vis : ultraviolet-visible light spectroscopy

XAFS : X-ray absorption fine structure

XANES : X-ray absorption near-edge spectroscopy

XPS : X-ray photoelectron spectroscopy

XRD : X-ray diffraction

CHAPTER 1

A review of advances made in nanoparticle research

1.1 Classifying Nanoparticles

Nanoparticles (NPs) research has seen tremendous growth over the past decade due to their unique aspects of atomic and molecular assembly, behaviour of the individual particles, magnetic and electrical properties, and also their applications in fields such as catalysis, medicine, and biosensors. Although NPs have already become well-established and geared for these and several other fields of interest during the relatively short time they have been known to researchers, many possible applications have still to be found and many areas of interest are still largely unexplored. [1,2]

The number of atoms in a NP cluster is based on the dense packing of atoms in a geometry that is often believed to be spherical or some other, similar geometry. [3] A discrete NP consists of a single, central atom which is surrounded by twelve other atoms in three-dimensional space. As a result, the smallest NP cluster contain thirteen atoms and the following layers after this first one contain $10n^2 + 2$ atoms, where n is the number of the layer. After the first layer of 12 atoms, the second layer contains 42 atoms, which will result in a total of 55 atoms for a NP cluster. The $[Au_{55}(PPh_3)_{12}Cl_6]$ complex is one such example of a NP cluster and it has been extensively characterized by Schmid *et al*. [4] Spectroscopic data has previously revealed that the core of such a Au_{55} cluster shows a discrete energy level spacing. Apart from this specific Au_{55} cluster, larger clusters containing 147, 309, 561, 923, 1415, and 2057 atoms have been isolated and these contain from 3 to 8 layers of atoms respectively (n = 3 – 8). [3–5] Besides these large clusters that can contain even thousands of atoms, discrete Au clusters are known to contain a small number of atoms, but with various three-dimensional geometries. [6–8] When these clusters become very large, they start to approach a figurative barrier between what is known to be a cluster and what is known to be a colloid. Colloids tend to be defined by some dispersity represented by a histogram constructed using transmission electron microscopy (TEM) images. [1]

NPs with diameters in the range of 1 – 10 nanometres (nm) are considered to be intermediate in size between that of small molecules and bulk metals. The resulting physical and electronic properties of these nanomaterials no longer tend to represent either those of molecular compounds, nor those of bulk metals. However, the physical and electronic properties of these nanomaterials depend on the NP size, distance between individual NPs, the shape of the NPs, and the nature of the organic stabiliser. [1,9]

The free electrons present in the NPs all show a characteristic collective oscillation frequency of the plasma resonance. This causes the plasmon resonance band (PRB) which is commonly observed near 530 nm for NPs with a diameter greater than 5 nm. One would typically find a gap between the valence band and the conduction band when analysing NPs, which is unlike what would be found in bulk metals. This size specific metal-insulator transition is generally observed if the metal particle is small enough (<20 nm), so that size-dependent quantization effects occur. [10]

Discrete metallic nanoclusters are well known to contain a small number of atoms and a range of different geometries, which is especially true for Au NPs which have been studied extensively. [1,6,7]

1.2 Monometallic Nanoparticle Synthesis

A. Nanoparticle Synthesis

Among the conventional methods for synthesising monometallic Au NPs by reducing Au(III) derivatives, the most common method for a considerable time since 1951 has been to use a citrate reduction of chloroauric acid ($HAuCl_4$) in water. [2] This method produces Au NPs with a size of roughly 20 nm in diameter. Another synthesis method reported by Frens in 1973, attempted to obtain Au NPs of predetermined size by means of a controlled formation, a method that was proposed where the ratio between the reducing and stabilizing agents (trisodium citrate and Au) was varied. [11] This method is still commonly used today when a less rigid ligand shell is desired around the NP and also when a material is prepared which requires Au NP precursors. A practical method has also been developed for the preparation of Au NPs which are stabilized with sodium 3-mercaptopropionate (Figure 1.1). This method requires the simultaneous addition of citrate salt and an amphiphilic surfactant, allowing the NP size to be controlled by changing the ratio of the stabilizer and the amount of Au ions. [12]

The $[Au_{55}(PPh_3)_{12}Cl_6]$ cluster which was reported by Schmid in 1981 remained unique for a considerable time due its narrow size distribution (1.4 ± 0.4 nm) for the study of nanomaterials despite the intricate method for its synthesis (Figure 1.2). [13] The stabilization of Au NPs with alkanethiols showed that it was possible to use thiols of different chain lengths and characterise them. [14,15]

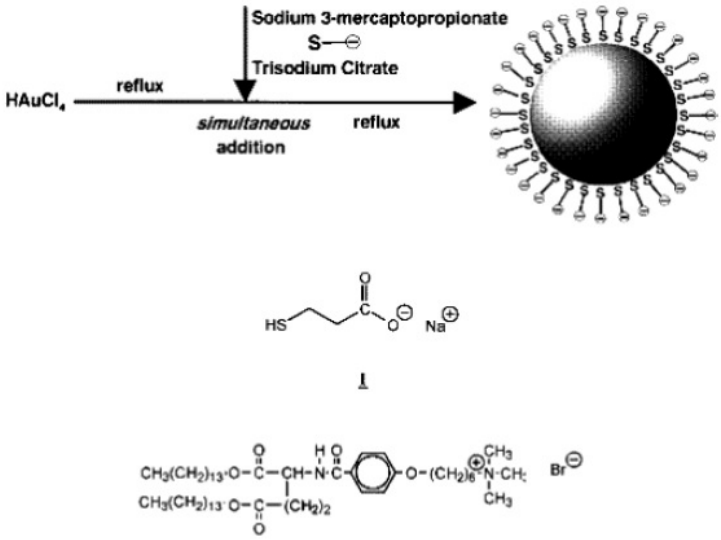

Figure 1.1 Preparation of anionic mercapto-ligand-stabilized Au NPs in water. [12]

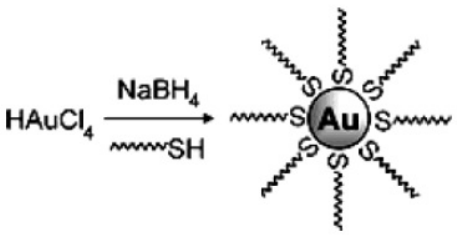

Figure 1.2 Au NPs coated with organic shells by reducing Au(III) compounds in the presence of thiols. [13]

The Brust-Schiffrin method has had a considerable impact on the synthesis of nanomaterials, because it allowed the facile synthesis of thermally stable and air-stable NPs of reduced size distributions and controlled NP size for the first time with the NP diameters ranging between 1.5 and 5.2 nm. These NPs were isolated and redissolved in organic solvents without any irreversible aggregation or decomposition and can easily be handled and functionalized (Figure 1.3). [16] Attempts to specifically study the stability of Au NPs has led to the development and use of various types of amphiphilic ligands. [17–19] All these ligands have unique properties that make them advantageous use in a biphasic system. These ligands, which include amphiphiles such as surfactants, reverse micelles, copolymer micelles, microemulsions, and membranes allow a favourable reaction environment in which hydrophilic metallic ions can be extracted to the organic phase. [1,18,19]

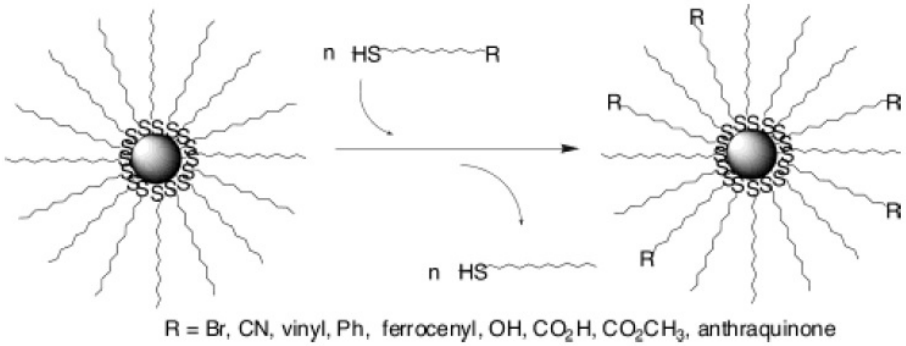

Figure 1.3 Generalized scheme representing the ligand-exchange between alkanethiol-stabilized Au NPs of the Brust type. [16]

This process would otherwise be hard to facilitate and thus it serves as an advantage over conventional biphasic systems. The amphiphilic ligand thereby allows the NPs to be extracted into the organic phase and subsequently it will also stabilize the NPs. [20,21] Since these types of amphiphilic ligands such as micelles and polymers have shown to be very favourable to the isolation of the Au NPs, many recent studies have focused on understanding the factors that contribute towards this stabilization. [22,23] Besides using various amphiphilic ligands such as polymers and micelles, the seeding-growth technique has proven capable to allow control over the size distribution of NPs. This method, being used for over a century, is a step-by-step process by which the nucleation of NPs is enlarged by reducing a metal salt onto an initial, smaller seed. [24–26] This method has shown to be much more effective in controlling the NPs' size distribution than a single step seeding method in which secondary nucleation is bound to occur when no stabilizers are present (Figure 1.4). [27,28]

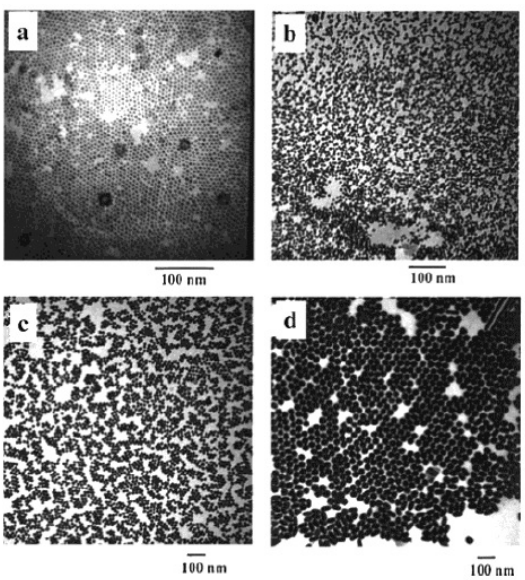

Figure 1.4 TEM images of large Au NPs prepared with the seeding-growth technique. [27]

Polyamidoamine (PAMAM) dendrimers are one example of dendrimers utilised to successfully stabilise Au NPs. [1] These PAMAM dendrimers were only able to stabilize the Au NPs when prepared in solution and when an excess of the dendrimer was added. However, only once the peripheries of these dendrimers were functionalised with thiol groups, were they able to completely stabilise the NPs and when being used in organic solvents, these PAMAM dendrimers were modified by adding hydrophobic groups to the peripheries. [29,30]

The direct reduction of dendrimer encapsulated nanoparticles (DENs) requires that a metal cation be extracted into the interior of a dendrimer and subsequently be reduced, commonly with $NaBH_4$ (Figure 1.5). [31–33] The reduction of the metal ions causes the formation of metal clusters inside the dendrimer framework.

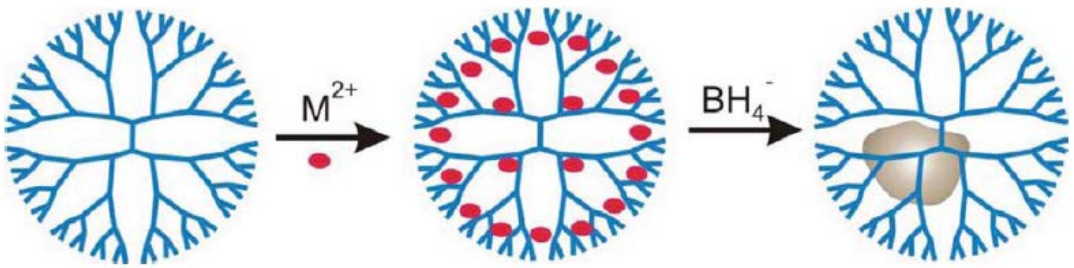

Figure 1.5 General reaction scheme showing how DENs are prepared via direct reduction. [34]

One obvious indication for the formation of NP's, is the colour change of the reaction solution. In the case of a fourth-generation hydroxyl-terminated PAMAM dendrimer loaded with Cu^{2+} (G4-OH$(Cu^{2+})_n$) the solution is blue, but changes to golden brown once reduction has been completed with $NaBH_4$. [31,32]

The direct reduction method for preparing dendrimer-encapsulated metal nanoclusters is not always suitable for encapsulating NPs whose precursor ions are not strongly complexed. [31,33] For instance, it is not possible to prepare Ag particles inside hydroxyl-terminated PAMAM dendrimers by allowing the direct reduction of interior ions, a metal displacement reaction has to be used to form stable dendrimer encapsulated Ag clusters, as shown in Figure 1.6. [35]

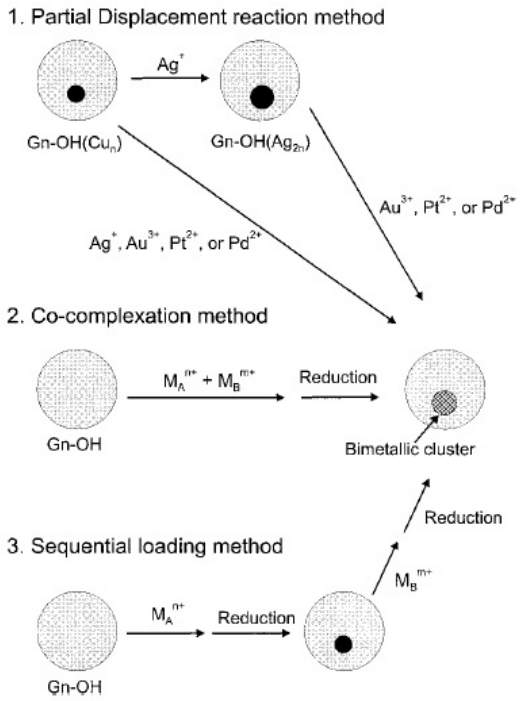

Figure 1.6 Schematic representation of different methods that can be utilized to prepare bimetallic NPs. [35]

B. Characterizing Nanoparticles

Characterizing NPs is critical for correlating their structures and functions. NP characterisation is made significantly more arduous because of their extremely small sizes. DENs are also hard to characterize due to the presence of their sizeable hydrocarbon structure. [34] It is important for the researcher to know what the surface structure is of the NP, because it will have a direct influence on the analysis results that will be obtained. As mentioned before, the small structures of NPs make them particularly hard to characterize. As a result, many spectroscopic techniques that utilize long-wavelength radiation, such as X-ray diffraction (XRD), are redundant for such analysis. Extended X-ray absorption fine structure (EXAFS) is a particularly useful method to utilize when characterizing NPs, because it provides detailed information about the environment in which an absorbing atom is situated. This includes information about the interactions that exist between a particular atom and the ones that are adjacent to it, such as the type and number of bonds as well as the bond distances. [34] EXAFS has become an indispensable technique to analyse DENs in particular. [34] Dendrimers have well-defined three-dimensional structures that can encapsulate and stabilize NPs. [36] This effect of the dendrimer causes the encapsulated NPs to be significantly smaller than when synthesized using a different template. This reduced diameter of the NP results in a lower average coordination number of the atoms in the NP due to a greater ratio of them being on the surface of the NP.

Frenkel reported an instance of this when he found that the ratio of surface to interior atoms in 147- and 55-atom cuboctahedra were 1.7 and 4.2, respectively, showing the sensitivity that EXAFS has towards both the size and shape of the NPs. [37] Previous work published showed that EXAFS is also fitting to characterize certain bimetallic NPs. The different homo and hetero metal-metal coordination numbers of core-shell and alloy NPs were used to investigate the structures of bimetallic PdAu, PdCu, and PtCu DENs. [38–41] Co-complexation and sequential reduction methods were used to synthesize 147-atom Pd-Au DENs where different ratios of Pd:Au were used. EXAFS was able to show that the DENs that were synthesized via the co-complexation method were alloys, while the DENs synthesized via sequential reduction possessed a core-shell structure.

EXAFS is also suitable to use for distinguishing between the different types of bimetallic structures that metallic NPs might have. These different structures are the cluster-on-cluster, alloy, and core-shell types and they all possess different homo and hetero metal-metal coordination numbers. Research has previously been done to determine what the structures of PdAu, PdCu, and PtCu DENs are. [31,35,39,42] In the instance of the PdAu DENs (with 147 atom NPs) containing different ratios of Pd to Au the synthesis was done via two different methods. The first of these methods was co-complexation. Analysis with EXAFS showed that this method for preparing bimetallic DENs produces random alloys. The second method, sequential reduction, showed that it forms core-shell bimetallic NPs. Size information may also be obtained from EXAFS data. This is because the ratio of surface to interior atoms increases significantly with decreasing size for particles less than 2 nm in diameter. Accordingly, predicted coordination numbers for cuboctahedral particles containing 55 and 147 atoms are 7.86 and 8.98, respectively, and such values can usually be distinguished.

Transition Electron Microscopy (TEM), X-ray photoelectron spectroscopy (XPS), energy-dispersive X-ray spectroscopy (EDS), and ultraviolet-visible spectrophotometry (UV-vis) used together can show certain indications that co-reduction of two different metals yields bimetallic DENs that have diameters comparable to the expected values.[34,40] Myers, *et al.* showed that using TEM in conjunction with single particle EDS was effective to determine the sizes and composition of bimetallic NPs. The TEM micrographs of bimetallic Pd-Cu DENs obtained after extraction indicated NP sizes of 0.5 – 2.2 nm, which was within the expected range. Single particle EDS was also used to prove the bimetallic composition of the particles.[40]

Mass spectrometry (MS) is a powerful method for determining the composition of small NPs. The ability of MS to measure the size of DENs depends on the nature of the dendrimer encapsulating the particle. In one instance, Yamamoto *et al.* used matrix-assisted laser desorption-ionization time of flight (MALDI-

TOF) MS to measure the size of Rh DENs synthesized in G4 DPA dendrimers. Informative spectra of DENs synthesized in PAMAM dendrimers using either MALDI-TOF or electrospray ionization (ESI) MS have not been easy to obtain though. In fact, obtaining reliable MS spectra for high-generation PAMAM dendrimers, even in the absence of an encapsulated NP, proves challenging. [43]

Au_{55} clusters have been studied by Mossbauer spectroscopy, EXAFS, electron spectroscopy for chemical analysis (ESCA), and conductivity measurements. These aforementioned techniques showed that the Au_{55} particles behave like a system with a few metallic electrons that are used for tunnelling between neighbouring clusters. This was observed by applying an alternating current in the 10-kHz range for impedance measurements.[10,16]

There are several techniques available to measure NP size which can corroborate TEM findings. One such technique is the optical plasmon band (SPR) of solution-phase DENs to estimate, or at least set an upper limit, on the NP size if they are comprised of appropriate metals, such as Ag, Au, or Cu. For instance, Cu NPs that are smaller than 3 nm in diameter do not exhibit a plasmon band during analysis with UV-Vis spectroscopy. [34]

The relative one-dimensional ^{1}H-NMR peak intensities of the internal dendrimer functional groups decrease in the presence of DENs.[44] It has been shown that a correlation exists between the size of the encapsulated NPs and the damping of the NMR signal. This principle was demonstrated by comparing the signal ratio for Pd NPs encapsulated in G6–OH dendrimers and it was found that it increased linearly with particle size.[34,44] This method of characterization may be useful in cases where high-resolution TEM is not available and it also allows the DENs to be analysed in situ.[34]

Ever since DENs were first reported a definitive case regarding encapsulation still had to be made and the only support regarding this idea came from TEM analysis of gold NPs. [45] Since then, various studies have been done to investigate the spatial relationship of the DEN and it surrounding dendrimer. [34]

One of these studies focused on the process during which carbon monoxide was adsorbed onto the surfaces of platinum DENs in several different solvents. [46] In the cases in which polar solvents were tested, strong and extensive adsorption of carbon monoxide would always be observed and the opposite trend was observed when the experiment was done with dry DENs in air. This experiment showed that when polar solvents were used, the dendrimer would essentially open up around the encapsulated NP, thereby opening up spaces that would allow nearby solvent molecules to interact with the NPs. However, when poor solvents were used, the dendrimer would collapse onto the NP and as a result, other molecules would be impeded from reaching the encapsulated NP. The experiment suggested that these observations could only be consistent if the NPs was completely encapsulated inside the dendrimer host.

In a related study, alkanethiols were used for solvent-selective adsorption on the surface of platinum DENs that were prepared for use as catalysts. [47] An electrode surface was used to immobilize PAMAM dendrimers that were modified with hydroxyl peripheries and the DENs were encapsulated within these modified dendrimers. After being immobilized on the electrode surface, these DENs were added to either a polar or apolar solvent, both of which contained alkanethiols. When polar solvents were used, it was found that the alkanethiols bound strongly to the DENs and as a result, the homogeneous catalytic reactions – hydrogenation, Heck coupling, and Suzuki reactions – were inhibited. [46] When apolar solvents were used, the opposite was observed and no alkanethiols adsorbed onto the DEN surfaces. These results were also consistent with what would be expected if the NPs were encapsulated within the modified dendrimer framework.

Experiments utilising high-resolution NMR have also been done with palladium DENs in hydroxyl-terminated PAMAM dendrimers in order to study NP encapsulation (Figure 1.7). [48,49] Peak assignments for the dendrimer were made using a variety of NMR experiments. These included ^{1}H, $^{1}H–^{1}H$ correlation spectroscopy (COSY), $^{1}H–^{15}N$ heteronuclear multiple bond correlation (HMBC), $^{1}H–^{13}C$ HMBC, and $^{1}H–^{13}C$ heteronuclear single quantum coherence (HSQC) NMR experiments. [50]

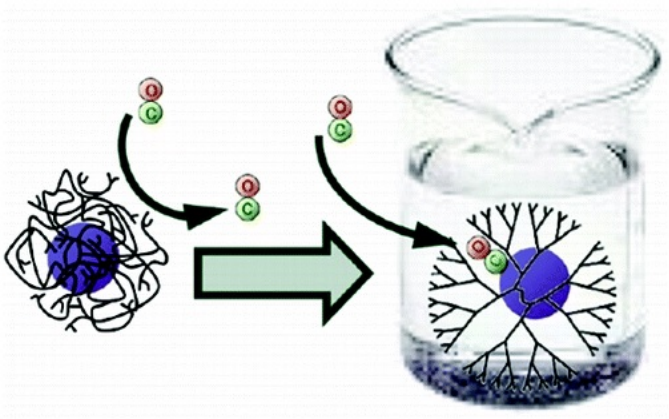

Figure 1.7 Graphical representation of how polar solvents can affect the access of substrates to the catalytic sites by affecting the dendrimer's structure. [47]

The peak assignments were done by shifting the peaks of the peripheral methylene groups relative to the peaks of the methylene groups closest to the interior. Once the palladium had been introduced as the Pd(II) precursor, all the ^{1}H peaks of the dendrimer disappeared as a result of the Pd(II) complexation. However, once the Pd(II) had been reduced with sodium borohydride ($NaBH_4$), the ^{1}H peaks of the

dendrimer returned, albeit with a lower intensity than before. It was also observed that the relative intensity of the internal methylene peaks had decreased. After this, short chain thiols were used to extract the palladium NPs from the dendrimer and as a result, the peak intensities of the methylene groups returned to their initial intensities as seen for the free dendrimer. This also suggested that the palladium NPs were encapsulated inside the dendrimer.

C. Dendrimers as Nanoparticle Stabilizers

Dendrimers possess two important properties that make them desirable hosts for metal NPs: they have large numbers of peripheral groups, and they possess internal void spaces in the interior with higher dendrimer generations. [33,51] These internal void spaces, however, are only present in dendrimers with a sufficiently high generation. One such instance where the internal cavities of a dendrimer is affected by the dendrimer generation is the PAMAM dendrimer (Figure 1.8). The G4 PAMAM dendrimer has a porous, three-dimensional structure, whereas the G1 counterpart has a much more open structure. [31]

Using dendrimer templates to prepare DENs has shown to have at least five potential advantages that make use of the dendrimers' unique chemical and structural properties. [31,33,52] Firstly, the dendrimer template allows for well-defined NP replicas due to their uniform composition and structure. Secondly, the NPs won't agglomerate during catalysis, because being encapsulated by the dendrimers allow for additional stabilization. Thirdly, a significant portion of the surface area of the NP, retained inside the dendrimer, is activated and can subsequently be used in catalysis. Fourthly, the access that molecules or substrates have to the surface of the encapsulated NP can be controlled selectively by the branches of the dendrimer. Finally, the peripheries of the dendrimer can be altered so that the solubility of the DENs can be controlled. The dendrimer interior can serve as a template in the preparation of dendrimer encapsulated NPs to control the size of NPs and to passivate the NP surface to some extent. [31] Passivating the NP surface is required to prevent seeding that leads to agglomeration, but when seeding does occur, the nanoclusters formed will not be isotropic, thereby forming nanoclusters with irregular shapes. [53,54] Because the NPs used for catalysis should be prepared with consistent sizes, this is usually done by reducing a metal salt in the presence of a stabilizer. These stabilizers may include either dendrimers (Figure 1.9), ligands, or surfactants amongst others. The stabilizers are used to inhibit agglomeration by passivating the surface, however, since these NPs are to be used for catalysis it must not be completely passivated. If this were to happen, the entire NP surface would be covered with the stabilizer and subsequently there would be no open, active sites for the substrate to access. [31,55,56]

Dendrimers' uses in catalysis stand out as one of their most promising applications. This is because they offer the unique ability of integrating advantages of both heterogeneous and homogeneous catalysis while still retaining their well-defined molecular features that are required for analysing the catalytic process. Dendrimers also enable control of the number of available catalytic sites. [33]

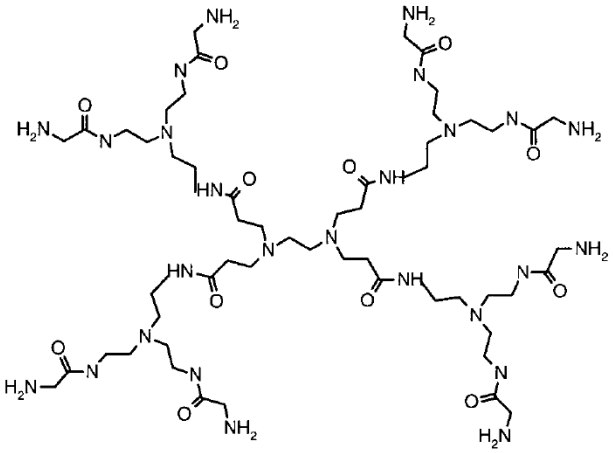

Figure 1.8 Representation of a G2 poly(amidoamine) (PAMAM) dendrimer. [31]

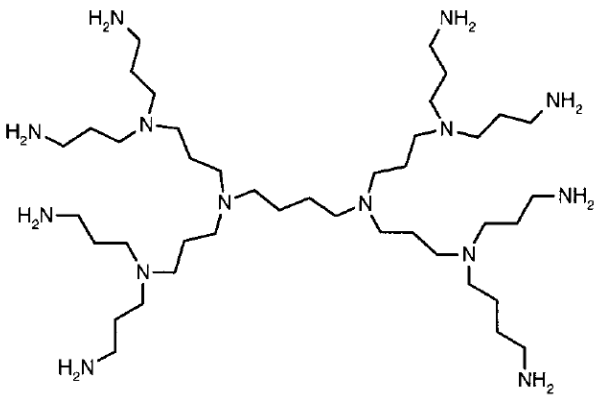

Figure 1.9 Representation of a G2 poly(propylene imine) (DAB-PPI) dendrimer. [31]

D. Polymeric supports

Organic ligands and polymers that have an affinity to metals are often used as stabilizers of metal NPs. [57,58] These substances also allow for control or manipulation of the reduction rate of metal ions coordinated to the ligands as well as the agglomeration of these metal NPs. The preparation of these polymer- or ligand-stabilized NPs involve two basic processes: reducing the metal ions in solution to metallic, zerovalent atoms and coordinating the polymer to metal NPs so that the NP can be stabilized. [59]

Ligands and polymers control and often prevent the agglomeration of metallic NPs in solution. The reduction of metal ions can either be preceded or followed by the interaction between the stabilizer and the NP.

In the instances where the reduction precedes the stabilizing interaction, the structural properties of the NPs will only be determined by the reaction conditions under which chemical reduction has occurred. However, in the instance where the stabilizing interaction precedes the chemical reduction, the interaction between the NPs and their stabilizers will affect the shapes and sizes of the NPs. As a result, when the NPs are prepared in the presence of a stabilizer, a stabilizing interaction will be maintained between these two. Conversely, if the chemical reduction were to precede this interaction, the stabilizers and NPs may not have any such interactions and significant agglomeration may occur as a result. Any type of stabilizing polymer, whether it may be natural or synthetic, can interact with and adsorb onto the surface of hydrophobic NPs. The hydrophobic part of the stabilizer will be adsorbed onto the surface of the NP and the other, hydrophilic part will spread out into the hydrophilic solvent. [58,59]

Any organic ligands with a functional group that displays an affinity to metallic NPs can be used as stabilizers for those NPs. Thiol derivatives, for instance, have been well-reported as effective and strong stabilizers for gold NPs. These same thiols and their derivatives can also be used to functionalize the NPs surface by forming a single layer on the NPs surface. [60–62]

1.3 Monometallic Nanoparticle Applications

A. Homogeneous catalysis

DENs possess great potential to be used as catalysts, as they combine the advantages of both homo- and heterogeneous catalysis. [33] NPs can serve as model catalysts for correlating the effects of their sizes to their activities during catalysis. In one instance, the effect of NP size on the rate of the catalytic hydrogenation of allyl alcohol was reported for palladium NPs encapsulated in 6th generation hydroxyl terminated PAMAM dendrimers (Figure 1.10). [34,63] In this particular study, the turnover frequency, normalized to the number of moles of palladium, was determined by measuring the rate of H_2 consumption. The results showed that the TOF increased as the NP size increased. Specifically, the TOF directly correlated to the theoretical number of atoms on the NP faces for the NPs that were smaller than 1.5 nm in diameter. Therefore, this observation was attributed to the effect of the NPs geometry rather than the diameter. By contrast, the TOF for the smallest particles did not correlate to any one specific category of surface atoms,

and it was subsequently proposed that the decreasing catalytic rates for particles less than 1.5 nm in diameter were due to electronic effects. [63]

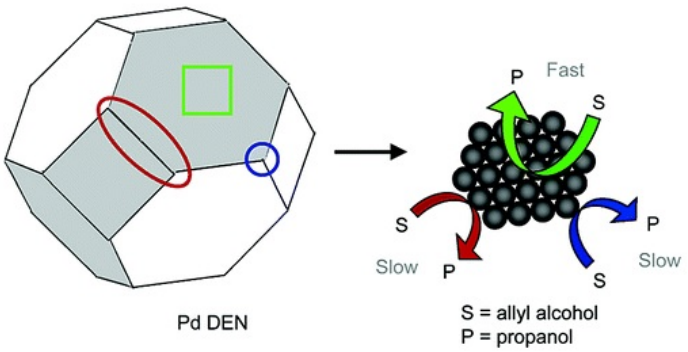

Figure 1.10 Graphical representation of the effect of the NPs morphology on the catalytic process. [64]

In addition to catalytic hydrogenation reactions, palladium NPs have also been used to catalyse carbon-carbon coupling reactions. [46,65,64] However, proposed mechanisms suggested that the active catalytic species may not have been the NP itself, but rather another palladium species that leached from the dendrimer in which the palladium NPs were stabilised. This point was particularly emphasized when it was found that $Pd(OAc)_2$ has activity for the aqueous Stille reaction - reactions in which the palladium catalyses the coupling between an aryl halide and organotin compound- similar to that of palladium NPs (Figure 1.11). [64] They also found that palladium NPs agglomerated during the Stille reaction. However, the NPs exhibited better recyclability and selectivity compared to $Pd(OAc)_2$. The rate of the Suzuki-Miyaura reaction catalysed by palladium DENs (dendrimer encapsulated NPs) and DSNs (dendrimer stabilised NPs) synthesised in triazolylferrocenyl dendrimers was also determined. [65] They found that the TOF was independent of both the amount of palladium used for catalysis and the method of NP stabilization (DEN and DSN). In fact, the TOF and stability improved upon dilution of the catalyst and it was concluded that the active catalyst is a leached palladium species. This was further confirmed by the observation of a palladium precipitate that had formed during catalysis. [34,65]

Due to the metal catalysts' active sites being on the surface of the NP, smaller metal particles are expected to be more efficient than what larger NPs would be. However, there are exceptions, particularly when the NPs are in the range of 1 – 3 nm. [66] One expected drawback of the smaller NPs is believed to arise from their higher surface energy, since it is a strong contributing factor for NP agglomeration. This drawback can be avoided by adding some form of stabilizer to the metal ion solution before it is reduced. This helps resolve the problem by interacting with the surface of the growing NPs and thereby lowering the

surface energy. This should lower the chances of any aggregation and precipitation from occurring. [66,67] The subsequent reduction of these metal ions in the reaction solution containing some sort of stabilizer will then result in the formation of NPs that are stabilized. [68–70]

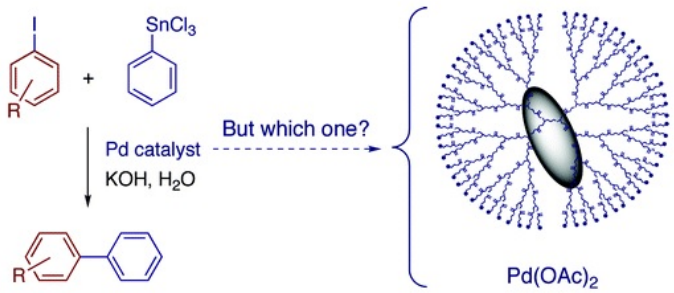

Figure 1.11 Stille reaction catalysed with Pd DENs. [64]

The irreversible adsorption of any stabilizers on the NP surface is undesirable when preparing homogeneous catalysts. This irreversible adsorption of the stabilizer will cause the catalyst's active sites to be sterically crowded and subsequently result in a loss of catalytic activity. These problems have created a need for methods that optimize both NP size and surface protection in order to obtain efficient NP catalysts. DENs, having the unique property of being retained within their dendrimer hosts to some extent, will inherently have a portion of their surface area unpassivated as a result of the dendrimer's stabilizing effect, thereby inhibiting these sites for catalysis. [71]

DENs can also be tailored to be used as homogeneous catalysts in various solvents, because the peripheries of the dendrimer can be modified to alter their solubility. [72] One such example that was reported is a fourth-generation, hydroxyl-terminated (G4-OH) PAMAM dendrimers that encapsulated palladium NPs made up of forty palladium atoms (G4-OH(Pd_{40})). These DENs were able to catalyse the hydrogenation of various linear and branched alkenes efficiently in an aqueous solution. [73] Such DENs with modified peripheries have also been used as catalysts in the Suzuki cross-coupling reactions of aryl halides and arylboronic acids in water. [74] In this study, palladium NPs were encapsulated in a third generation, hydroxyl-terminated PAMAM dendrimer (G3-OH(Pd_{10})). These catalysts proved to be more efficient in the coupling phenylboronic acid and iodobenzene than its fourth generation counterpart (G4-OH(Pd_{10})), although it was found to be less stable. These observations are believed to result from the relatively open structure of the dendrimer. The relatively open dendritic structure allows for easier access of the substrates to the catalytic surface, but it doesn't prove to be as effective at stabilizing the NP. [72]

B. Heterogeneous catalysis

Colloidal DENs not significantly tend to block the access of small molecules to the surface of the DEN in aqueous solutions, but when drying it, the dendrimer tends to collapse around the encapsulated NP. [46,63,75,76] As a result, any gaseous catalytic reaction will usually proceed very slowly. [77] One exception to this was reported when it was found that even after drying rhodium and platinum DENs that were immobilized on a three dimensional silica support, these DENs still exhibited high catalytic activity towards the hydrogenation of ethylene and pyrrole. [78] It was proposed that interactions between 4th generation hydroxyl terminated dendrimers and the channel walls of the silica support prevented the dried dendrimer from passivating the encapsulated NPs. Further thermal treatment under mildly reducing conditions resulted in higher catalytic activity and XPS analysis indicated that the DENs were incompletely reduced during synthesis and that further reduction of the metal occurred during the heating process. As such it was deemed impossible to attribute the enhanced catalytic activity to increased surface exposure of the DEN. Previous efforts to remove the dendrimer from the encapsulated NP, without changing the composition or structure of the DENs, have so far proved unsuccessful and it is believed to be a problem that warrants further investigation. [77,79]

Since heterogeneous catalysts allow for easy separation of the catalyst from the rest of the reaction mixture, they are commonly used in various industrial processes and applications. However, one drawback of heterogeneous catalysts that are immobilized on a support such as silica, alumina, or highly cross-linked polymer beads is that they often tend to have decreased catalytic activity and selectivity when compared to their homogeneous counterparts. This drawback is believed to result from the substrate's limited accessibility to the catalytic surface as a result of the support (Figure 1.12). [80] Several important factors to consider when studying DENs as catalysts are the fundamental questions raised regarding the size, shape, and location of these NPs. Gröhn, *et al* [45] used TEM and various scattering methods to confirm that gold NPs were slightly offset from the centre of G_n (n = 6 – 9) PAMAM dendrimers terminated with amine groups (G_n – NH_2). The difficulty of interpreting the data obtained from these methods and correlating the results to the dendrimer's conformation in solution is very complex and dependant on constructed models. [72] It has been observed in some cases that TEM analysis can possibly over-estimate the size of DENs by more than 50 % in some cases. [73] This, along with the steric crowding commonly seen with DENs, would suggest that these encapsulated NPs may all have a variety of complex shapes. [72]

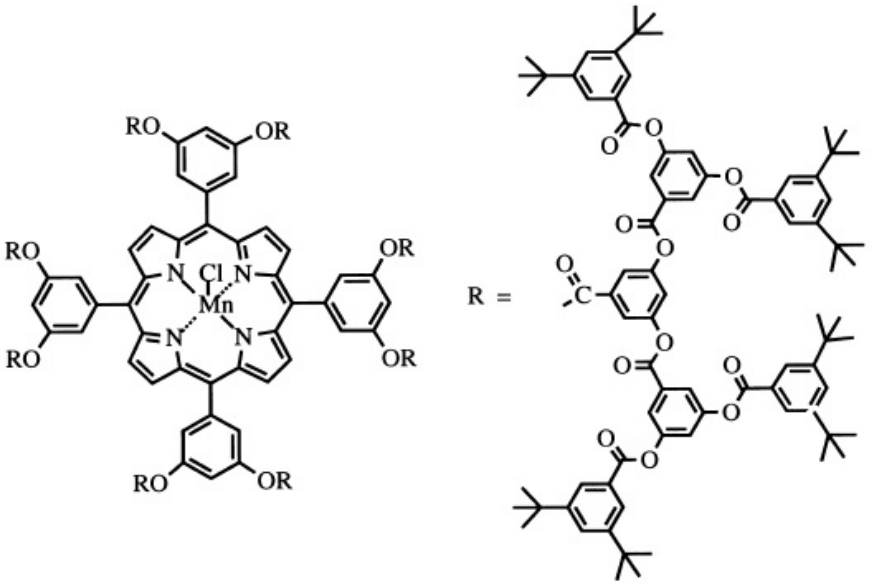

Figure 1.12 Graphical representation of the large sizes of immobilized catalysts that can lead to lowered activity as a result of steric effects. [79]

1.4 Monometallic Nanoparticle Limitations and Introduction to Bimetallic Nanoparticles

A. Advantages of Bimetallic nanoparticles

Bimetallic NPs are unique and important materials, since their unique bimetallic characteristics are different than those of the individual metals from which they are made and this sets them apart from monometallic NP's. [31] This allows for the synthesis of bimetallic NPs as catalysts with improved activity. [81] The combination of different metals (Au and Pd) in one NP was proposed in the 1970's. [82]

When preparing metal NPs, the ideal is to have them all be perfectly monodispersed. However, even if such perfectly monodispersed NPs cannot be obtained, they will still possess unique properties that will be based on their metal compositions. One of the biggest goals at this point concerning NPs is to be able to prepare them on a large scale while preserving the uniformity of all the NPs and thus a lot of attention is being devoted to this. [59]

The unique chemical and physical properties of NPs are amongst their most remarkable characteristics. Since NPs are very small, these chemical and physical properties are governed by the quantum size effect (QSE). This effect has already been well-established in the field of physics. [83] Another

unique property of NPs derives from the large proportion of surface atoms to the total number of atoms that make up the NP. A well-documented example of these unique properties can be observed when using NMR spectroscopy to analyse the NPs. [84] When platinum NPs with sizes ranging from 0.7 – 1.2 nm were analysed with ^{195}Pt NMR, a broad peak was observed. This occurred as a result of the quantum effect of the free electrons in the NPs. Some of these platinum atoms reacted in a manner consistent with those that are in the metallic state while others reacted in a fashion consistent with an oxidized state. [85]

Even though there are many possibilities for the uses of NPs, one of the fields in which great interest has been generated is catalysis. [55,86,87] A greatly desirable characteristic of NPs is that their sizes can be tailored depending on the reaction conditions and very importantly also the stabilizer being used. Researchers would want to capitalize on this specific property since the NP size affects the activity and selectivity during catalytic reactions. [87] Bimetallic NPs which are made up of two different metals are of great interest to many researchers since they have an enhanced catalytic activity. [88,89] This is caused by their bimetallic nature which can improve the catalytic properties of the conventional single-metal NPs utilized as catalysts. The bimetallic composition of these NPs might possibly even be able to yield unique properties with regards to activity, selectivity and stability not observed with either of their monometallic counterparts.

1.5 Bimetallic Nanoparticle Synthesis

Bimetallic NP synthesis via two metal salt precursors can be categorised into two synthetic methods, as shown in Figure 1.13. [34] The first of these is the co-reduction method. It is the simplest method used to prepare bimetallic NPs and is essentially the same as the general method used for preparing monometallic NPs. The only difference would be the number of metal precursors used. The second method is the successive reduction method. This method is generally used to prepare bimetallic NPs with a core-shell structure.

The first report of core-shell bimetallic NPs was published long after the bimetallic alloys were reported and studied. Schmid's group was the first to report on this new synthetic method used to prepare bimetallic NPs that have a distinctly different core and shell based on the different metals that these two parts are composed of. [34,90] Sequential reduction, also known as sequential loading, requires that the metal ions of one metal complex to the dendrimer interior. Subsequent reduction will form the corresponding NPs of these metal precursors. This step of reducing the ions to form NPs is a direct reduction method and is followed by adding the metal salt of the second metal. These metal ions will be able to complex to the

dendrimer interior since the previous metal ions would already have been reduced to their corresponding metallic NPs.

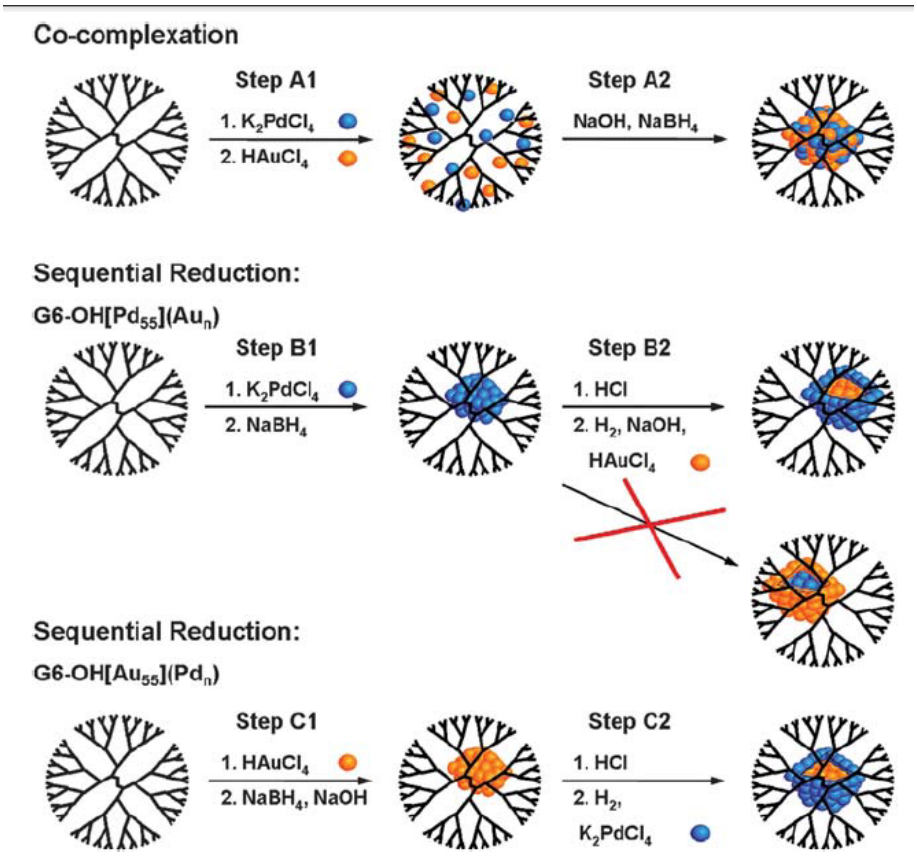

Figure 1.13 Scheme representing the different structures of bimetallic NPs that are obtained with different synthesis methods as confirmed with EXAFS. [34]

Miner *et al.* [91] have reported the synthesis of gold-platinum bimetallic NPs. These NPs were prepared with the two appropriate metal salts, tetrachloroauric acid and hexachloroplatinic acid. Once dissolved, the metal precursors were reduced by means of citrate reduction. The metal ions were completely reduced within four hours after the addition of the citrate. These citrate-stabilized NPs were analysed by means of UV-Vis spectroscopy and it revealed that the spectrum of these bimetallic NPs wasn't simply a sum of the spectra of the two monometallic Au and Pt NPs, but rather a unique spectrum, indicating that the bimetallic NPs are an alloy.

Richard *et al.* [92] successfully utilised the co-reduction method for the preparation of Pt-Ru bimetallic NPs in the presence of glucose. When analysed with EXAFS, it was revealed that a Pt-Ru bond existed, thereby proving that bimetallic NPs had formed.

The successive reduction method, when used with two metal precursors, is widely considered to be one of the most suitable methods used to prepare core-shell bimetallic NPs. Turkevich and Kim [93] have attempted to layer Au onto Pd NPs and this method of depositing one metal on a NP made of one other metal was found to be very effective. A recorded attempt to prepare polyvinylpyrrolidone (PVP)-stabilized Au-Pd bimetallic NPs was done by following the successive reduction method. [94] When the Au NPs were prepared first and then followed by reducing the Pd precursor, a mixture of individual Au and Pd NPs were produced. However, when the Pd NPs were prepared before the Au precursors were reduced, bimetallic NPs were found to have formed. Analysis found that these bimetallic NPs did not possess a core-shell structure, even though the bimetallic NPs prepared by the co-reduction method possessed a core-shell structure. The differences in these bimetallic NP structures was attributed to the differences in the redox potentials of the Pd and Au ions. When the gold ions were added to the reaction mixture that already contained the palladium NPs, some Pd^0 atoms of the NPs were oxidized and reduced some of the Au^{3+} ions to Au^0 atoms. Following this reduction of the Au^{3+} ions, the oxidized palladium ions are, in turn, reduced by the reducing agent. This process, as seen in this example, is capable of forming NPs that have complex cluster-in-cluster structures.

Gold-palladium and gold-platinum bimetallic NPs stabilized by trisulfonated triphenylphosphine and sodium sulfanilate ligands were prepared by Schmid *et al*. [90,95] by utilizing the successive reduction method. Gold colloids, which have an average diameter of approximately 18 nm, were able to be covered by an outer layer of platinum or palladium shells when different chloride salts of the metal precursors were used. The initial red colour which resulted from the gold NPs changed to a dark brown solution when the gold NPs were covered with a layer of either the platinum or palladium atoms. The addition of a water-soluble ligand enabled the newly-formed bimetallic NPs to be stabilized in solution. In the instances when the gold-platinum bimetallic NPs were prepared, uniform, heterogeneous agglomerates containing a large, spherical gold core surrounded by smaller, spherical platinum particles of approximately 5 nm were obtained. When these NPs were analysed with energy-dispersive X-ray spectroscopy (EDX), it was found that the surface of these bimetallic agglomerates contained only platinum and no gold. [90] When the gold-palladium NPs were analysed with high resolution transmission electron microscopy (HRTEM), they were found to be homogeneous and contained well-ordered shells of Pd atoms. Investigating these gold-palladium bimetallic NPs with TEM revealed structures that mostly had irregular shapes, although no smaller NPs were observed to have agglomerated and EDX analysis showed that the surface only contained palladium.

1.6 Bimetallic Nanoparticles in Catalysis

A. Catalysis

Bimetallic DENs have been utilised for multiple applications and the research arena has now progressed beyond the synthesis of NPs. The primary application for metallic NPs includes homogeneous and heterogeneous catalysis. Crooks *et al.* have previously distinguished the two by referring to DENs dissolved in solution as homogeneous catalysts, and those immobilised on a solid support as heterogeneous catalysts. [42] Catalysis with bimetallic NPs prepared via a dendrimer template, in particular the active oxide supported ones, is now an expanding field of interest and a number of new catalytic systems for various reactions, such as allyl alcohol hydrogenation, CO oxidation, and electrocatalytic O_2 reduction, are now being explored.

Investigations have shown that bimetallic DENs were efficient catalysts for the hydrogenation of unsaturated substrates. Crooks *et al*. measured the turnover frequency (TOF) for the hydrogenation of allyl alcohol in water with G4-OH[$(Pd)_x(Pt)_{40-x}$] DENs at various ratios of Pd and Pt. [96] The results showed that their ability to hydrogenate allyl alcohol was at higher rates than physical mixtures of monometallic DENs with equal composition. In the optimal composition, these bimetallic NPs were more active than what only the monometallic Pd or Pt DENs were. Such an enhancement observed at Pd-Pt bimetallic NPs of 1 – 2 nm in diameter was believed to be due to synergistic electronic and ligand effects. The similar experimental results also appeared in the hydrogenation of allyl alcohol when the PdAu bimetallic DEN alloys were used as catalysts.

Sinfelt *et al*. [81] have investigated inorganic oxide-supported bimetallic NPs extensively in their roles as catalysts. They have also been able to analyse the NPs' micro-structures by means of EXAFS. [97–98] These NPs supported by the inorganic oxide have already shown to be effective catalysts for olefin hydrogenation and the alloy structure of the bimetallic NP has been examined carefully in order to understand their catalytic properties.

1.7 Project Scope and Aims

In this project, dendrimer micelles were employed as templates and stabilizers to prepare DENs. Alkyl chains with varying lengths (C_{15}, C_{11}, and C_5) were used to determine whether the hydrocarbon periphery is able to influence and control the size of newly-formed NPs and also whether the steric hindrance caused by these alkyl chains will have a positive effect on the activity and product selectivity during solvent-free styrene oxidation. Various mono- and bimetallic NPs will be investigated in order to determine the effect of the metal and NP type on the activity and selectivity of the catalyst. The bimetallic NPs will also be investigated to determine whether the presence of two different metals in a single NP will be able to enhance that NP's catalytic performance.

This project entails the synthesis of monometallic Au and Cu DENs as well as bimetallic Au-Cu DENs. Once these have been prepared, an investigation on the effects of the peripheral alkyl chains on the NP sizes, is performed. Once the DENs have successfully been prepared, we will also be able to investigate the effects of the peripheral alkyl chains and NP composition on the catalytic process, which is the oxidation of styrene.

1.8 References

1. Daniel, M. & Astruc, D. Gold Nanoparticles: Assembly, Supramolecular Chemistry, Quantum-Size-Related Properties, and Applications toward Biology, Catalysis, and Nanotechnology. *Chem. Rev.* **104,** 293–346 (2004).
2. Turkevitch, J., Stevenson, P. & Hillier, J. Nucleation and Growth Process in the Synthesis of Colloidal Gold. *Discuss. Faraday Soc.* **1,** 55–75 (1951).
3. Schmid, G. *et al.* Current and Future Applications of Nanoclusters. *Chem. Soc. Rev.* **28,** 179–185 (1999).
4. Zhang, H., Schmid, G. & Hartmann, U. Reduced Metallic Properties of Ligand-Stabilized Small Metal Clusters. *Nano Lett.* **3,** 305–307 (2003).
5. Schmid, G. *et al.* Ligand-stabilized Giant Palladium Clusters: Promising Candidates in Heterogeneous Catalysis. *J. Am. Chem. Soc.* **115,** 2046–2048 (1993).
6. Puddephat, R. The Chemistry of Gold. *Elsevier* (1978).
7. Schmidbauer, H. *Gold, Progress in Chemistry, Biochemistry and Technology*. (Wiley, 1999).
8. Laguna, A. *In Metal Clusters in Chemistry*. (Wiley-VCH, 1999).
9. Brust, M. & Kiely, C. Some Recent Advances in Nanostructure Preparation from Gold and Silver: A Short Topical Review. *Colloids Surf. A Physiochem. Eng. Asp.* **202,** 175–186 (2002).
10. Daniel, M. C. & Astruc, D. Gold Nanoparticles: Assembly, Supramolecular Chemistry, Quantum-Size-Related Properties, and Applications Toward Biology, Catalysis, and Nanotechnology. *Chemical Reviews* **104,** 293–346 (2004).
11. Frens, G. Controlled Nucleation for the Regulation of the Particle Size in Monodisperse Gold Suspensions. *Nat. Phys. Sci.* **241,** 20–22 (1973).
12. Yonezawa, T. & Kunitake, T. Practical Preparation of Anionic Mercapto Ligand-Stabilized Gold Nanoparticles and Their Immobilization. *Colloids Surf. A Physiochem. Eng. Asp.* **149,** 193–199 (1999).
13. Schmid, G. *et al.* [Au55{P(C6H5)3}12Cl6] - A Gold Cluster of Unusual Size. *Chem. Ber.* **114,** 3634–3642 (1981).
14. Giersig, M. & Mulvaney, P. Preparation of ordered colloid monolayers by electrophoretic

deposition. *Langmuir* **9,** 3408–3413 (1993).

15. Hasan, M., Bethell, D. & Brust, M. The Fate of Sulfur-Bound Hydrogen on Formation of Self-Assembled Thiol Monolayers on Gold: 1H NMR Spectroscopic Evidence from Solutions of Gold Clusters. *J. Am. Chem. Soc.* **125,** 1132–1133 (2003).

16. Daniel, M.-C. & Astruc, D. Gold Nanoparticles: Assembly, Supramolecular Chemistry, Quantum-Size-Related Properties, and Applications toward Biology, Catalysis, and Nanotechnology. *Chem. Rev.* **104,** 293–346 (2003).

17. Belloni, J. Metal Nanocolloids. *Curr. Opin. Colloid Interface Sci.* **1,** 184–196 (1996).

18. Latters, A., Rico, I., de Savignac, A. & Samii, A. Formamide, a Water Substitute in Micelles and Microemulsions: Structural Analysis Using a Diels-Alder Reaction as a Chemical Probe. *Tetrahedron* **43,** 1725–1735 (1987).

19. Sohn, B. *et al.* Directed Self-Assembly of Two Kinds of Nanoparticles Utilizing Monolayer Films of Diblock Copolymer Micelles. *J. Am. Chem. Soc.* **125,** 6368–6369 (2003).

20. Hassenkam, T., Nørgaard, K., Iversen, L., Kiely, C. & Bjørnholm, T. Fabrication of 2D Gold Nanowires by Self-Assembly of Gold Nanoparticles on Water Surfaces in the Presence of Surfactants. *Adv. Mater.* **14,** 1126–1130 (2002).

21. Gittins, D. & Caruso, F. Tailoring the Polyelectrolyte Coating of Metal Nanoparticles. *J. Phys. Chem. B* **105,** 6846–6852 (2001).

22. Hayat, M. *Colloidal Gold, Principles, Methods and Applications*. (Academic Press, 1989).

23. Pellizzetti, E. *Fine Particles Sciences and Technology From Micro- to New Particles*. (1996).

24. Jana, N., Gearheart, L. & Murphy, C. Evidence for Seed-Mediated Nucleation in the Chemical Reduction of Gold Salts to Gold Nanoparticles. *Chem. Mater.* **13,** 2313–2322 (2001).

25. Sau, T., Pal, A., Jana, N., Wang, Z. & Pal, T. Size Controlled Synthesis of Gold Nanoparticles Using Photochemically Prepared Seed Particles. *J. Nanopart. Res.* **3,** 257–261 (2001).

26. Meltzer, S. *et al.* Fabrication of Nanostructures by Hydroxylamine Seeding of Gold Nanoparticle Templates. *Langmuir* **17,** 1713–1718 (2001).

27. Carrot, G. *et al.* Gold Nanoparticle Synthesis in Graft Copolymer Micelles. *Colloid Polym. Sci.* **276,** 853–859 (1998).

28. Busbee, B., Obare, S. & Murphy, C. An Improved Synthesis of High-Aspect-Ratio Gold Nanorods.

Adv. Mater. **15,** (2003).

29. Chechik, V. & Crooks, R. Monolayers of Thiol-Terminated Dendrimers on the Surface of Planar and Colloidal Gold. *Langmuir* **15,** 6364–6369 (1999).

30. Esumi, K., Hosoya, T., Suzuki, A. & Torigoe, K. Preparation of Hydrophobically Modified Poly(amidoamine) Dendrimer-Encapsulated Gold Nanoparticles in Organic Solvents. *J. Colloid Interface Sci.* **229,** 303–306 (2000).

31. Crooks, R. M., Zhao, M., Sun, L., Chechik, V. & Yeung, L. K. Dendrimer-Encapsulated Metal Nanoparticles: Synthesis, Characterization, and Applications to Catalysis. *Acc. Chem. Res.* **34,** 181–190 (2001).

32. Parker, J. F., Fields-Zinna, C. A. & Murray, R. W. The Story of a Monodisperse Gold Nanoparticle: Au25L18. *Acc. Chem. Res.* **43,** 1289–1296 (2010).

33. Peng, X., Pan, Q. & Rempel, G. L. Bimetallic dendrimer-encapsulated nanoparticles as catalysts: a review of the research advances. *Chem. Soc. Rev.* **37,** 1619–1628 (2008).

34. Myers, S. V. *et al.* Dendrimer-encapsulated nanoparticles: New synthetic and characterization methods and catalytic applications. *Chem. Sci.* **2,** 1632–1646 (2011).

35. Zhao, M. & Crooks, R. M. Intradendrimer Exchange of Metal Nanoparticles. *Chem. Mater.* **11,** 3379–3385 (1999).

36. Vögtle, F., Richardt, G. & Werner, N. *Dendrimer Chemistry: Concepts, Syntheses, Properties, Applications*. (Wiley-VCH Verlag GmbH & Co., 2009).

37. Frenkel, A. I. Solving the 3D structure of metal nanoparticles. *Zeitschrift für Krist.* **222,** 605–611 (2007).

38. Weir, M. G., Knecht, M. R., Frenkel, A. I. & Crooks, R. M. Structural Analysis of PdAu Dendrimer-Encapsulated Bimetallic Nanoparticles. *Langmuir* **26,** 1137–1146 (2010).

39. Knecht, M. R., Weir, M. G., Frenkel, A. I. & Crooks, R. M. Structural Rearrangement of Bimetallic Alloy PdAu Nanoparticles within Dendrimer Templates to Yield Core/Shell Configurations. *Chem. Mater.* **20,** 1019–1028 (2008).

40. Myers, S. V., Frenkel, A. I. & Crooks, R. M. X-ray Absorption Study of PdCu Bimetallic Alloy Nanoparticles Containing an Average of ~64 Atoms. *Chem. Mater.* **21,** 4824–4829 (2009).

41. Carino, E. V. & Crooks, R. M. Characterization of Pt@Cu Core@Shell Dendrimer-Encapsulated

Nanoparticles Synthesized by Cu Underpotential Deposition. *Langmuir* **27,** 4227–4235 (2011).

42. Scott, R. W. J., Datye, A. K. & Crooks, R. M. Bimetallic Palladium-Platinum Dendrimer-Encapsulated Catalysts. *J. Am. Chem. Soc.* **125,** 3708–3709 (2003).

43. Yamamoto, K. & HiguchiM. Fine-control of Metal Assembling in Dendritic Polyphenylazomethines. *Polym. J.* **36,** 577–586 (2004).

44. Toshima, N. & Yonezawa, T. Bimetallic nanoparticles - novel materials for chemical and physical applications. *New J. Chem.* 1179–1201 (1998).

45. Groehn, F., Bauer, B., Akpalu, Y., Jackson, C. & Amis, E. Dendrimer Templates for the Formation of Gold Nanoclusters. *Macromolecules* **33,** 6042–6050 (2000).

46. Scott, R. W. J., Wilson, O. M. & Crooks, R. M. Synthesis, Characterization, and Applications of Dendrimer-Encapsulated Nanoparticles. *J. Phys. Chem. B* **109,** 692–704 (2005).

47. Vohs, J. & Fahlman, B. Advances in the controlled growth of nanoclusters using a dendritic architecture. *New J. Chem.* 1041–1051 (2007).

48. Peng, X., Pan, Q. & Rempel, G. Bimetallic dendrimer-encapsulated nanoparticles as catalysts: a review of the research advances. *Chem. Soc. Rev.* **37,** 1619–1628 (2008).

49. Chandler, B. & Gilbertson, J. Dendrimer-Encapsulated Bimetallic Nanoparticles: Synthesis, Characterization, and Applications to Homogeneous and Heterogeneous Catalysis. *Top. Organomet. Chem.* **20,** 97–120 (2006).

50. Aikens, C. Electronic Structure of Ligand-Passivated Gold and Silver Nanoclusters. *J. Phys. Chem. Lett.* **2,** 99–104 (2011).

51. Matthews, O. A., Shipway, A. N. & Stoddart, J. F. Dendrimers—Branching out from curiosities into new technologies. *Prog. Polym. Sci.* **23,** 1–56 (1998).

52. Andrés, R., de Jesús, E. & Flores, J. C. Catalysts based on palladium dendrimers. *New J. Chem.* **31,** 1161–1191 (2007).

53. Cloete, J., Mapolie, S. F. & Malgas-Enus, R. Facile synthesis and characterization of PTA stabilized hydrophilic Au55 nanoparticles via a DEN-MPC method. *Polyhedron* **102,** 469–478 (2015).

54. Mackay, A. L. A dense non-crystallographic packing of equal spheres. *Acta Crystallogr.* **15,** 916 (1962).

55. Lewis, L. N. Chemical Catalysis by Colloids and Clusters. *Chem. Rev.* **93,** 2693–2730 (1993).

56. Schmid, G. *Clusters and Colloids: From Theory to Applications*. *Clusters and Colloids: From Theory to Applications* (2007). doi:10.1002/9783527616077

57. Hirai, H. & Toshima, N. *Tailored Metal Catalysts*. (1986).

58. Hirai, H., Nakao, Y., Toshima, N. & Adachi, K. *Chem. Lett.* 905 (1976).

59. Toshima, N. & Yonezawa, T. Bimetallic nanoparticles - novel materials for chemical and physical applications. *New J. Chem.* **22,** 1179–1201 (1998).

60. Brust, M., Walker, M., Bethell, D., Schriffrin, D. & Whyman, R. *J. Chem. Soc. Chem. Comm.1* 801 (1994).

61. Brust, M., Fink, J., Bethell, D., Schriffrin, D. & Kiely, C. *J. Chem. Soc. Chem. Comm.* 1655 (1995).

62. Yonezawa, T., Sutoh, M. & Kunitake, T. *Chem. Lett.* 619 (1997).

63. Wilson, O. M., Knecht, M. R., Garcia-Martinez, J. C. & Crooks, R. M. Effect of Pd Nanoparticle Size on the Catalytic Hydrogenation of Allyl Alcohol. *J. Am. Chem. Soc.* **128,** 4510–4511 (2006).

64. Bernechea, M., de Jesús, E., Lopez-Mardomingo, C. & Terreros, P. Dendrimer-Encapsulated Pd Nanoparticles versus Palladium Acetate as Catalytic Precursors in the Stille Reaction in Water. *Inorg. Chem.* **48,** 4491–4496 (2009).

65. Diallo, A., Ornelas, C., Salmon, L., Aranzaes, J. & Astruc, D. ‘“Homeopathic”’ catalytic activity and atom-leaching mechanism in Miyaura–Suzuki reactions under ambient conditions with precise dendrimer-stabilized Pd nanoparticles. *Angew. Chem. Int. Ed.* **46,** 8644–8648 (2007).

66. Hirai, H. *J. Macromol. Sci.-Chem. A* **13,** 633 (1979).

67. Kiwi, J. & Graetzel, M. *J. Am. Chem. Soc.* **101,** 7214 (1979).

68. Templeton, A., Wuelfing, W. & Murray, R. *Acc. Chem. Res.* **33,** 27 (2000).

69. Brust, M., Fink, J., Bethell, D., Schiffrin, D. & Kiely, C. *Chem. Commun.* **16,** 1655 (1995).

70. Pileni, M. *Supramol. Sci.* **5,** 321 (1998).

71. Niu, Y. & Crooks, R. M. Preparation of Dendrimer-Encapsulated Metal Nanoparticles Using Organic Solvents. *Chem. Mater.* **15,** 3463–3467 (2003).

72. Niu, Y. & Crooks, R. M. Dendrimer-encapsulated metal nanoparticles and their applications to

catalysis. *C. R. Chim.* **6,** 1049–1059 (2003).

73. Zhao, M. & Crooks, R. M. Homogeneous Hydrogenation Catalysis with Monodisperse, Dendrimer-Encapsulated Pd and Pt Nanoparticles. *Angew. Chemie - Int. Ed.* **38,** 364–366 (1999).

74. Li, Y. & El-Sayad, M. *J. Phys. Chem. B* **105,** 8938 (2001).

75. Ye, H. & Crooks, R. M. Electrocatalytic O2 Reduction at Glassy Carbon Electrodes Modified with Dendrimer-Encapsulated Pt Nanoparticles. *J. Am. Chem. Soc.* **127,** 4930–4934 (2005).

76. Albiter, M., Crooks, R. & Zaera, F. Adsorption of Carbon Monoxide on Dendrimer-Encapsulated Platinum Nanoparticles: Liquid versus Gas Phase. *J. Phys. Chem. Lett.* **1,** 38–40 (2010).

77. Lang, H., May, R., Iversen, B. & Chandler, B. Dendrimer- Encapsulated Nanoparticle Precursors to Supported Platinum Catalysts. *J. Am. Chem. Soc.* **125,** 14832–14836 (2003).

78. Huang, W. *et al.* Dendrimer Templated Synthesis of One Nanometer Rh and Pt Particles Supported on Mesoporous Silica: Catalytic Activity for Ethylene and Pyrrole Hydrogenation. *Nano Lett.* **8,** 2027–2034 (2008).

79. Lafaye, G., Siani, A., Marécot, P., Amiridis, M. & Williams, C. Particle Size Control in Dendrimer-Derived Supported Ruthenium Catalysts. *J. Phys. Chem.* **10,** 7725–7731 (2006).

80. Inoue, K. Functional dendrimers, hyperbranched and star polymers. *Prog. Polym. Sci.* **25,** 453–571 (2000).

81. Sinfelt, J. H. Structure of bimetallic clusters. *Acc. Chem. Res.* **20,** 134–139 (1987).

82. Sinfelt, J. H. Catalysis by alloys and bimetallic clusters. *Acc. Chem. Res.* **10,** 15–20 (1977).

83. Marzke, R. *Catal. Rev.-Sci. Eng.* **19,** 43 (1979).

84. Bucher, J. *et al. Colloids Surf.* **36,** 155 (1989).

85. Tong, Y., Yonezawa, T., Toshima, N. & van der Klink, J. *J. Phys. Chem.* **100,** 730 (1996).

86. Schmid, G. *Clusters and Colloids*. (VCH, 1994).

87. Boennemann, H. *et al. Angew. Chem. Int. Ed.* **30,** 1312 (1991).

88. Sinfelt, J. *J. Catal.* **29,** 308 (1973).

89. Toshima, N. *J. Macromol. Sci.-Chem.* **A27,** 1225 (1990).

90. Schmid, G., Lehnert, A., Malm, J.-O. & Bovin, J.-O. Ligand-Stabilized Bimetallic Colloids Identified by HRTEM and EDX. *Angew. Chemie - Int. Ed.* **30,** 874–876 (1991).

91. Miner, R., Namba, S. & Turkevitch, J. Proceedings of the 7th International Congress on Catalysis. in 160 (1981).

92. Richard, D., Couves, J. & Thomas, J. *Faraday Discuss. Chem. Soc.* **92,** 109 (1991).

93. Turkevitch, J. & Kim, G. *Science (80-.).* **169,** 873 (1970).

94. Harada, M., Asakura, K. & Toshima, N. Catalytic activity and structural analysis of polymer-protected gold/palladium bimetallic clusters prepared by the successive reduction of hydrogen tetrachloroaurate(III) and palladium dichloride. *J. Phys. Chem.* **97,** 5103–5114 (1993).

95. Schmid, G., West, H., Malm, J., Bovin, J. & Grenthe, C. *Chem. Eur. J.* **2,** 1099 (1996).

96. Zhao, M. & Crooks, R. M. Homogeneous hydrogenation catalysis with monodisperse, dendrimer-encapsulated Pd and Pt nanoparticles. *Angew. Chemie - Int. Ed.* **38,** 364–366 (1999).

97. Meitzner, G., Via, G., Lytle, F. & Sinfelt, J. *J. Chem. Phys.* **78,** 882 (1983).

98. Meitzner, G., Via, G., Lytle, F. & Sinfelt, J. *J. Chem. Phys.* **83,** 4793 (1988).

CHAPTER 2

Mono- and bimetallic Au-Cu dendrimer micelle stabilized nanoparticles as catalysts in the solvent-free oxidation of styrene.

2.1 Introduction

As was mentioned in Chapter 1, the ability of dendrimers to encapsulate nanoparticles allows for their utility in a variety of applications including drug delivery and catalysis.[2,6] Two major advantages have been recognized in the preparation of DENs via the dendrimer template method for use in catalysis.[7,8] Firstly, the template yields well-defined NPs with uniform structure and composition thus resulting in uniformity of available catalytic sites. These encapsulated NPs are then also stabilized within these dendrimers, thereby limiting agglomeration which results in a retention of surface area and a subsequent increase in catalyst lifetime.

A further advantage is that the peripheral groups on the dendrimer can be tailored to achieve a desired solubility. The template can thus be fine-tuned to be hydrophilic or hydrophobic in nature. In the work presented here, the dendrimer's peripheral groups were functionalized with alkyl chains resulting in an inverse micelle being formed *i.e.* the hydrophilic dendrimer is converted to a hydrophobic dendrimer micelle which is soluble in organic solvents.[9] Consequently, encapsulation of metal salts is solubility driven and subsequent reduction results in nanoparticles which are retained within the dendrimer micelle largely due to steric effects rather than through coordination with functional groups. This therefore allows the bulk of the available surface area of the NPs to be available for catalysis. Furthermore, since the metal-ion interaction does not depend on the specific coordination to ligand sites within the dendrimer, but rather on solubility differences between the solvent and the dendrimer interior, metal loading is not limited by the number of coordination sites which in turn means it is not limited to dendrimer generation. [10] It was aimed to exploit the above mentioned advantages of a dendrimer micelle by using it as a template and stabilizer to produce monometallic Au_n and Cu_n as well as bimetallic Au_nCu_m NPs. Commercially available third generation DAB-PPI (diaminobutane poly(propylene imine)) dendrimers were modified with alkyl chains on their peripheries to give **M1** (C_{15} alkyl chain), **M2** (C_{11} alkyl chain) and **M3** (C_5 alkyl chain) inverted micelles. The effect that the varying peripheral alkyl chain lengths had on

NP stabilization during synthesis was investigated. After these dendrimer stabilized NPs were synthesized and characterized, they were evaluated as catalysts in the solvent-free oxidation of styrene. The effect of the peripheral alkyl chain length on catalyst activity was also evaluated.

2.2 Nanoparticle synthesis and characterization

The mono- and bimetallic Au, Cu and Au-Cu dendrimer stabilized NPs were prepared by a template approach in which metal uptake into the dendrimer interior was followed by chemical reduction with excess $NaBH_4$.[2] Metal uptake and reduction was monitored by UV-Vis spectroscopy. The dendrimer micelle (**M1**, **M2**, and **M3**) and metal salt:dendrimer micelle molar ratios were varied to obtain the different sets of mono- and bimetallic NPs. In the case of the monometallic Au and Cu NPs, metal ion uptake coincided with the formation of absorbance bands in the range 323 - 325 nm and 276 - 297 nm, respectively. These absorbances were attributed to ligand-to-metal charge transfer (LMCT).[11] In the case of the bimetallic Au-Cu NPs, the Au(III)-LMCT bands were observed in the range of 319 - 325 nm, but the Cu(II)-LMCT bands were not observed due to the relatively low Cu(II) concentration versus the Au(III).[12] The bands shifted from a lower to higher wavelength as the Au content was decreased and the Cu content increased. Upon chemical reduction, the monometallic Au NPs showed surface plasmon resonance (SPR) peaks in the range 533 – 556 nm, indicative of the formation of zerovalent Au atoms.[13] The Au(III)-micelle solution shows two distinct absorbances at 240 nm and 321 nm resulting from the ligand-metal charge transfer bands. The sample taken from the reduced reaction mixture (Au DENs) shows a very characteristic absorbance at 533 nm, indicating that nanoparticles larger than 2 nm in diameter had formed. The situation for the monometallic Cu NPs appears more complex, though. The UV-Vis spectrum of the reduced **M1**-Cu_n NPs show a characteristic monotonic absorbance increase in the direction of higher energy, without the presence of an absorbance peak at higher wavelength which is typical for Cu NPs.[11] In contrast, the UV-Vis spectrum of the reduced **M2**-Cu_n and **M3**-Cu_n NPs, shows a plasmon absorbance band at 584 nm and 591 nm, respectively.[14] The Cu(II)-micelle solution shows a distinct absorbance at 277 nm indicating ligand-metal charge transfer. The reduced Cu DENs show an absorbance peak at 591 nm which indicates that the Cu DENs had indeed formed. This absorbance peak is distinctly different than that of the Au DENs which have a more intense absorbance peak which appears at 533 nm. The UV-Vis spectra of the reduced bimetallic AuCu NPs show SPR bands, due to the presence of Au, in the range of 548 – 577 nm. The UV-Vis spectrum of the Au(III)-Cu(II)-micelle solution shows an absorbance at 323 nm, which can be assigned to the LMCT of the Au(III) ions. The expected absorbance of the Cu(II) which is present in much lower concentration

should be present near 280 nm, but this is masked by the absorbance peaks of the Au(III) (Figure 2.1). The bimetallic AuCu DENs show a SPR peak at 547 nm, indicating that the bimetallic DENs formed.

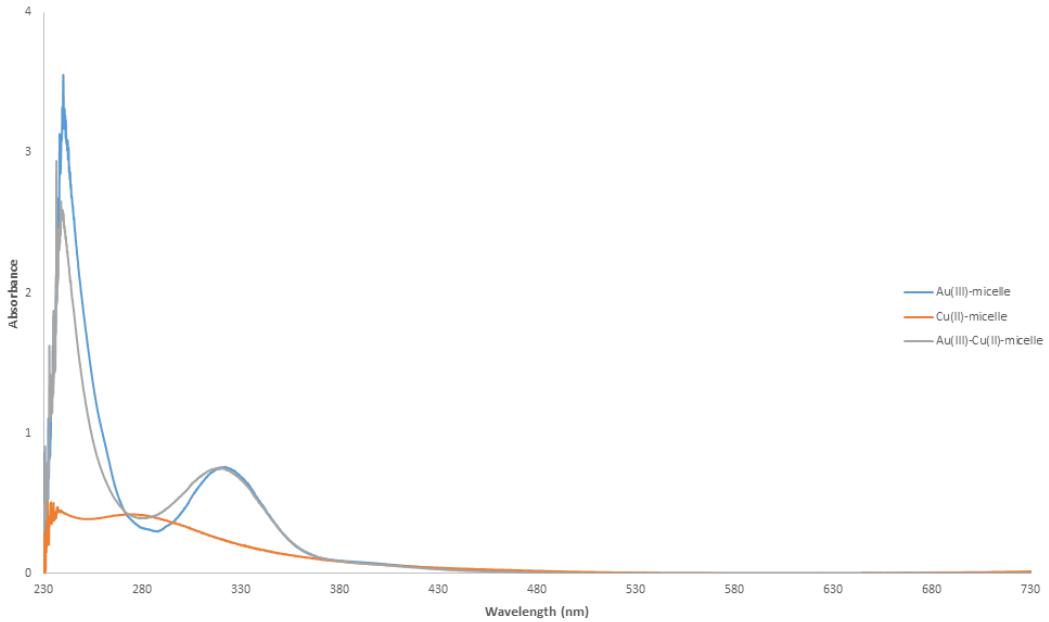

Figure 2.1 UV-Vis spectra of the M1-Au_{55}, M1-Cu_{55}, and M1-$Au_{42}Cu_{13}$ NPs.

This SPR peak differs from both that of the **M1**-Au_{55} and **M1**-Cu_{55} DENs which have SPR peaks at 533 nm and 591 nm, respectively (Figure 2.2). This is a clear indication of a different SPR compared to either of the monometallic DENs, however it is still more similar to that of the Au_{55} DENs due to the higher ratio of Au to Cu. Further confirmation of the formation of bimetallic DENs should become more evident once those with different ratios of Au:Cu are used, since the SPR peak at 548 nm should change accordingly.

A comparison of the UV-Vis spectra of the mono- and bimetallic NPs show distinct differences in their plasmon bands. These differences are attributable to clear differences in the composition of Au and Cu atoms which constitute the bimetallic NPs.

To ascertain whether or not the bimetallic alloyed NPs (as opposed to a mixture of two different monometallic NPs) had indeed formed during synthesis, separate solutions of the DAB-PPI G3 **M1**-Au and **M1**-Cu NPs were combined in a 3:1 ratio and analysed by means of UV-Vis spectroscopy (Figure 2.3). This would indicate any differences in the UV-Vis spectrum between the bimetallic Au-Cu DENs and the monometallic Au and Cu DENs by comparing the shapes of the respective SPR peaks and the wavelengths at which these peaks occur.

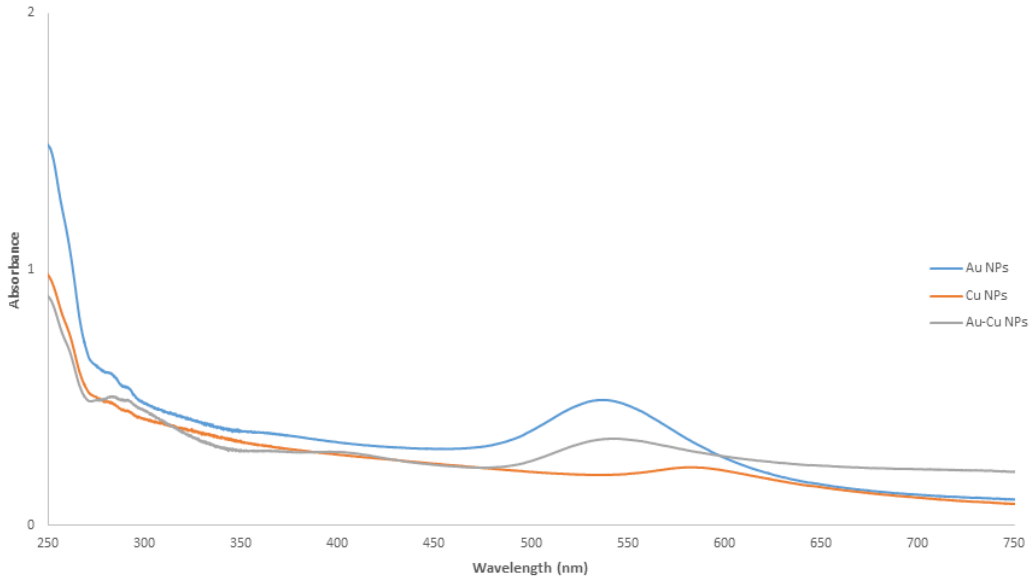

Figure 2.2 Overlay of the UV-Vis spectra of M1-Au_n, M1-Cu_n and M1-Au_nCu_m NPs showing the differences in the position and shape of the plasmon absorbance band.

The prepared bimetallic Au_nCu_m NPs show an absorbance peak at 548 nm and the mixture of monometallic NPs (Au-Cu mix) shows an absorbance at 543 nm. This latter peak arises mostly due to the presence of the Au NPs and its intensity is approximately three-quarters that of the Au_n NP sample, due to three-quarters of the metal in the NP being Au. The shape of the peak is also different to that of either the monometallic **M1**-Au_n, **M1**-Cu_n or bimetallic **M1**-Au_nCu_m NPs, since it is broader than the Au_n NPs and also follows the contour of the Cu_n NPs beyond 590 nm. It is also worth noting the similar absorbances around 408 nm. The mixture of monometallic NPs shows an absorbance peak at this wavelength, whereas the same, albeit fainter peak, is present for the bimetallic NPs. The comparative UV-Vis data would thus suggest that the prepared nanoparticles are bimetallic alloys and not a mixture of monometallic NPs.

The Au(III)-micelle solution of the **M2**-Au_n NPs shows an absorbance band at 325 nm resulting from the LMCT bands indicating that the Au(III) ions have coordinated to the tertiary amines inside the structure of the dendrimer micelle. The sample of Au DENs taken from the reduced reaction mixture shows a broad absorbance band at 556 nm, indicating that NPs larger than 2 nm in diameter had formed. The UV-Vis spectrum of the Cu(II)-micelle solution shows a distinct absorbance at 283 nm, an LMCT band, indicating that the Cu(II) ions have interacted with the tertiary amines inside the structure of the dendrimer micelle. The reduced Cu DENs show a weak absorbance peak at 584 nm which indicates that the Cu DENs had indeed formed.[11]

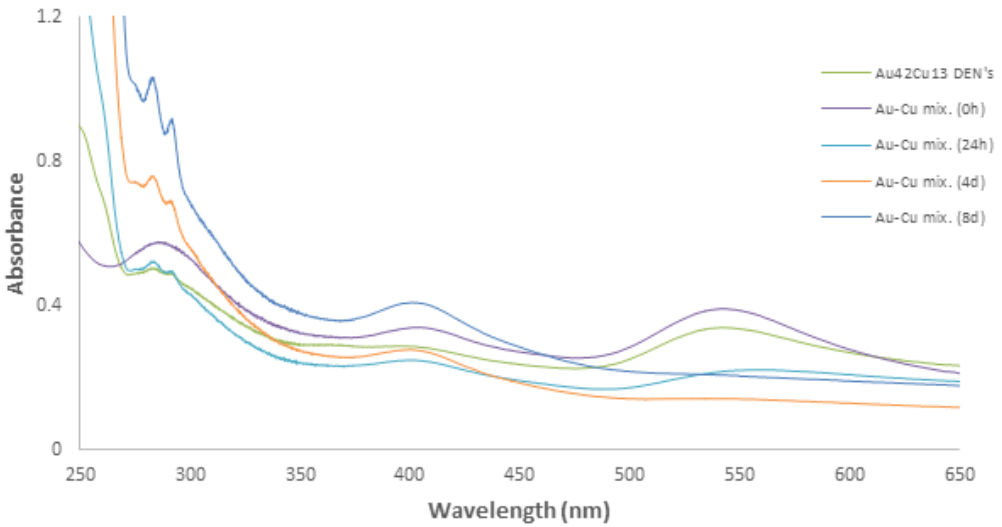

Figure 2.3 Overlay of the UV-Vis spectra of the prepared bimetallic M1-Au_nCu_n DENs and the 3:1 mixture of monometallic M1-Au_n and M1-Cu_n DENs.

The UV-Vis spectra of the Au(III) and Cu(II) ions in the micelle solution show an LMCT band at 323 nm for the Au and Cu. The bimetallic Au-Cu DENs show a SPR peak at 562 nm, indicating that the bimetallic DENs formed. This SPR peak differs from both that of the **M2**-Au_n and **M2**-Cu_n DENs which have SPR peaks at 556 nm and 584 nm, respectively. This is a clear indication of a different SPR compared to either of the monometallic DENs.

The Au(III)-micelle solution of the **M3**-Au_n NPs shows an absorbance at 324 nm resulting from the LMCT bands indicating that the Au(III) ions have interacted with the tertiary amines inside the structure of the dendrimer micelle. The sample of Au DENs taken from the reduced reaction mixture shows a broad absorbance at 547 nm, indicating that NPs larger than 2 nm in diameter had formed. The UV-Vis spectrum of the Cu(II)-micelle solution shows a distinct LMCT band at 276 nm indicating that the Cu(II) ions have coordinated to the tertiary amines inside the structure of the dendrimer micelle. The reduced Cu DENs shows a weak absorbance peak at 591 nm which indicates that the Cu DENs had formed.[11]

The UV-Vis spectra of the Au(III) and Cu(II) ions in the micelle solution shows an LMCT band at 325 nm for the Au(III) and Cu(II), respectively. The bimetallic Au-Cu DENs show a SPR peak at 560 nm, indicating that the bimetallic DENs formed. This SPR peak differs from both that of the **M3**-Au_{55} and **M3**-Cu_{55} DENs which have SPR peaks at 547 nm and 591 nm, respectively. This is a clear indication of a

different SPR peak compared to that of either of the monometallic DENs. The UV-Vis data has been tabulated in Table 2.1.

Table 2.1 LMCT and SPR values observed during UV-Vis analysis of the various mono- and bimetallic M1, M2, and M3 DENs

DENs	Au(III) LMCT band (nm)	Cu(II) LMCT band (nm)	SPR band (nm)
M1-Au	323	N/A	533
M1-Cu	N/A	297	588
M1-AuCu	319	-	545
M2-Au	352	N/A	556
M2-Cu	N/A	283	584
M2-AuCu	323	-	562
M3-Au	324	N/A	547
M3-Cu	N/A	276	591
M3-AuCu	325	-	560

The average size and size distribution of the mono- and bimetallic NPs were investigated by means of HR-TEM analysis. We initially set-out to synthesize nanoparticles consisting of 55 atoms, i.e. n = 55 in the case of **M1**-Au_n and **M1**-Cu_n, and n = 42, m = 13 for **M1**-Au_nCu_m. Figure 2.4 shows these HR-TEM results for the **M1** NP systems. The monometallic Cu NPs were found to have the smallest average diameter size and was also the most monodisperse of the NP systems analyzed (2.5 nm ± 0.8). On the other hand, the monometallic Au NPs displayed the largest average diameter size with a high degree of polydispersity (14.8 nm ± 12.5). In the case of the bimetallic Au-Cu NPs, intermediate average diameter sizes with relatively high polydispersity was observed (9.2 nm ± 7.1). The relatively large size of the prepared NPs led us to conclude that we had not formed NPs of 55 atoms that we initially set out to obtain. If this were the case, the average sizes of the NPs would be approximately 1.18 nm. Instead, the NPs that were synthesized were dendrimer stabilised nanoparticles (DSNs). [15]

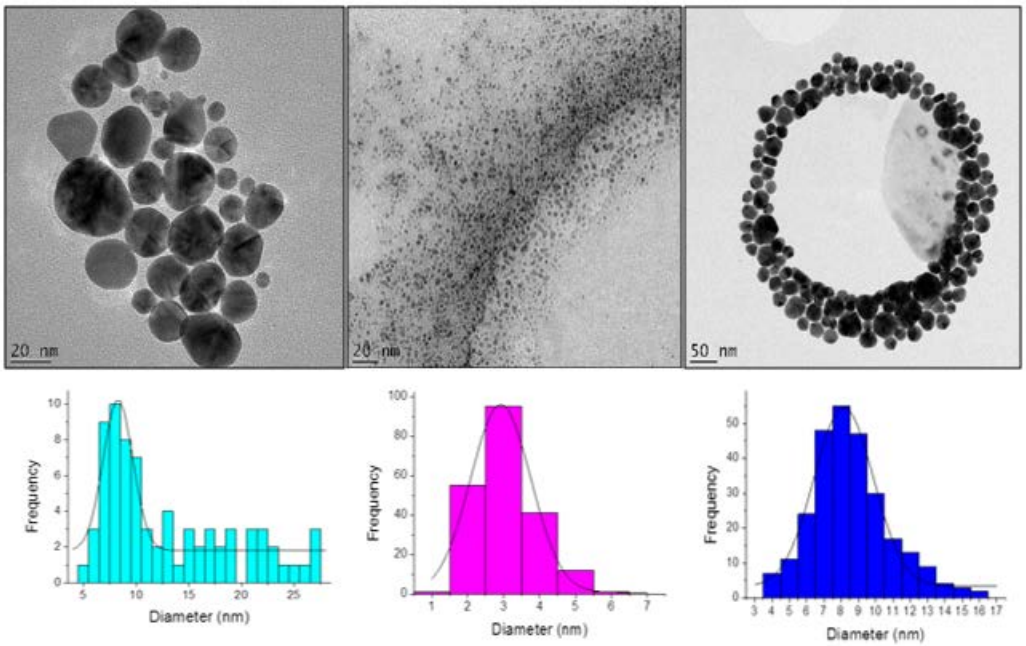

Figure 2.4 HR-TEM images and histograms representing the size distribution of the M1-Au (left), M1-Cu (centre), and M1-AuCu (right) DSNs.

The average sizes and size distributions of the **M2** NPs are summarized in Figure 2.5. The monometallic Au NPs had the greatest average diameter size and was also the most polydisperse of the NP systems analyzed (27.4 nm ± 11.2). The monometallic Cu DSNs showed the smallest average diameter size and was fairly monodisperse (2.3 nm ± 0.7). In the case of the bimetallic Au-Cu DSNs, intermediate average diameter sizes with a high polydispersity was observed (11.5 nm ± 12.1).

The average sizes and size distributions of the **M3** NPs are shown in Figure 2.6. The observed trend of the NP size and size distribution follow the same trend as seen with the **M1** and **M2** NP systems (Figures 2.4 and 2.5, Table 2.2). The monometallic **M3**-Au DSNs had the greatest average diameter size and are the most polydisperse of the NP systems (39.4 nm ± 16.0). The monometallic **M3**-Cu DSNs showed the smallest average diameter size and was fairly monodisperse (5.9 nm ± 3.5). In the case of the bimetallic **M3**-AuCu DSNs, intermediate average diameter sizes with a lower polydispersity was observed (12.8 nm ± 4.5).

The NPs that were prepared were monometallic Au DSNs with 77,000 Au atoms on average, monometallic Cu DSNs with 309 Cu atoms on average and bimetallic Au-Cu DSNs with approximately 18,000 Au and Cu atoms combined on average. Such large atom clusters would therefore imply that the NPs that were formed are too large to be encapsulated by the dendrimer micelle, but is instead stabilized

by it, i.e. DSN formation. [15] The bimetallic Au-Cu DSNs were often observed as rings or arcs (Figure 2.4). These shapes are believed to arise from interactions between the Au and Cu atoms in the bimetallic NPs.

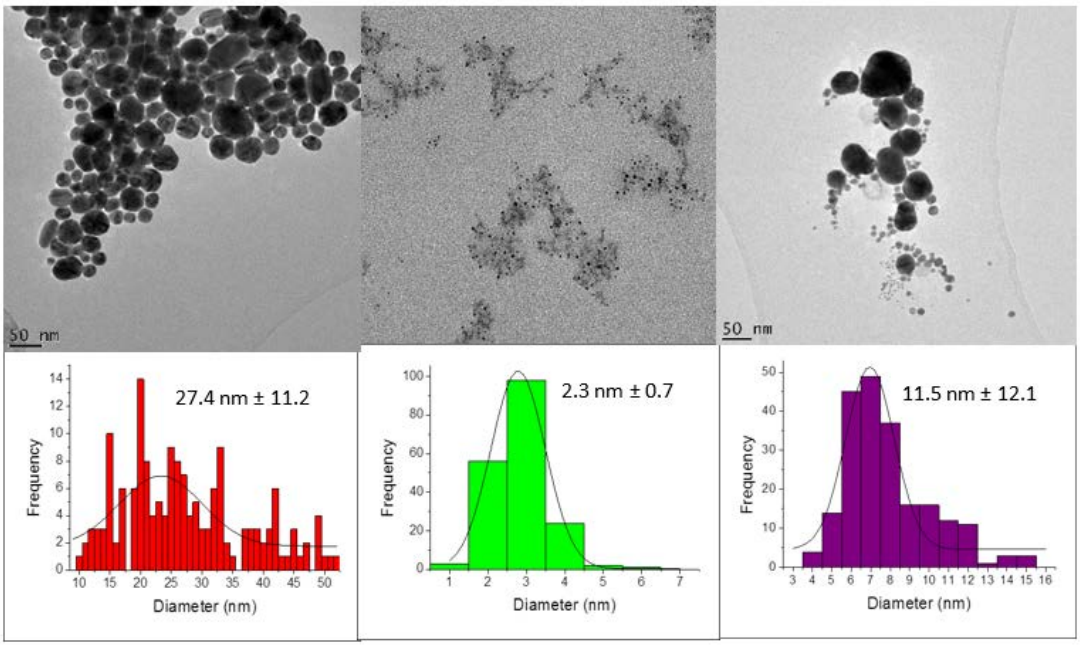

Figure 2.5 HR-TEM images and histograms representing the size distribution of the M2-Au (left), M2-Cu (centre), and M2-AuCu (right) DSNs.

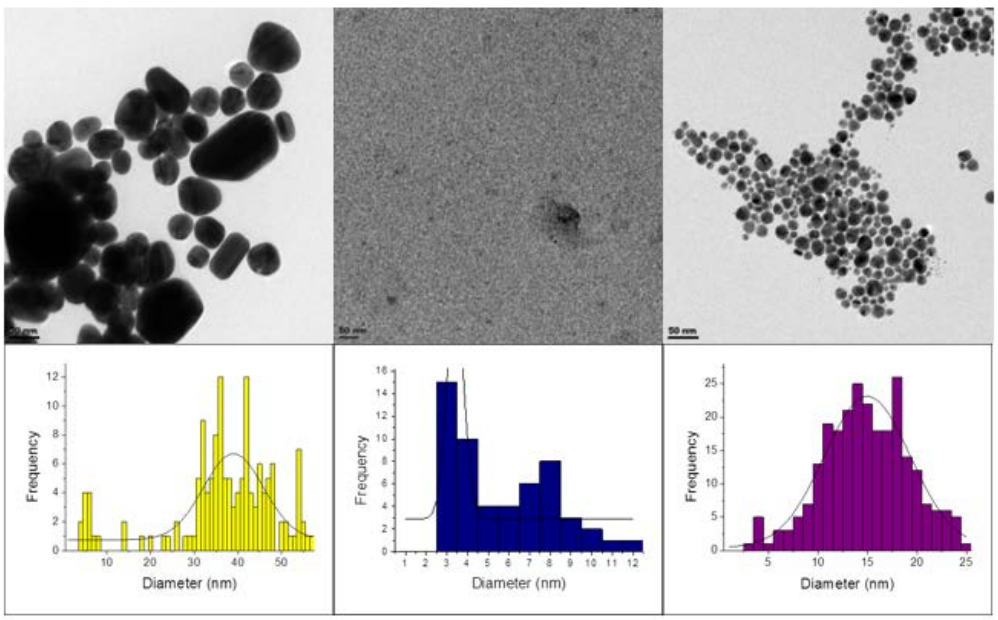

Figure 2.6 Histograms representing the size distribution of the M3-Au (left), M3-Cu (center), and M3-AuCu (right) NPs.

Table 2.2 List of the DSN sizes and polydispersity for the various M1, M2, and M3 DSNs

DENs	DEN sizes (nm)
M1-Au	14.8 ± 12.5
M1-Cu	2.5 ± 0.8
M1-AuCu	9.2 ± 7.1
M2-Au	27.4 ± 11.2
M2-Cu	2.3 ± 0.7
M2-AuCu	11.5 ± 12.1
M3-Au	39.4 ± 16.0
M3-Cu	5.9 ± 3.5
M3-AuCu	12.8 ± 4.5

Figure 2.7 shows the effect of micelle chain length on the average NP size. For the Au DSNs, a clear trend can be observed as the DSNs increase in size as the dendrimer micelle chain length decreases. This finding was consistent with what was expected based on the stabilizing effect that the peripheral alkyl chains would have on the NPs.

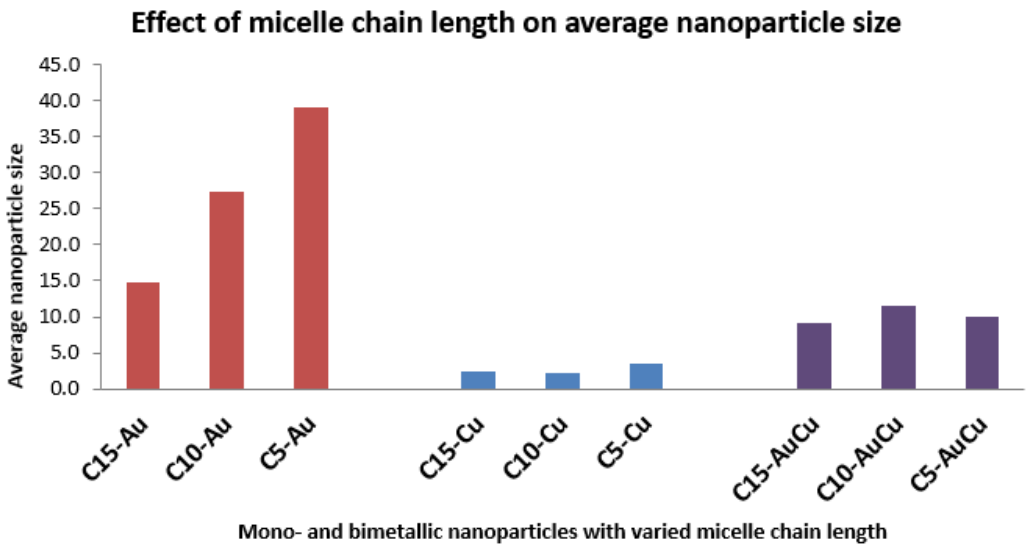

Figure 2.7 Graph of average DSN sizes as a function of micelle chain length.

The tendency of the longest dendrimer micelle chain lengths (**M1** NP systems) to generate some of the smallest NPs is due to the more effective stabilization of these longer chains of the DSNs because of the greater steric radius provided by these longer peripheral alkyl chains. The sizes of the Cu DSNs remain

largely similar throughout the range of dendrimer micelle chain lengths, yet showed a larger average NP size for the **M3** chain considering the size distribution of all these three different Cu nanoparticles. The average sizes of the bimetallic Au-Cu nanoparticles showed very similar sizes considering the average sizes as well as the size distributions.

In addition, the greater polydispersity of the monometallic Au DSNs is indicative of the fact that the Au DSNs are less stable than either the monometallic Cu or bimetallic Au-Cu DSNs.

2.3 Evaluation of DSNs in the Solvent-Free Oxidation of Styrene

The mono- and bimetallic DSN systems were evaluated as catalysts in the solvent-free oxidation of styrene at 70 °C with a metal loading of 0.025 mmol and 0.040 mmol H_2O_2 as oxidant. The metal content was kept constant for each different oxidation reaction, irrespective of the catalyst employed. The effect of time, metal loading, dendrimer micelle chain lengths, and different metals on activity and selectivity were examined. Our point of departure was a comparative study of reaction time: 3 h vs 16 h at 70 °C (Table 2.3). An increase in conversion was observed with an increase in reaction time, but the **M3**-Cu DSN was the only exception where a slight decrease was observed. At 16 h of reaction the **M1**-AuCu DSNs displayed superior activity to their monometallic **M1**-Au and **M1**-Cu counterparts, with a maximum conversion of 88 % observed for the **M1**-AuCu DSNs. It was observed that for each catalyst that the conversions were generally similar despite the difference in reaction time.

When considering the effect of micelle chain length, greater activity for the **M2** monometallic Au and Cu DSNs was observed as compared to their **M1** counterparts. This trend was not seen for the bimetallic Au-Cu DSNs where the activity decreased upon using the **M2** catalyst instead of the **M1** (Figure 2.8). This is in accordance with what we had expected to happen: the longest alkyl chain's superior stabilization of the nanoparticles would cause it to be more active than the nanoparticles stabilized by the shorter alkyl chains. The lowest activity was observed for the **M3** DSNs for all three different metal nanoparticles and this is due to the fact that the **M3** DSNs of the three different metal catalysts were larger than the **M1** and **M2** DSNs. After 16 h, the Au DSNs show the lowest conversion, because its average nanoparticle size is much greater than that of either the monometallic Cu or the bimetallic Au-Cu DSNs. This leads to a lower total surface area which can account for this lower conversion. The smaller average nanoparticle size of the

Cu and Au-Cu DSNs results in a much larger surface area of metal and thus more of the substrate can be converted.[16]

Table 2.3 Conversions observed for all DSNs applied to solvent-free styrene oxidation after 3 hours and 16 hours and with 0.025 mmol metal loading.

DEN	Conversion (%) after 3 h	Conversion (%) after 16 h
M1-Au	70.1	75.4
M1-Cu	66.2	77.0
M1-AuCu	69.9	88.1
M2-Au	73.4	78.3
M2-Cu	72.4	80.1
M2-AuCu	62.8	82.3
M3-Au	57.1	61.8
M3-Cu	65.8	65.0
M3-AuCu	60.4	67.0

Reaction conditions: Temperature = 70 °C, metal loading = 0.025 mmol; substrate = styrene (3 mL); oxidant = 30 % H_2O_2 (4.50 mL).

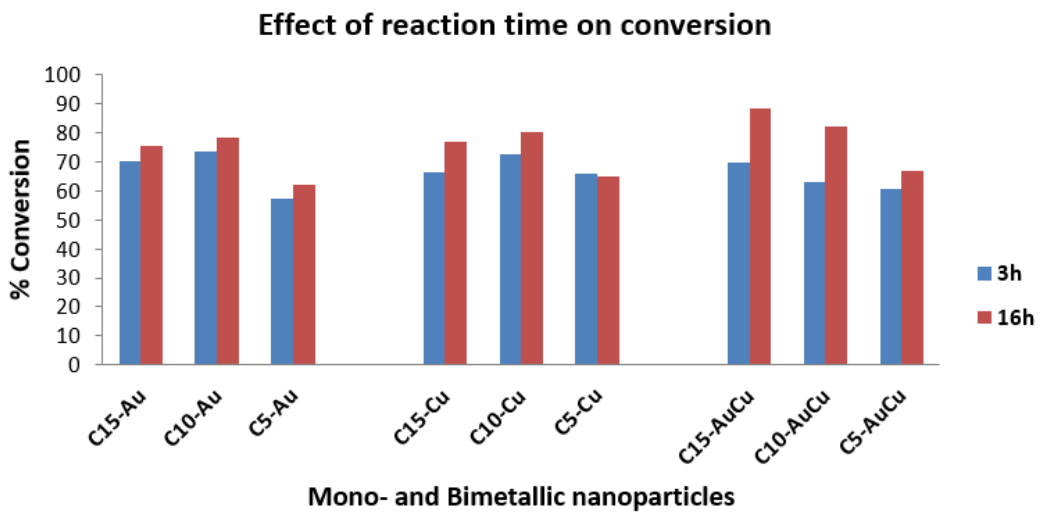

Figure 2.8 Effect of reaction time on the catalytic conversion of styrene.

The Au-Cu DSNs are believed to yield the highest conversions after 16 h due to the combined effects of both metals of the DSNs. Micelle chain length was found to further impact on catalysis by providing varying degrees of stabilisation to the nanoparticles (Figure 2.9). The longer micelle chain length provides greater stabilisation for the DSNs and thus less agglomeration is believed to occur during synthesis as well as catalysis. Less agglomeration results in smaller average nanoparticles sizes and larger metal particle surface area, and this effect is maintained during catalysis.

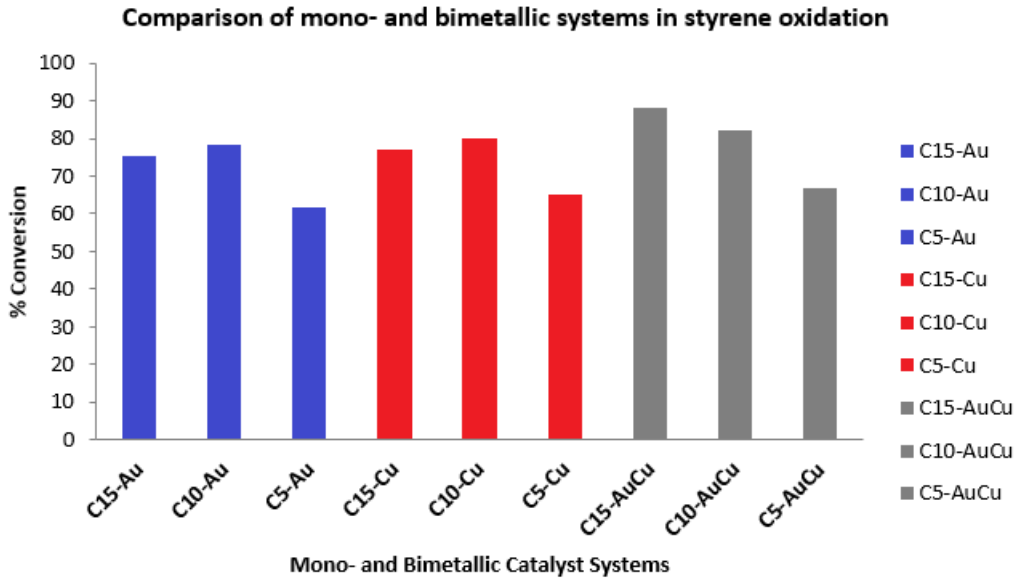

Figure 2.9 Comparison of mono- and bimetallic DSN systems in styrene oxidation.

The effect of metal loading was evaluated after 3 h and 16 h of reaction time (Figure 2.10). We observed a decrease in activity with increasing load for the Cu DSNs, but varying trends were observed for the Au and Au-Cu DSNs. Most of the differences between the lower and higher metal loads are relatively small and there were not generally significant differences in activity.

The oxidation of styrene showed selectivity towards benzaldehyde and styrene oxide (Figure 2.11). Benzaldehyde was the major product with it constituting at least 72 % and as high as 97 % of the products formed. Styrene oxide constituted the rest of the oxidation products and this formed in much smaller amounts than benzaldehyde, only being a maximum of 28 % of the converted product. This trend is in accordance to what has been reported by Nemanashi, *et al*. who also observed that benzaldehyde tended to be the favoured product over styrene oxide when using Au nanoparticles as catalysts for styrene oxidation. [17]

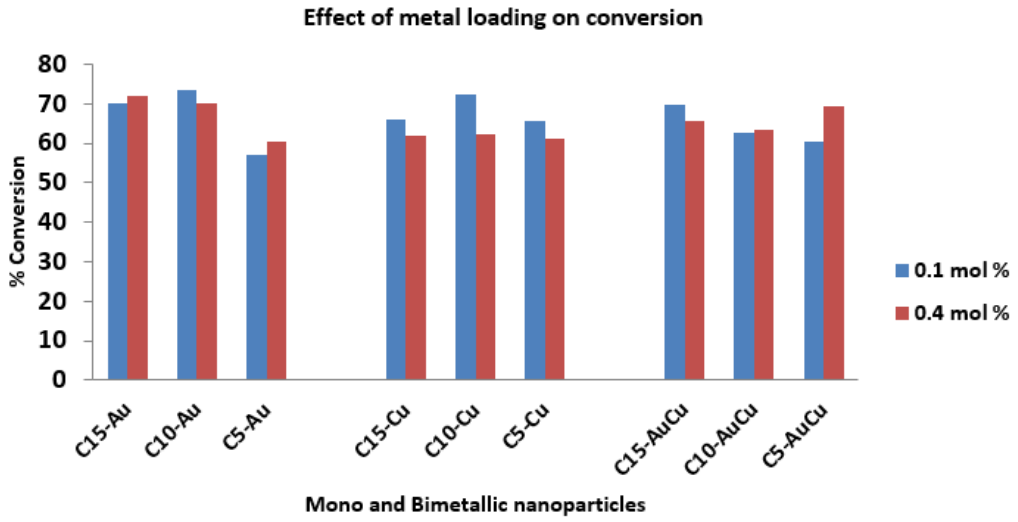

Figure 2.10 The effect of metal loading on the conversion of styrene.

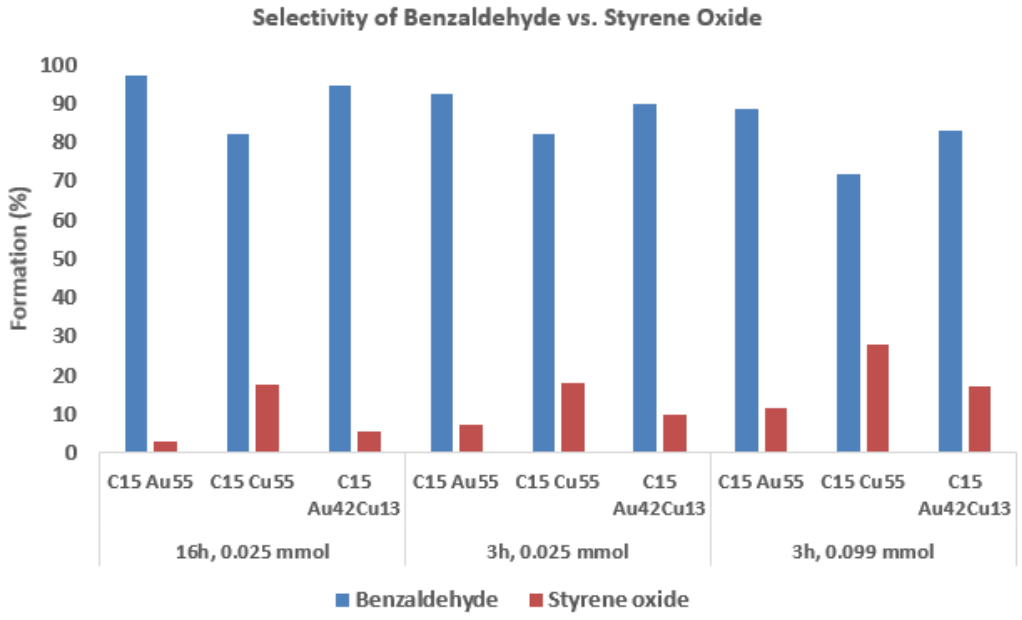

Figure 2.11 Selectivity of all M1 DSNs with metal loadings of 0.025 and 0.099 mmol and differences in time of 3 h and 16 h.

The Cu DSN systems showed the greatest selectivity towards styrene oxide regardless of the dendrimer micelle that was used. It was also consistently observed that the bimetallic Au-Cu DSN systems had higher selectivity towards styrene oxide than the Au DSN systems

which showed the lowest selectivity towards styrene oxide. It was also found that increasing the load of the catalyst caused an increase in formation of styrene oxide.

2.4 Conclusions

Dendrimer micelles with varying alkyl chain lengths (**M1**, **M2**, **M3**) have been successfully synthesized, and subsequently used as templates and stabilizers for the synthesis of dendrimer stabilized nanoparticles (DSNs). Both mono- and bimetallic DSNs were prepared and it was found that the length of the peripheral alkyl chain of the dendrimer micelle had a direct influence on the average nanoparticle size obtained. These DSNs were then evaluated in the catalytic oxidation of styrene, using H_2O_2 as oxidant. It was observed that the bimetallic nanoparticles showed a higher conversion towards styrene oxidation products, benzaldehyde and styrene oxide, than the monometallic nanoparticles at optimal reaction conditions. Greater conversion was observed for longer dendrimer micelle chain nanoreactors (**M1**) due to the stabilisation that it provided compared to the shorter micelle chain length catalytic systems (**M3**). In terms of catalytic activity, the bimetallic DSNs resulted in the highest styrene conversion, followed by the monometallic Cu DSNs, with the monometallic Au DSNs exhibiting the lowest conversion. Comparing the effect of alkyl chain length, the **M3** DSNs showed the lowest conversion, whereas conversion increased when using the **M2** DSNs systems. For the monometallic **M1** Au and Cu DSNs, a decrease in conversion was observed. The bimetallic **M1** DSNs, however, showed an increase in conversion. The bimetallic nanoparticles displayed a superior activity when compared to its monometallic analogues under the same reaction conditions.

2.5 Experimental Section

2.5.1 General considerations

All chemical transformations were performed under ambient conditions, unless otherwise stated. All commercially available reagents were used as received. Solvents were dried by refluxing over the appropriate drying agents followed by distillation prior to use and all other

reagents were employed as obtained. NMR (^{1}H: 300 and 400 MHz; ^{13}C: 75 and 100 MHz) spectra were recorded on Varian VNMRS 300 MHz; Varian Unity Inova 400 MHz spectrometers and chemical shifts were reported in ppm, referenced to the residual protons of the deuterated solvents and tetramethyl silane (TMS) as internal standard. FT-IR analysis was performed on a Thermo Nicolet AVATAR 330 instrument, and spectra were recorded neat (ATR) unless otherwise specified. UV-Vis analysis was performed on a GBC UV-Vis 920 instrument. TEM analysis was performed on a FEI Tecnai G^2 Field Emission Gun (FEG) TEM operating at 200 kV and having a 2.5 Å point-to-point resolution, 1.02 Å line resolution and 1.4 Å information limit. GC analysis was performed on a Varian 3900 instrument with an Agilent Technologies 50 m × 0.21 mm × 0.5 μm column, using p-xylene as reference.

2.5.2 Synthesis of dendrimer micelles (M1 – M3)

The C_{15} (**M1**), C_{11} (**M2**) and C_5 (**M3**) dendrimer micelles were prepared according to a previously reported literature procedure.[10]

2.5.2.1 Synthesis of **M1** dendrimer micelle

DAB G3 PPI (0.469 g, 0.282 mmol) was added to a RBF, dissolved in THF (25 ml), and set to stir. After the DAB G3 PPI had dissolved, triethylamine (5 ml, 35.85 mmol) was added to the clear solution. Thereafter, palmitoyl chloride (1.35 ml, 4.45 mmol) was added and the reaction mixture subsequently turned white. The solution was left to stir at room temperature for 52 hours. After the 52 hours had elapsed, the reaction mixture was filtered and washed with cold THF (20 ml). The white crystals obtained after filtration was transferred to a RBF, diethyl ether (30 ml) was added, and set to reflux for at 70 °C for 30 minutes. Following reflux, the reaction mixture was left to cool, then filtered and washed with cold diethyl ether (20 ml). The white crystals obtained were added to a RBF and aqueous Na_2CO_3 solution (0.449 g, 4.233 mmol in 50 ml H_2O) was added. This mixture was left to reflux at 90 °C for 16 hours. The mixture was filtered and washed with cold H_2O. The product was obtained as white crystals following filtration and it was dried overnight at 60 °C (0.3509 g, 0.0640 mmol, 22.7 %). The product was characterized with FT-IR and ^{1}H- and ^{13}C NMR.

FTIR: 3288.50 cm^{-1} (amide N-H stretch), 3080.17 cm^{-1} (amide N-H stretch), 2915.35 cm^{-1} (saturated C-H), 1638.9 cm^{-1} (amide carbonyl), and 1549.01 cm^{-1} (N-H bend). ^{1}H NMR (300 MHz, $CDCl_3$) δ 7.16 (s), 3.26 (d, J = 5.9 Hz), 2.23 (dd, J = 36.6, 29.2 Hz), 1.77 (s), 1.77 – 0.64 (m), 0.80 – 0.52 (m). ^{13}C NMR (75 MHz, $CDCl_3$) δ 173.93 (s), 77.16 (s), 76.74 (s), 52.36 (s), 51.59 (s), 37.93 (s), 36.84 (s), 32.10 (s), 30.05 – 29.41 (m), 27.29 (s), 26.16 (s), 22.86 (s), 14.28 (s).

2.5.2.2 Synthesis of **M2** dendrimer micelle

DAB G3 PPI (0.246 g, 0.148 mmol) was added to a RBF, dissolved in THF (25 ml), and set to stir. After the DAB G3 PPI had dissolved, triethylamine (3 ml, 21.509 mmol) was added to the clear solution. Thereafter, lauroyl chloride (0.564 ml, 2.377 mmol) was added to the reaction mixture and it subsequently turned white. The solution was left to stir for 72 hours at room temperature. After the 72 hours had elapsed, the reaction mixture was filtered and washed with cold THF (20 ml). The solid, white product was transferred to a RBF, diethyl ether (30 ml) was added and subsequently set to reflux at 70 °C for one hour. The reaction mixture was left to cool, then filtered and washed with cold diethyl ether (20 ml). The white crystals were transferred to a RBF and aqueous solution of Na_2CO_3 (0.501 g, 4.727 mmol) in H_2O (50 ml) was added. This mixture was left to reflux for 22 hours at 90 °C. After the time had elapsed, the mixture was filtered and washed with cold H_2O. The product was obtained as pale white crystals. The product was characterized with FT-IR and ^{1}H- and ^{13}C NMR.

FTIR: 3296.55 cm^{-1} (amide N-H stretch), 3080.17 cm^{-1} (amide N-H stretch), 2916.01 cm^{-1} (saturated C-H), 1634.83 cm^{-1} (amide carbonyl), and 1548.96 cm^{-1} (N-H bend). ^{1}H NMR (300 MHz, $CDCl_3$) δ 7.28 (d, J = 0.8 Hz), 3.28 (s), 2.40 (s), 2.30 – 2.00 (m), 1.61 (d, J = 12.0 Hz), 1.27 (s), 0.90 (t, J = 6.7 Hz). ^{13}C NMR (75 MHz, $CDCl_3$) δ 173.91 (s), 77.75 – 76.99 (m), 76.74 (s), 52.65 – 51.18 (m), 36.84 (s), 32.09 (s), 30.10 – 29.41 (m), 27.54 – 26.95 (m), 26.15 (s), 22.86 (s), 14.28 (s).

2.5.2.3 Synthesis of **M3** dendrimer micelle

DAB G3 PPI (0.396 g, 0.238 mmol) was added to a RBF, dissolved in THF (25 ml), and set to stir. After the DAB G3 PPI had dissolved, triethylamine (3 ml, 21.509 mmol) was added to the clear solution. Thereafter, hexanoyl chloride (0.57 ml, 4.510 mmol) was added to the reaction mixture and it subsequently turned white. The solution was left to stir for four days at room temperature. After four days had elapsed, the solvent was removed under vacuum. The oily, light orange product was transferred to a RBF, diethyl ether (30 ml) was added and subsequently set to reflux at 70 °C for one hour. The diethyl; ether was removed under vacuum. A solution of Na_2CO_3 (0.501 g, 4.727 mmol) in H_2O (50 ml) was added to the light orange oil. This mixture was left to reflux for 24 hours at 90°C. After this time had elapsed, chloroform (25 ml) was added to separate the product from the aqueous layer, which was then extracted and the chloroform was removed under vacuum. The product was obtained as a viscous, sticky, light orange oil. The product was characterized with FT-IR and ^{1}H- and ^{13}C NMR.

FTIR: 3285.955cm^{-1} (amide N-H stretch), 3074.64 cm^{-1} (amide N-H stretch), 2927.80 cm^{-1} (saturated C-H), 1632.04 cm^{-1} (amide carbonyl), and 1548.75 cm^{-1} (N-H bend). ^{1}H NMR (300 MHz, $CDCl_3$) δ 7.29 – 6.96 (m), 3.25 (d, *J* = 5.8 Hz), 2.69 (s), 2.24 (dt, *J* = 7.8, 4.8 Hz), 1.89 – 1.22 (m), 1.22 – 1.04 (m), 0.87 (t, *J* = 6.8 Hz), 0.05 (s). ^{13}C NMR (75 MHz, $CDCl_3$) δ 173.89 (s), 77.75 – 77.03 (m), 76.74 (s), 51.96 (d, *J* = 45.2 Hz), 51.50 – 51.06 (m), 37.98 (s), 36.73 (s), 31.69 (s), 31.05 (s), 29.95 – 29.68 (m), 27.12 (s), 25.74 (s), 24.66 (s), 22.58 (s), 14.12 (s).

2.5.3 Synthesis of mono- and bimetallic DSNs with dendrimer micelle **M1**

2.5.3.1 Synthesis of **M1**-Au_n DSNs

To a stirring solution of the **M1** dendrimer micelle (0.0502 g, 0.00916 mmol) in chloroform (100 ml) was added $HAuCl_4$ (0.170 g, 0.501 mmol). To the resulting bright yellow solution was added a solution of $NaBH_4$ (0.0497 g, 1.314 mmol) in methanol (1 ml). The addition of the reducing agent resulted in the formation of a deep-purple solution which was stirred for one hour. UV-Vis analysis was employed to monitor the reaction prior to and after reduction. Before reduction: λ_{max} 240 and 231 nm (LMCT). After reduction: λ_{max} 533 nm (SPR peak).

2.5.3.2 Synthesis of **M1**-Cu_n DSNs

To a stirring solution of the **M1** dendrimer micelle (0.0502 g, 0.00916 mmol) in chloroform (100 ml) was added a solution of $CuCl_2$ (0.0668 g, 0.497 mmol) in methanol (0.6 ml). To the resulting bright yellow solution was added a solution of $NaBH_4$ (0.0497 g, 1.314 mmol) in methanol (1 ml). The addition of the reducing agent resulted in the formation of a brown which was stirred for one hour. UV-Vis analysis before reduction: λ_{max} 277 nm (LMCT). UV-Vis analysis after reduction: λ_{max} 591 nm.

2.5.3.3 Synthesis of **M1**-Au_nCu_m DSNs

To a stirring solution of the **M1** dendrimer micelle (0.0502 g, 0.00916 mmol) in chloroform (100 ml) was added a solution of $HAuCl_4$ (0.1513 g, 0.3842 mmol) and $CuCl_2$ (0.0202 g, 0.1185 mmol) in methanol (0.3 ml) under an inert atmosphere. The resulting bright yellow solution was stirred for 1 hour. After the allotted time, a solution of $NaBH_4$ (0.0602 g, 1.591 mmol) in methanol (1 ml) was added to the metal-micelle solution. A colour change from bright-yellow to dark purple-brown was observed. UV-Vis analysis before reduction: λ_{max} 322 and 240 nm (LMCT to Au). LMCT to Cu not observed. UV-Vis analysis after reduction: λ_{max} 548 nm (SPR).

2.5.4 Synthesis of mono- and bimetallic DSNs with dendrimer micelle **M2**.

2.5.4.1 Synthesis of **M2**-Au_n DSNs

The same synthetic procedure as outlined above for **M1**-Au_n DSNs was employed for the synthesis of **M2**-Au_n DSNs, using the **M2** dendrimer micelle (0.0401 g, 0.00920 mmol) as a stabilizer. UV-Vis analysis before reduction: λ_{max} 323 and 240 nm (LMCT). UV-Vis analysis after reduction: λ_{max} 555 nm (SPR).

2.5.4.2 Synthesis of **M2**-Cu_n DSNs

The same synthetic procedure as outlined above for the **M1**-Cu_n DSNs was employed for the synthesis of **M2**-Cu_n DENs, using the **M2** dendrimer micelle (0.0399 g, 0.00916 mmol) as a stabilizer. UV-Vis analysis before reduction: λ_{max} 283 nm (LMCT). UV-Vis analysis after reduction: λ_{max} 577 nm.

2.5.4.3 Synthesis of **M2**-Au_nCu_m DSNs

The same synthetic procedure as outlined above for **M1**-Au_nCu_m DSNs was employed for the synthesis of **M2**-Au_nCu_m DSNs, using the **M2** dendrimer micelle (0.0391 g, 0.00897 mmol) as a stabilizer. UV-Vis analysis before reduction: λ_{max} 324 and 240 nm (LMCT to Au). LMCT to Cu not observed. UV-Vis analysis after reduction: λ_{max} 577 and 303 nm.

2.5.5 Synthesis of mono- and bimetallic DENs with dendrimer micelle **M3**

2.5.5.1 Synthesis of **M3**-Au_n DSNs

The same synthetic procedure as outlined above for **M1-Au_n** DSNs was employed for the synthesis of **M3**-Au_n DSNs, using the **M3** dendrimer micelle (0.0296 g, 0.00915 mmol) as a stabilizer. UV-Vis analysis before reduction: λ_{max} 324 and 240 nm (LMCT). UV-Vis analysis after reduction: λ_{max} 552 nm (SPR).

2.5.5.2 Synthesis of **M3**-Cu_n DSNs

The same synthetic procedure as outlined above for **M1-Cu_n** DSNs was employed for the synthesis of **M3**-Cu_n DSNs, using the **M3** dendrimer micelle (0.0291 g, 0.00899 mmol) as a stabilizer. UV-Vis analysis before reduction: λ_{max} 276 nm (LMCT). UV-Vis analysis after reduction: No λ_{max} observed.

2.5.5.3 Synthesis of **M3**-Au_nCu_m DSNs

The same synthetic procedure as outlined above for **M1-Au_nCu_m** DSNs was employed for the UV-Vis as a stabilizer. UV-Vis analysis before reduction: λ_{max} 330 and 240 nm (LMCT to Au). LMCT to Cu not observed. UV-Vis analysis after reduction: λ_{max} 560 nm.

2.5.6 Catalytic styrene oxidation

2.5.6.1 General procedure for catalytic oxidation of styrene

For a typical solvent-free oxidation reaction procedure, styrene (3 ml, 2.718 g, 0.026 mol), H_2O_2 (4.5 ml, 30 wt %, 1.35 g, 0.040 mol), and various DENs were refluxed at 70 °C for either three or sixteen hours. Metal loadings of 0.025, 0.050 and 0.099 mmol were evaluated. After the allotted time had elapsed, the organic layer was extracted and filtered. The filtrate was analysed by GC-FID using p-xylene as internal standard to determine styrene conversion and selectivity.

2.6 References

1. Klajnert, B.; Bryszewska, M., *Acta Biochimica Polonica*, 2001, **48**, 199-208.
2. Myers, V. S.; Weir, M. G.; Carino, E. V.; Yancey, D. F.; Pande, S.; Crooks, R. M., *Chem. Sci.*, 2011, **2**, 1632-1646.
3. Chung, Y. M.; Rhee, H. K., *J. Colloidal Interface Sci.*, 2004, **271**, 131-135.
4. Wang, C.; Zhu, G.; Li, J.; Cai, X.; Wei, Y.; Zhang, D., Qiu, S., *Chem. Eur. J.*, 2005, **11**, 4975-4982.
5. Endo, T., Kuno, T., Yoshimura, T., & Esumi, K., *J. Nanosci. Nanotechnol.*, 2005, **5**, 1875-1882.
6. Peng, X.; Pan, Q.; Rempel, G. L, *Chem. Soc. Rev.*, 2008, **37**, 1619-1628.
7. Andrés, R.; de Jesus, E.; Flores, J. C., *New J. Chem.*, 2007, **31**, 1161-1191.
8. Crooks, R. M.; Zhao, M.; Sun, L.; Chechik, V.; Yeung, L. K., *Acc. Chem. Res.*, 2001, **34**, 181-190.
9. Niu, Y.; Crooks, R. M., 2003, **6**, 1049-1059.
10. Stevelmans, E. W. M. S.; van Herst, J. C. M.; Jansen, J. F. G. A.; van Boxtel, D. A. F. J.; de Brabander-van den Berg, E. M. M., *J. Am. Chem. Soc.*, 1996, **7863**, 7398-7399.
11. (a) R. M. Crooks, M. Zhao, L. Sun, V. Chechik and L. K. Yeung, *Acc. Chem. Res.*, 2001, **34**, 181-190; (b) M. Zhao and R. M. Crooks, *Chem. Mater.*, 1999, **11**, 3379-3385.
12. M.V. Sujitha, S. Kannan, *Spectrochimica Acta Part A: Molecular and Biomolecular Spectroscopy*, 2013, **102**, 15-23.
13. (a) M.-C. Daniel, D. Astruc, *Chem. Rev.*, 2004, **104**, 293–346; (b) S. Eustis, M. A. El-Sayed, *Chem. Soc. Rev.*, 2006, **35**, 209–217; (c) M. E. Stewart, C. R. Anderton, L. B. Thompson, J. Maria, S. K. Gray, J. A. Rogers, R. G. Nuzzo, *Chem. Rev.*, 2008, **108**, 494–521; (d) A. Llevot, D. Astruc, *Chem. Soc. Rev.* 2012, **41**, 242–257; (e) C. Louis, O. Pluchery, *Gold Nanoparticles for Physics, Chemistry, Biology*, Imperial College, London, 2012; (f) N. Li, P. Zhao, D. Astruc, *Angew. Chem. Int. Ed.*, 2014, **53**, 1756–1789.

14. (a) A. C. Curtis, D. G. Duff, P. P. Edwards, D. A. Jefferson, B. F. G. Johnson, A. I. Kirkland and A. S. Wallace, *Angew. Chem., Int. Ed. Engl.*, 1988, **27**, 1530–1533; (b) M. P. Pileni and I. Lisiecki, *Colloids Surf., A*, 1993, **80**, 63–68.

15. N. Krasteva, B. Guse, I. Besnard, A. Yasuda, T. Vossmeyer, *Sens. and Act. B*, 2003, **92**, 137-143.

16. N. Linares, C. P. Canlas, J. Garcia-Martinez and T. J. Pinnavaia, *Catal. Commun.*, 2014, **44**, 50-53.

17. M. Nemanashi, R. Meijboom, *Catal. Lett.*, 2013, **143**, 324-332.

CHAPTER 3

Synthesis methods applied for mono- and bimetallic gold-copper dendrimer-stabilised nanoparticles

3.1 Introduction

In Chapter 2, the synthesis of the Au and Cu monometallic and bimetallic Au-Cu dendrimer-stabilised nanoparticles (DSNs) was reported. The bimetallic NPs that was initially set out to prepare were $Au_{42}Cu_{13}$, where the entire NP is a closed-shell cluster of 55 atoms – approximately 42 being Au and the remaining 13 being Cu. However, HR-TEM analysis showed that the NPs that formed were much larger than a cluster of 55 atoms. In the case of Au_{55}, the bimetallic NPs should only have been approximately 1.4 nm in diameter, but our results showed that their diameters were 12.8 nm on average. This indicated that we did not make $Au_{42}Cu_{13}$ bimetallic NPs, but rather larger DSNs with a Au-to-Cu ratio of 3:1.

The template method was sufficient for preparing mono- and bimetallic DSNs, however, it was difficult to control the NP size very effectively. Other researchers have reported that the template method was very effective for their ends of preparing mono- or bimetallic NPs, regardless of whether the desired NP size was only a few atoms or several hundred. [1–3] Since the template method follows two steps in order to synthesise the NPs, we decided to focus our efforts on one of these two steps in order to gain better control over the NP size. [1] In the first step, the appropriate metal ions, Au(III) and Cu(II), in our case, are mixed with the dendrimer template. This will allow specific stoichiometric amounts of these metal ions to interact with the interior structure of the dendrimer. [4–6] The second step requires the subsequent reduction of the metal ions with an appropriate reducing agent (Scheme 3.1). Some authors have reported the use of reducing agents that also act as stabilisers, including citric and ascorbic acid amongst others. However, our method only required the use of a $NaBH_4$ solution since the dendrimer micelle was already present as a stabiliser for any newly-formed NPs.[7,8]

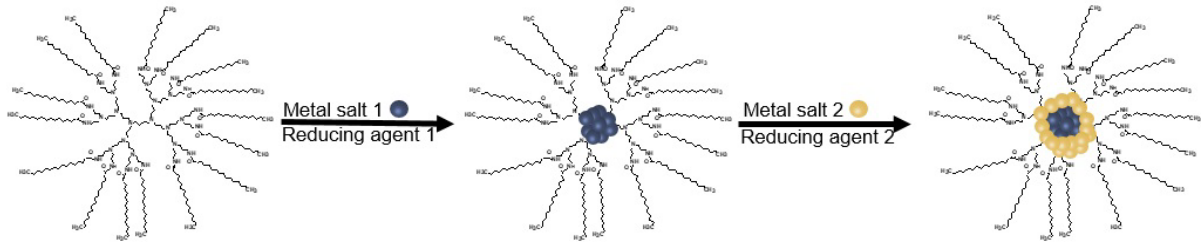

Scheme 3.1 Example of a template method in which two metals are reduced in subsequent order to form bimetallic NPs. [9]

Since our specific template method for the synthesis of DENs requires a solution of $NaBH_4$ for reduction of the metal ions, we decided to focus our efforts on the optimisation of this step. We chose this since it is the more critical of the two steps in the NP formation and it allowed us to alter various parameters such as the concentration of the reducing agent and the rate at which the solution is added to the reaction mixture.

Our previous method's reduction step simply required that the appropriate amount of the $NaBH_4$ reducing agent be dissolved in methanol and this mixture was quickly added to the reaction mixture. This mixture consisted of either Au^{3+} or Cu^{2+} metal ions in the presence of the dendrimer micelles to prepare monometallic DENs. Conversely, both Au^{3+} and Cu^{2+} were present in the mixture with the dendrimer micelles to prepare the bimetallic DENs. Once the reducing agent was added, we were able to confirm by means of observation and analyses that the various mono- and bimetallic NPs had formed based on the stoichiometric amount of each metal salt used. [10,11] Although analysis with HR-TEM confirmed the presence of the NPs, it also indicated that these NPs were much larger than what we had hoped to obtained: 9.2 nm ± 7.1 for the bimetallic NPs and 14.8 nm ± 12.5 and 2.5 nm ± 0.8 for the monometallic Au and Cu NPs, respectively. [1,10]

Throughout the process of attempting to find a more controllable reduction method for producing NPs with controlled sizes, we altered the concentration and volume of the $NaBH_4$-methanol solution as well as the rate at which it was added to the reaction mixture of metal salts and dendrimer micelles. Continued attempts eventually led us to obtain a method that allowed us to consistently produce NPs of similar sizes, even though they were larger than expected due to the metal ratio and concentration of the metal precursors. [1,3,10] Hence our synthetic method was reproducible.

Many reported instances have shown that when NPs are synthesised in the presence of a dendrimer to form DENs, the NP sizes are uniform and relatively monodispersed. [12] HR-TEM analysis indicated that neither of the mono- nor bimetallic NPs were sufficiently small to be encapsulated within the dendrimer interior which is commonly referred to as DENs. A factor believed to contribute to the difference of NP sizes is that we used relatively small, 3rd generation (G3) dendrimers, whereas the afore-mentioned researchers used higher dendrimer generations – at least from the 4th generation up to the 6th generation (G4 – G6). [1,3,12] The G3 DAB-PPI dendrimers that we used were not able to encapsulate the NPs or stabilise all the metal surfaces of the NPs. As a result of these unstabilized surfaces, the NPs were still relatively free to agglomerate, resulting in their larger sizes.

The method that we used in an attempt to synthesise DENs was not successful; instead it led to the formation of dendrimer stabilised nanoparticles (DSNs) as shown in Figure 3.1. Although the average NP sizes were still larger than expected, we know that some differences in the reaction conditions such as dendrimer type and generation and solvent hydrophilicity played a significant role. [1,3,10]

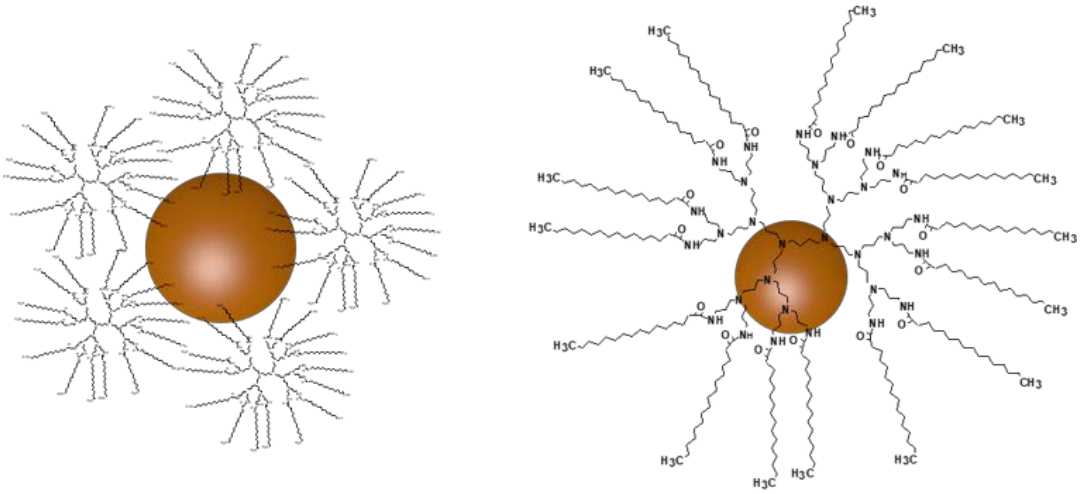

Figure 3.1 Structure of DSN (left) and DEN (right). [13]

Various authors have reported that dendrimers possess several advantages based on their structural and chemical properties. Many of these advantages can be utilised advantageously for catalysis. The templates of these dendrimers contribute to the formation of well-defined nanoparticles with uniform compositions and structures. The dendrimers are also believed to inhibit the agglomeration of NPs during catalysis due to their stabilising effect. Dendrimers' branches are also able to be controlled selectively, thus controlling the access that

substrates might have to the NPs. Another important feature is that the peripheries can also be modified in order to control the solubility of the DENs (Figure 3.2). [3,12,14]

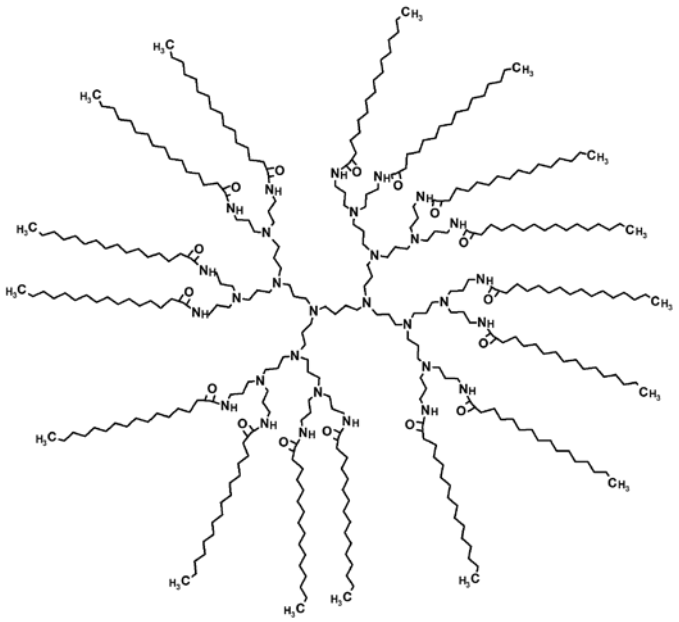

Figure 3.2 Representation of a 3rd generation DAB-PPI dendrimer modified with alkyl chains on the peripheries to form a dendrimer micelle.

The dendrimer interior can serve as a template in the preparation of dendrimer encapsulated NPs to control the size of NPs and to passivate the NP surface. [3] Passivating the NP surface is required to prevent seeding that leads to agglomeration, but when seeding does occur, the nanoclusters formed will not be isotropic, thereby forming nanoclusters with irregular shapes. [11,15] Because the NPs used for catalysis should be prepared with consistent sizes, this is usually done by reducing a metal salt in the presence of a stabilizer. These stabilizers may include either dendrimers, ligands, or surfactants amongst others. The stabilizers are used to inhibit agglomeration by passivating the surface, however, since these NPs are to be used for catalysis it must not be completely passivated. If this were to happen, the entire NP surface would be covered with the stabilizer and subsequently there would be no open, active sites for the substrate to access. [3,16,17]

Utilising dendrimers of different generations can be helpful in order to control the rate at which catalysis occurs. This is due to dendrimers' generation-dependent dendrimer porosity which means that higher generation dendrimers are less porous (and more sterically hindered) than lower generation dendrimers. If they are less porous, it will result in the dendrimer being less likely to allow substrates to access the interior where the NPs are encapsulated. This will

effectively result in the dendrimer acting as a selective filter to control the rate at which catalysis occurs. [18–20]

Despite the positive attributes of DENs, particularly with regard to the dendrimer stabilisers, which makes it well-suited for use as catalysts, there are two challenges that need to be overcome. Firstly, the NPs must be stabilised in such a way that agglomeration can be overcome, yet the active sites of the NPs must not be blocked and prevent the substrate from reaching the NP surface. Secondly, since the size, size distribution, and NP shape are influenced by the dendrimer being used as a stabiliser, it would be beneficial to gain an understanding as to how the dendrimers influence these parameters, especially since they have an effect in catalysis. [3]

This chapter will describe how we prepared other bimetallic NPs, namely the Au_1Cu_1 and Au_1Cu_3 types, in order to compare them to the Au_3Cu_1 NPs. Instead of referring to the NPs by the specific size of the 55-atom nanocluster, they will be named according to the ratios of gold to Cu used in the synthetic procedure. Changes were made in order to optimise the synthetic procedure that was discussed in Chapter 2. This chapter will discuss these changes as well as their effectiveness to repeatedly produce NPs that have approximately the same sizes and narrow size distributions.

The $Au_{42}Cu_{13}$, $Au_{28}Cu_{27}$, and $Au_{13}Cu_{42}$ NPs will be referred to as Au_3Cu_1, Au_1Cu_1, and Au_1Cu_3, respectively. The Au_{55} and Cu_{55} NPs will simply be referred to as monometallic Au and Cu NPs, respectively. This is due to the fact that the NPs that were synthesised were too large to be dendrimer encapsulated NPs, hence they are classified as dendrimer stabilised NPs.

3.2 Results and Discussion

Various mono- and bimetallic Au, Cu, and Au-Cu DSNs were prepared using the template approach. In this approach, the metal is taken up into the interior of the dendrimer, followed by the addition of excess $NaBH_4$ to facilitate chemical reduction. [9] Initially, the molar ratio of metal-to-micelle was kept at 55:1 for all three different dendrimer micelles and the Au:Cu ratio was altered accordingly to obtain three sets of different mono- and bimetallic NPs. The reaction was monitored by means of UV-Vis spectroscopy, recording the spectra before and after chemical reduction with $NaBH_4$. These spectra were also compared to those of the

empty micelles. These results are shown in Figure 3.3. The relevant peaks in the UV-Vis spectra are summarized in Table 3.1.

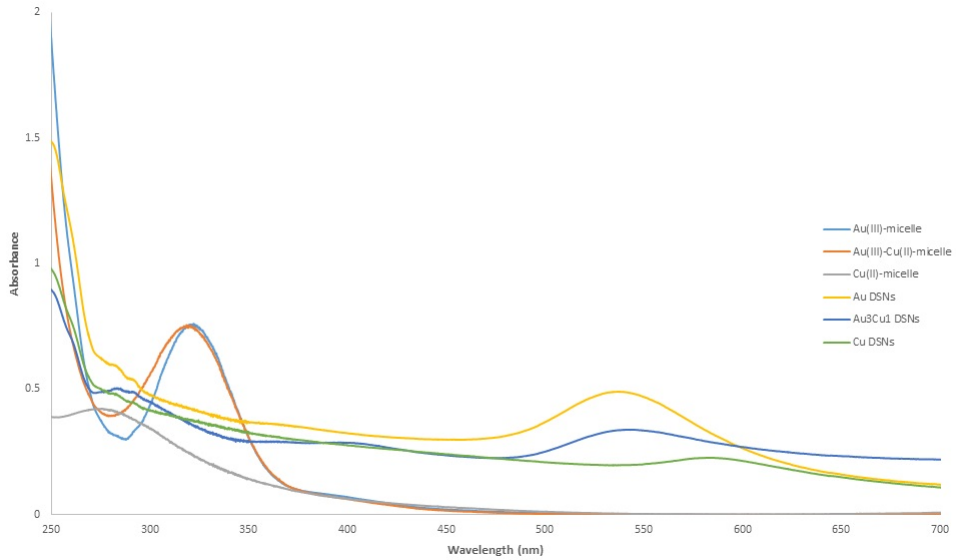

Figure 3.3 Overlaid UV-Vis spectra of the Au, Cu, and Au-Cu (mixture) salts in the dendritic micelle M1 and the mono- and bimetallic M1- Au, Cu, and Au_3Cu_1 DSNs.

The analysis of the three different bimetallic DSNs by means of UV-Vis spectroscopy showed distinct LMCT bands in the range of 239 – 319 nm. [21] The masking and overlap of these absorbance peaks can clearly be observed in Figures 3.3 and 3.4.

In Figure 3.3, the bimetallic Au_3Cu_1 NPs shows an absorbance peak at 548 nm, whereas the mixture of monometallic Au and Cu NPs show an absorbance at 543 nm after 0 hours. This peak of the Au and Cu NP mixture occurs due to the presence of the Au NPs and its intensity is approximately three-quarters that of the monometallic Au NP samples due to three-quarters of the metal in the bimetallic Au_3Cu_1 NPs being Au. The shape of the peak observed for the mixture of monometallic Au and Cu NPs also differs from that of the separate monometallic Au, Cu, and bimetallic Au_3Cu_1 NPs, being broader than the peak of the Au NPs and it also closely resembles the contour observed with the Cu NPs beyond 590 nm. Similar absorbances near 408 nm are also worth noting. The mixture of the monometallic NPs show an absorbance peak at this wavelength, but a similar yet smaller peak is present for the bimetallic NPs. This leads us to conclude, based on the comparative UV-Vis spectroscopy data, that the NPs we were able to prepare were indeed bimetallic alloys as opposed to a mixture of monometallic NPs.

Table 3.1 LMCT bands and SPR peaks for UV-Vis spectra of mono- and bimetallic DSNs of dendrimer micelles M1 - M3.

DSN	Au LMCT (nm)	Cu LMCT (nm)	SPR (nm)
M1-Au	321	N/A	533
M1-Cu	N/A	277	591
M1-Au_3Cu_1	322	-	548
M2-Au	323	N/A	555
M2-Cu	N/A	283	577
M2-Au_3Cu_1	324	-	577
M3-Au	324	N/A	552
M3-Cu	N/A	276	-
M3-Au_3Cu_1	330	-	560

*Note that "N/A" means that no band is expected, whilst "–" indicates that no band was observed.

The UV-Vis spectrum shown in Figure 3.4 compares the UV-Vis spectra obtained for the NPs varying in their metal composition. The UV-Vis spectra reveals similar absorbance bands to the absorbance spectrum shown in Figure 3.3, but the most notable difference is that a shoulder appears on the broad absorbance at 319 nm. This latter absorbance arises due to the presence of the Au(III) species and the shoulder at 290 nm is the LMCT band of the Cu(II). Upon reduction with $NaBH_4$, a single, broad SPR peak was seen at 551 nm. When observing the UV-Vis spectrum of the **M1**-Au_1Cu_3 DSNs in Figure 3.4, the stark contrast of visible LMCT bands compared to the **M1**-Au_3Cu_1 and M1-Au_1Cu_1 bands are easily identified. The significantly higher concentration of the Cu(II) over the Au(III) causes this difference so that only the band caused by the Cu(II) is visible at 296 nm. After this mixture of Au(III) and Cu(II) was reduced, an SPR peak was observed at 574 nm. This absorbance, however, is much weaker than what was seen with the **M1**-Au_3Cu_1 and **M1**-Au_1Cu_1 DSNs. This occurs due to the high Cu content of the NPs. Monometallic Cu NPs would typically only indicate a very weak SPR peak near 580 nm or even none and this characteristic is reflected in these **M1**-Au_1Cu_3 DSNs.

The average NP size and size distributions of the various bimetallic DSNs were investigated by means of HR-TEM analysis (Figure 3.5). The **M1**-Au_3Cu_1 DSNs were found to have the largest average diameter size and were the most polydisperse of the three different DSNs analyzed (24.5 nm ± 8.3).

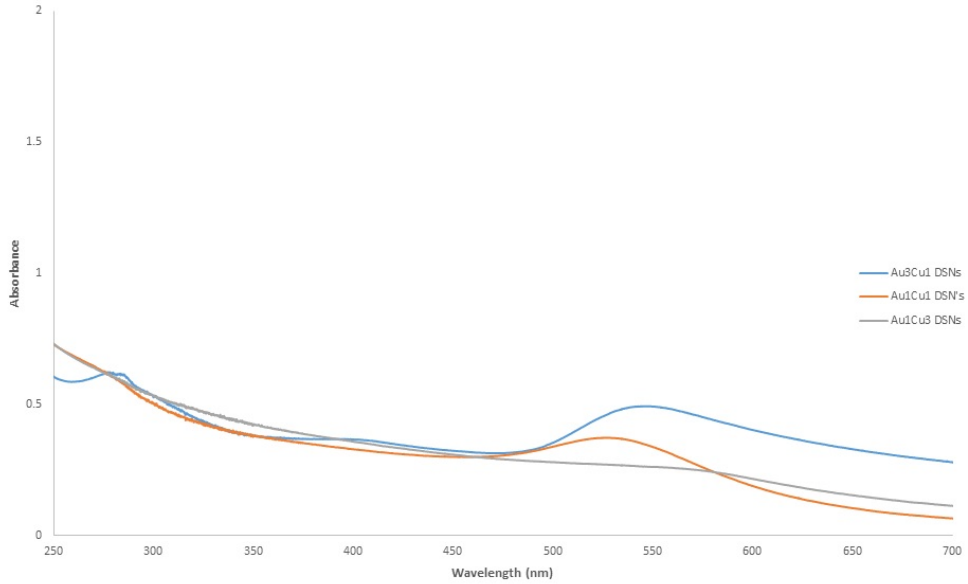

Figure 3.4 Overlaid UV-Vis spectra obtained for the M1- Au_3Cu_1, Au_1Cu_1, and Au_1Cu_3 DSNs.

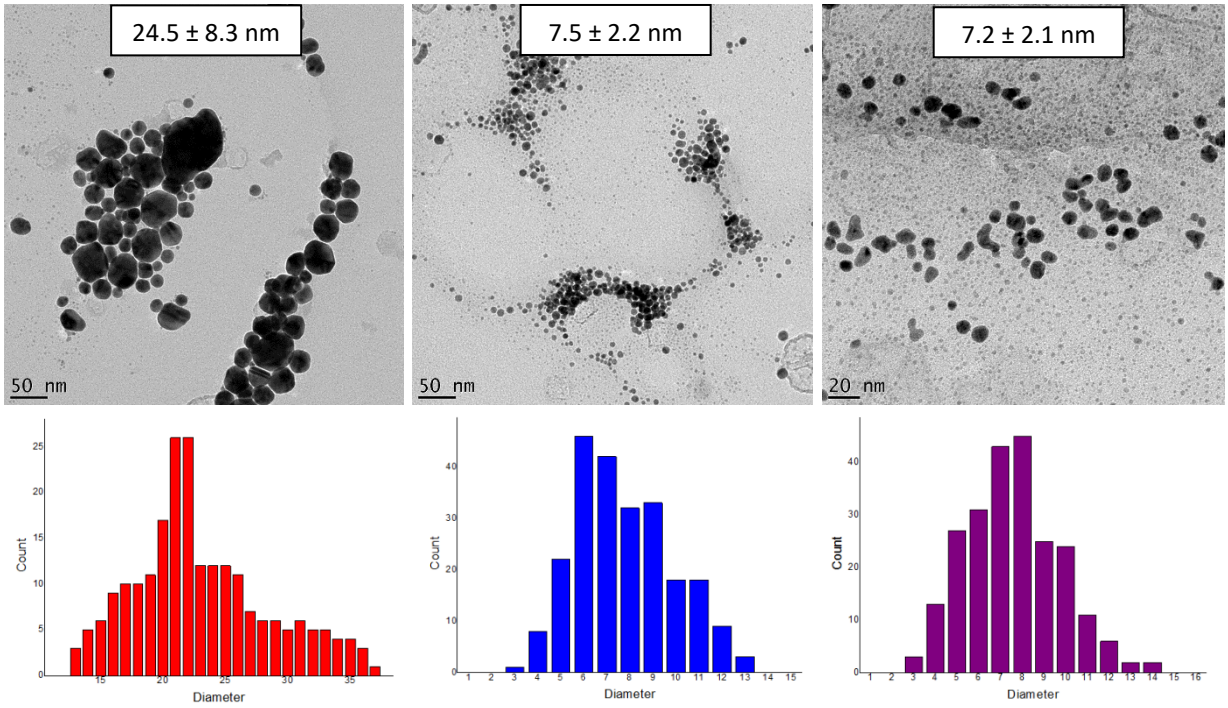

Figure 3.5 HR-TEM images of the M1-Au_3Cu_1 (left), M1-Au_1Cu_1 (middle), and M1-Au_1Cu_3 (right) DSNs with the respective histograms.

The **M1**-Au_1Cu_1 and **M1**-Au_1Cu_3 DSNs, however, showed very similar average NP sizes and size distributions. These were measured to be 7.5 nm ± 2.2 and 7.2 nm ± 2.1, respectively. This shows a significantly smaller average NP size than observed for the **M1**-Au_3Cu_1 DSNs and the size distributions are also relatively low. These large difference in sizes

between the **M1**-Au_3Cu_1 DSNs versus the **M1**-Au_1Cu_1 and **M1**-Au_1Cu_3 DSNs is as a result of the Au and Cu in these NPs. In Chapter 2, the results of HR-TEM analysis of the monometallic gold and Cu DSNs and bimetallic **M1**-Au-Cu DSNs showed that the NPs with the highest gold content is the largest on average and has a greater polydispersity and the converse was seen to be true of the Cu DSNs. The bimetallic DSNs, being Au-Cu alloys, showed NP sizes between the two different monometallic DSNs. Therefore, since the **M1**-Au_1Cu_1 and **M1**-Au_1Cu_3 DSNs have a significantly higher Cu content than the **M1**-Au_3Cu_1 DSNs, we would expect their average sizes to be smaller and that they would be more monodisperse. Although UV-Vis analysis of these DSNs were sufficient to indicate that NPs had indeed formed, it did not definitively conclude that these NPs were indeed bimetallic alloys. To confirm this, we also utilised EDS in conjunction with HR-TEM to determine whether the bimetallic alloys had indeed formed (Figures 3.6 – 3.8). The common Cu grids generally used for EDS analysis were not suitable for our analyses, since the grid would affect the data obtained for the NPs. Due to this we used nickel grids that do not contain Cu. The results conclusively showed that the NPs contained both gold and Cu, thereby enabling us to confirm that the NPs we had prepared were indeed bimetallic.

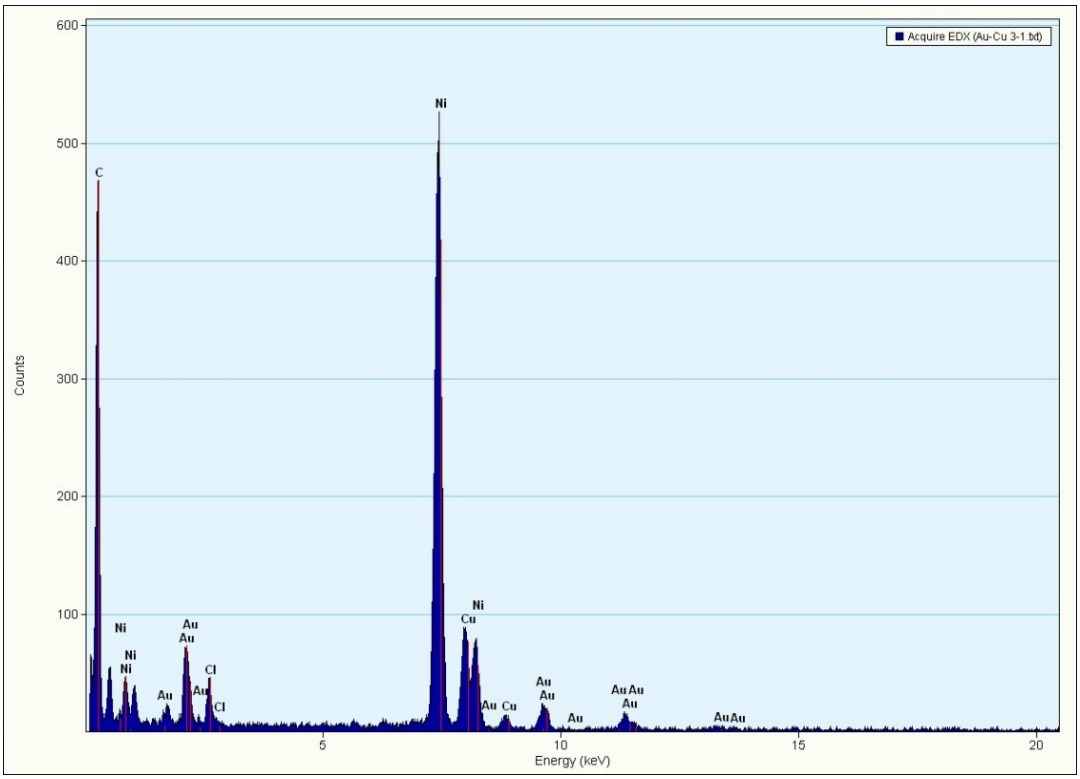

Figure 3.6 TEM-EDS spectrum obtained for the bimetallic M1-Au_3Cu_1 DSNs.

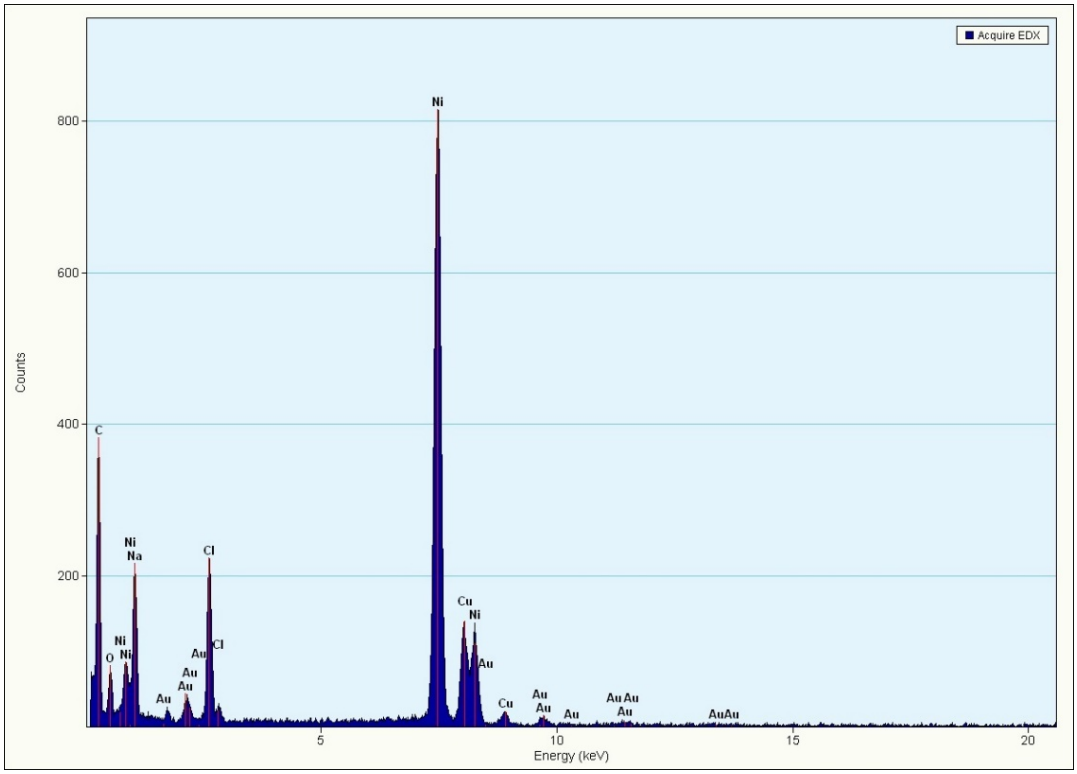

Figure 3.7 TEM-EDS spectrum obtained for the bimetallic M1-Au_1Cu_1 DSNs.

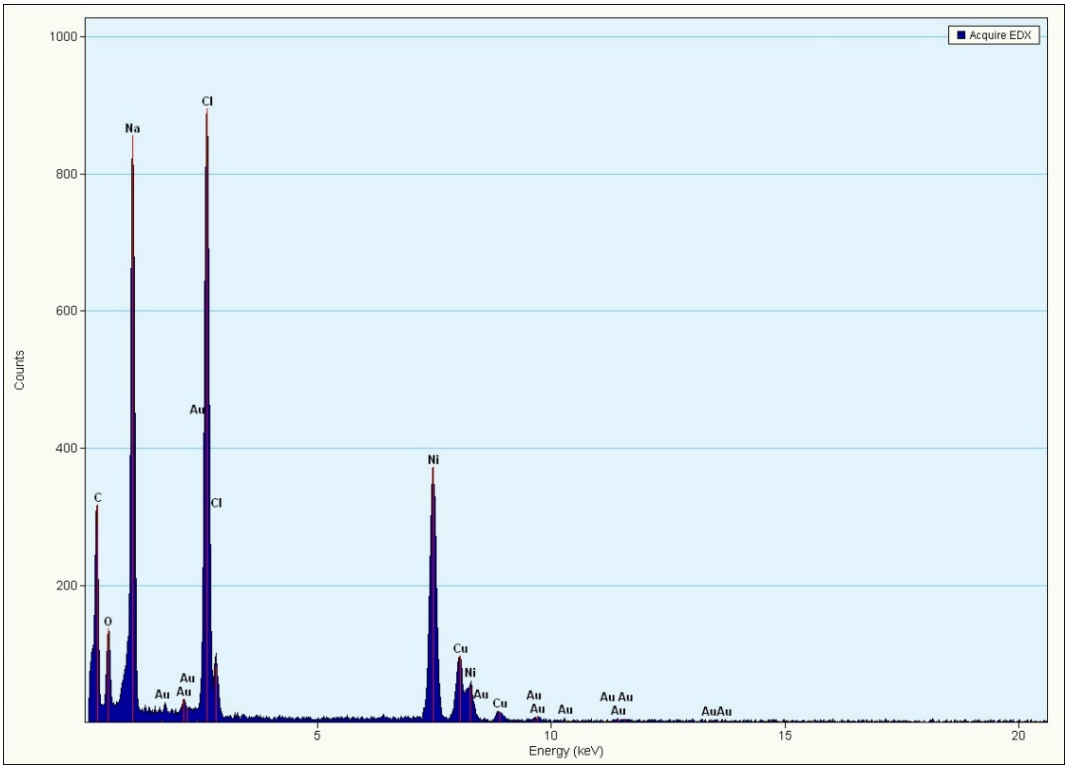

Figure 3.8 TEM-EDS spectrum obtained for the bimetallic M1-Au_1Cu_3 DSNs.

After we had established a successful method for preparing mono- and bimetallic alloy NPs, we attempted to optimise these synthetic methods for reproducibility. The most important step in preparing NPs is the reduction, hence we focused our efforts on this specific step. In previous reactions, the reducing agent, $NaBH_4$ in methanol, was added to the reaction mixture quickly, but we believed that the rate at which the reducing reagent is added would have a marked effect on NP formation and the subsequent NP size. This was first tested with the monometallic **M1**-Au and **M1**-Cu NPs and later duplicated in order to investigate the reproducibility of the method.

In previous instances when **M1**-Au syntheses were attempted, the Au DSNs could range greatly in size between a range of 20 nm to over 40 nm. Significant differences were also seen in the SPR peaks of these DSNs which could range from 531 nm to over 540 nm which is indicative of a change in size of the NPs. Such results show that the previous method was not well suited to reproducibility. When the new method was attempted and subsequently analysed by means of UV-Vis spectroscopy (Figure 3.9), repeating the same method showed extensive overlapping of the spectra and the broad SPR peaks differed only by 2 nm at their maxima (532 nm and 530 nm), showing that this new method is more reproducible for consistent sizes than the one used in previous instances.

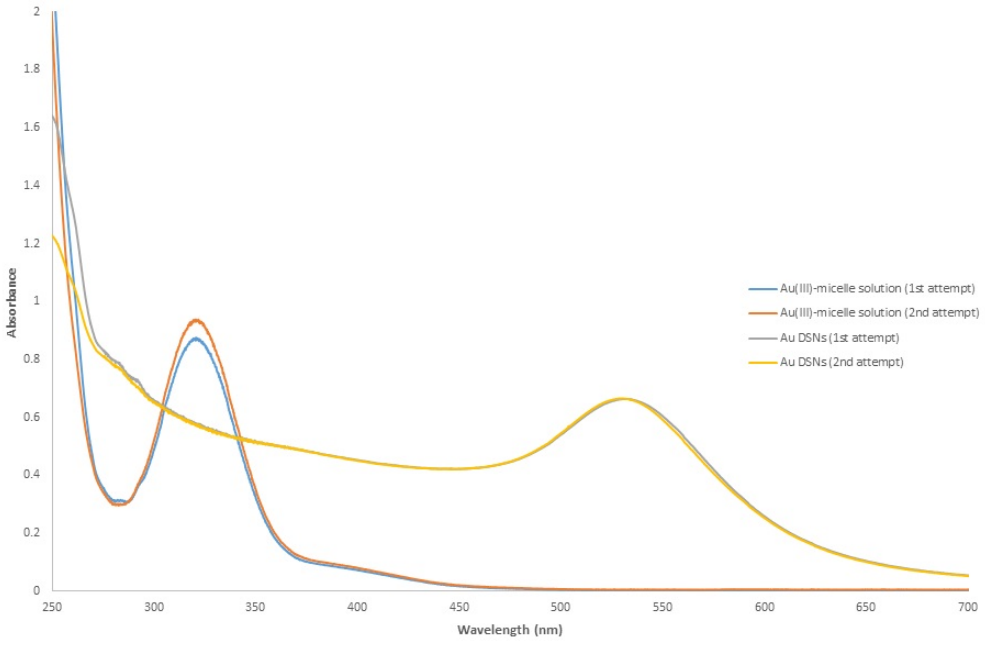

Figure 3.9 Overlaid UV-Vis spectra obtained for two different samples of M1-Au DSNs prepared with the same method.

When this method was applied for the synthesis of the **M1**-Cu DSNs, the same trend was observed. Again, the two spectra were very identical to each other with regards to the LMCT bands and the absence of any SPR peak (Figure 3.10). The absence of a SPR peak indicates that the Cu NPs that formed were sufficiently small to not produce a SPR peak upon UV-Vis analysis. No HR-TEM analysis was available to determine the actual sizes of the NPs.

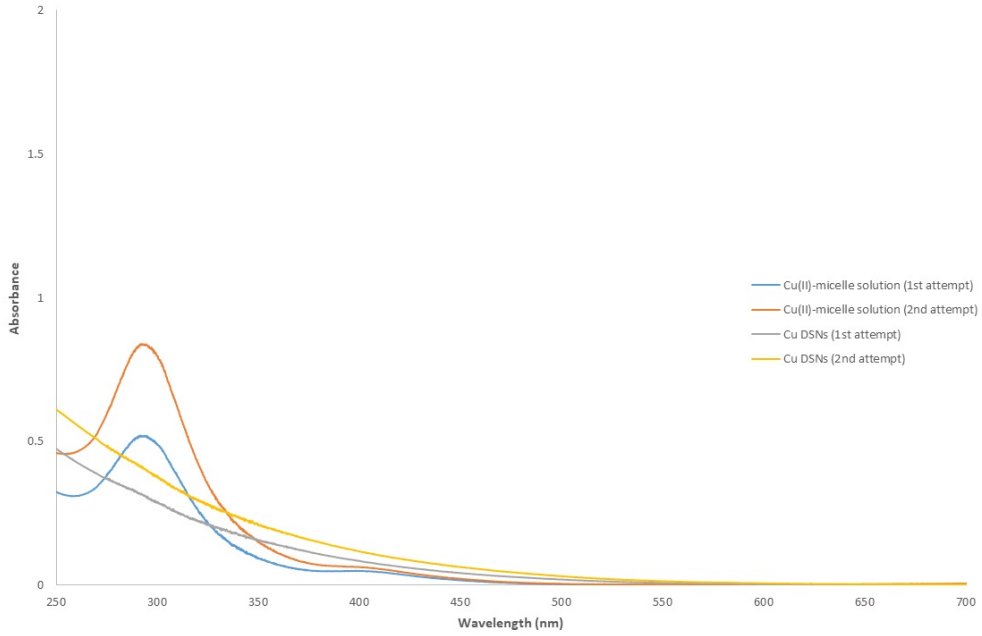

Figure 3.10 Overlaid UV-Vis spectra obtained for two different samples of M1-Au DSNs prepared with the same method.

Both of these methods utilised the template method represented in Scheme 3.2. This synthetic method requires two distinct steps. First, the metal ion has to be taken up into the dendrimer interior and, secondly, chemical reduction which is facilitated by $NaBH_4$. In order to optimise this method, we shifted our focus to the second of these synthetic steps: the chemical reduction. We attempted to do this by setting out to find a procedure that is both repeatable and able to give us more control over the metal reduction. This was done by testing the effects of the concentration, volume, and addition of the $NaBH_4$. We chose to focus on these parameters rather than testing other reducing agents, since the dendrimer micelles that we were using already accounted for stabilising effects. Using other reducing agents would consequently affect the overall stabilising effect. [7,8]

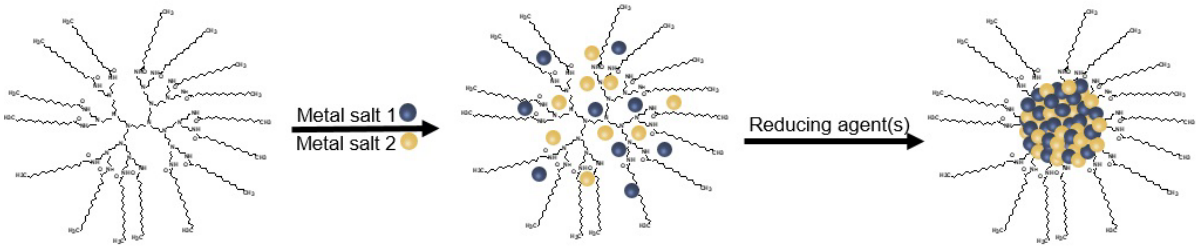

Scheme 3.2 Example of a co-complexation method in which two metals are reduced in the same step. [9]

Following extensive preparation and several alterations to the method, we were finally able to develop a method that allowed us to consistently produce NPs of similar sizes. While developing this method, it was found that the most important changes were to add the metal ion and reducing agent solutions in a slower, dropwise fashion which is more efficient. The reducing agent was also added as a solution of lower concentration, yet in greater quantity. Data acquired by HR-TEM made it possible for us to confirm that the new method we had developed produced NPs with consistent sizes and a narrower polydispersity (Figures 3.11 – 3.13).

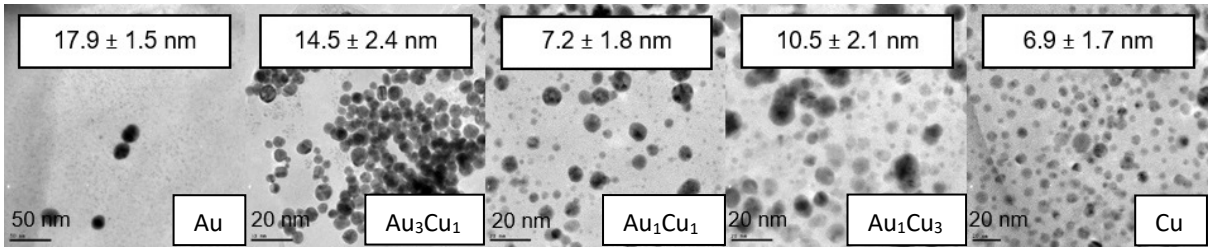

Figure 3.11 HR-TEM images for the monometallic M1-Au, M1-Cu, and bimetallic M1-Au_3Cu_1, M1-Au_1Cu_1, and M1-Au_1Cu_3 DSNs prepared on the first attempt using the new, reproducible method.

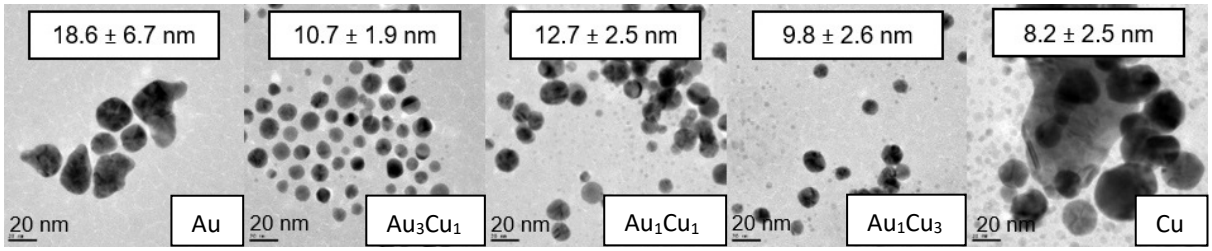

Figure 3.12 HR-TEM images for the monometallic M1-Au, M1-Cu, and bimetallic M1-Au_3Cu_1, M1-Au_1Cu_1, and M1-Au_1Cu_3 DSNs prepared on the second attempt using the new, more reproducible method.

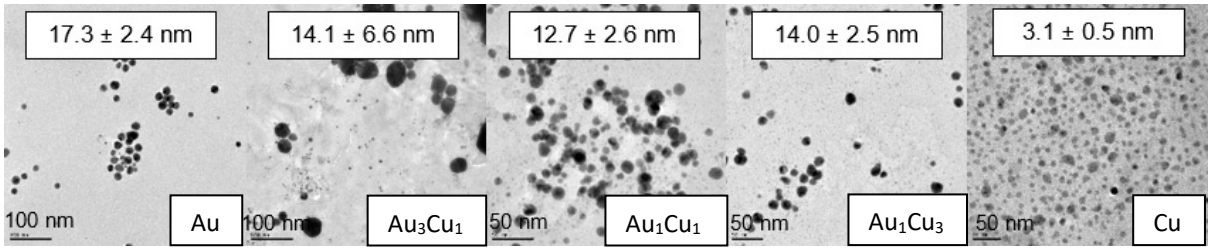

Figure 3.13 HR-TEM images for the monometallic M1-Au, M1-Cu, and bimetallic M1-Au_3Cu_1, M1-Au_1Cu_1, and M1-Au_1Cu_3 DSNs prepared on the third attempt using the new, more reproducible method.

Table 3.2 Reproducibility of DSN sizes that were prepared three different times with the same method, where the size was determined by HR-TEM.

DSN	DSN size (nm) Old method	DSN size (nm) New method Attempt 1	DSN size (nm) New method Attempt 2	DSN size (nm) New method Attempt 3
Au	14.8 ± 12.5	17.9 ± 1.5	18.6 ± 6.7	17.3 ± 2.4
Au_3Cu_1	9.2 ± 7.1	14.5 ± 2.4	10.7 ± 1.9	14.1 ± 6.6
Au_1Cu_1	-	7.2 ± 1.8	12.7 ± 2.5	12.7 ± 2.6
Au_1Cu_3	-	10.5 ± 2.1	9.8 ± 2.6	14.0 ± 2.5
Cu	2.5 ± 0.8	6.9 ± 1.7	8.2 ± 2.5	3.1 ± 0.5

After we had developed a new, effective method to prepare mono- and bimetallic DSNs with different metal ratios, we set out to evaluate and compare the stabilities of these various DSNs. These DSNs were analysed by means of UV-Vis spectroscopy (Figures 3.14 and 3.15; Table 3.3). After this experiment was conducted, we found that the monometallic Au NPs were the most unstable and most prone to agglomeration despite optimising the synthetic method and the dendrimer micelle's stabilising effect. The monometallic Cu NPs, however, were the smallest NPs.

The five different DSNs that were prepared in the afore-mentioned reactions (Table 3.3) were kept for a duration of 9 months. During this time the DSNs were analysed directly after synthesis and again after 3 and 9 months. During this time the DSNs were kept in solution in order to observe how these NPs changed over this time, especially with respect to agglomeration which affects both the average NP sizes and size distributions.

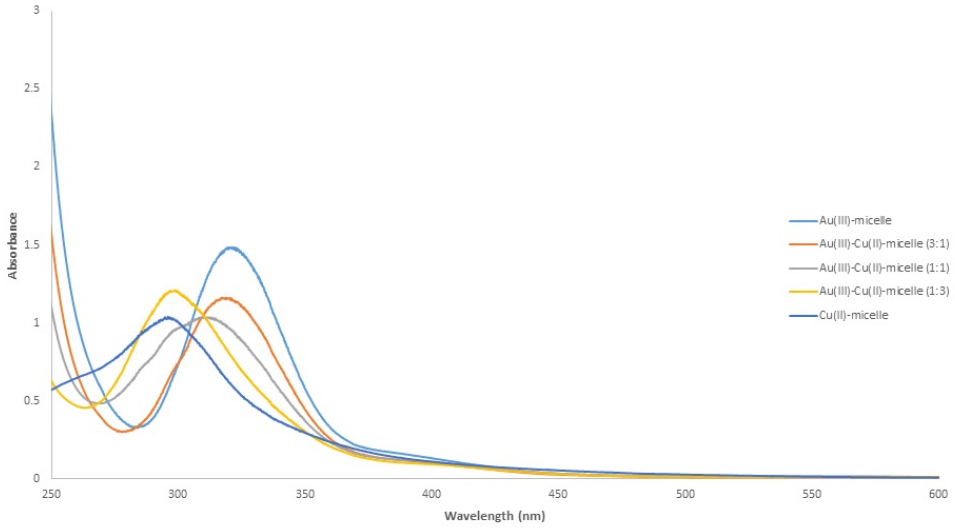

Figure 3.14 Overlaid UV-Vis spectra of the appropriate metal salt and M1 dendritic micelle solutions used to prepare the Au, Au_3Cu_1, Au_1Cu_1, Au_1Cu_3, and Cu DSNs.

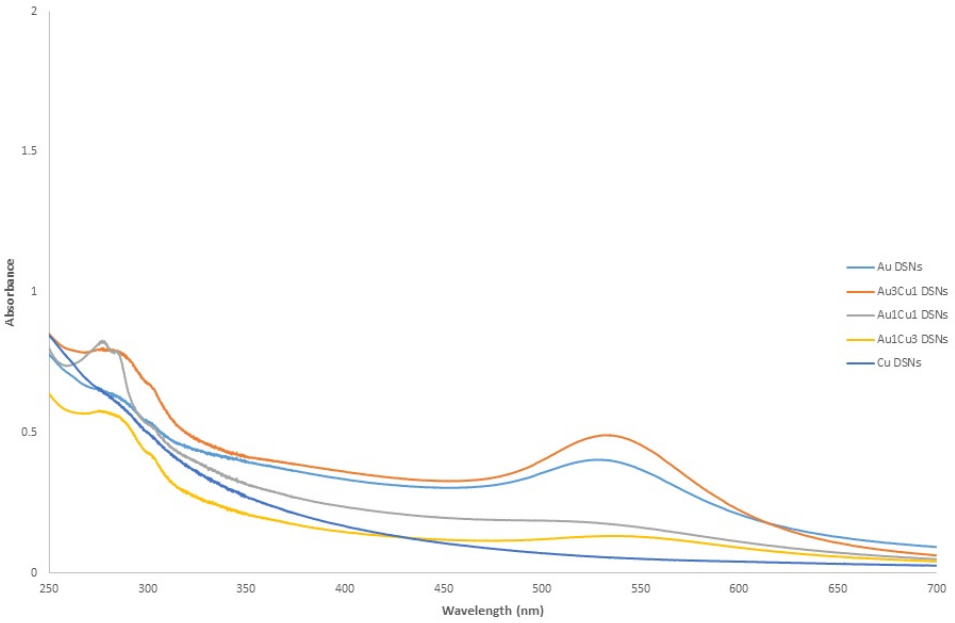

Figure 3.15 Overlaid UV-Vis spectra of the Au, Au_3Cu_1, Au_1Cu_1, Au_1Cu_3, and Cu DSNs prepared with the M1 dendritic micelle.

In the case of the **M1**-Au and **M1**-Au_3Cu_1 DSNs, a SPR peak was observed at a wavelength of 534 nm. This confirmed the formation of NPs with a diameter greater than 2 nm. However, the **M1**-Cu DSNs did not display any SPR peak, which suggests that the NPs that formed were smaller than 2 nm in diameter. The SPR peaks of the three different bimetallic DSNs did not appear to follow any trend based on the metal composition of the NPs.

Table 3.3 LMCT bands and SPR peaks for the UV-Vis spectra of the Au, Au_3Cu_1, Au_1Cu_1, Au_1Cu_3, and Cu DSNs prepared with the M1 dendritic micelle.

DSN	Au LMCT (nm)	Cu LMCT (nm)	SPR (nm)
M1-Au	326	-	534
M1-Au_3Cu_1	321	-	534
M1-Au_1Cu_1	325	310	530
M1-Au_1Cu_3	-	300	548
M1-Cu	-	300	-

In the instances of the three different bimetallic NPs, the sizes differed based on their metal compositions. After keeping these NPs in solution for nine months, HR-TEM analysis confirmed that they were very stable and showed little change in size and dispersity over such an extended time (Figures 3.16-3.20). This showed that the composition of metallic NPs affects the stability of the NP cluster. Bimetallic NPs have commonly been used to enhance the activity and selectivity of each of the metals. However, in this work, the results showed that the bimetallic nature of the NPs is very well suited to enhance the stability of the NPs. This is advantageous, because it will allow for a longer catalyst lifetime. This finding also opens up possibilities to use a bimetallic approach for enhanced stabilisation effects, as opposed to more conventional methods that require ligands, dendrimers, etc. Since our results showed the monometallic Cu NPs are much more stable than the monometallic Au NPs, it is believed that the Cu atoms in the bimetallic NPs stabilise the Au atoms.

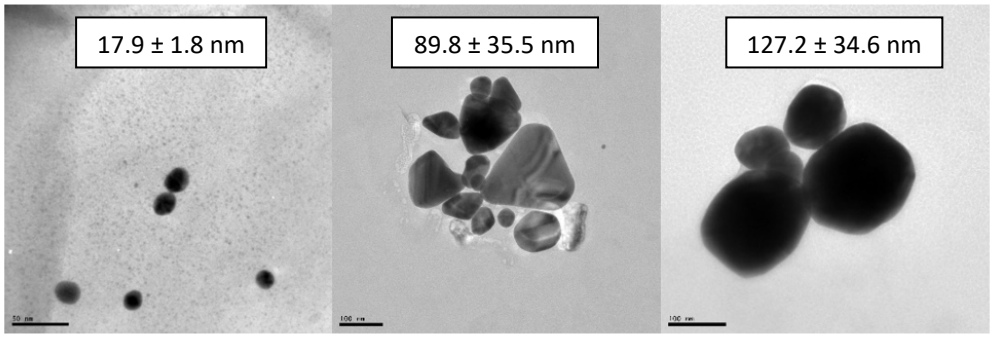

Figure 3.16 HR-TEM images of the M1-Au DSNs listing their sizes and size distributions directly after synthesis (left), after 3 months (middle), and after 9 months (right).

The Au DSNs showed a great degree of agglomeration over time due to the NPs only consisting of gold. Besides the extensive agglomeration, these NPs also tend to possess high degrees of crystallinity.

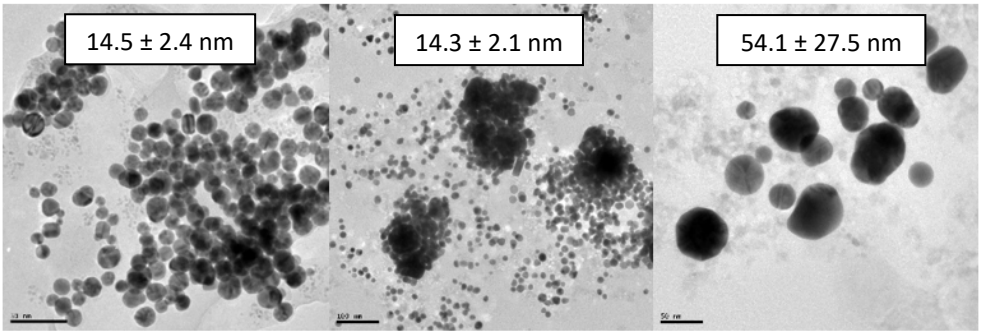

Figure 3.17 HR-TEM images of the M1-Au_3Cu_1 DSNs listing their sizes and size distributions directly after synthesis (left), after 3 months (middle), and after 9 months (right).

The bimetallic Au_3Cu_1 DSNs initially appeared to be very stable in solution with no extensive agglomeration or changes in size and size distribution observed. However, during the time of the second and third HR-TEM analyses (3 and 9 months, respectively), significant agglomeration and changes in the size and size distribution were observed (Figure 3.17). This phenomenon is believed to arise due to the majority Au content in these NPs, since Au is prone to agglomeration.

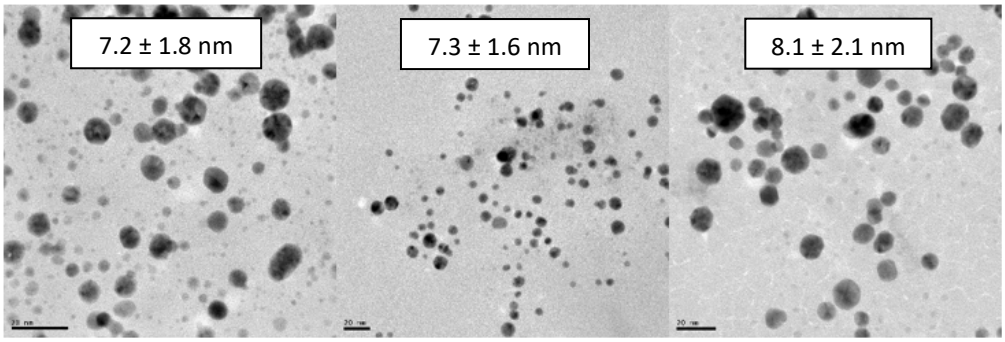

Figure 3.18 HR-TEM images of the M1-Au_1Cu_1 DSNs listing their sizes and size distributions directly after synthesis (left), after 3 months (middle), and after 9 months (right).

The Au_1Cu_1 DSNs showed great stability over the entire 9 month duration. Unlike the Au and Au_3Cu_1 DSNs which have high gold contents in the NPs, the Au_1Cu_1 DSNs have an equal molar mixture of the Au and Cu (Figure 3.18). This shows that the Cu is effective at stabilizing the Au atoms in the NPs.

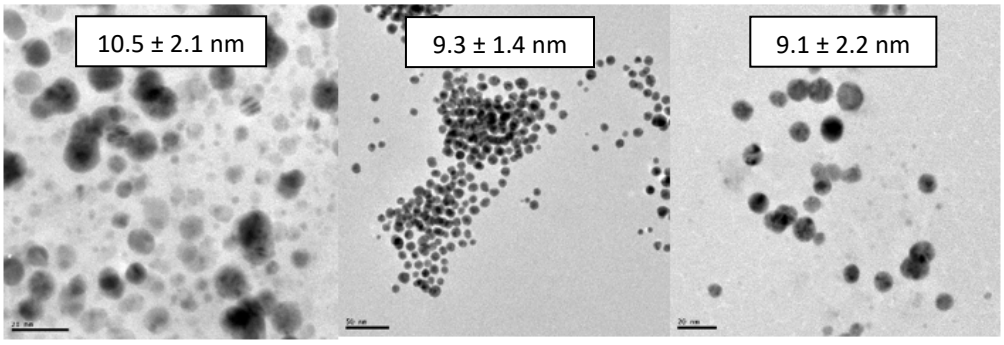

Figure 3.19 HR-TEM images of the M1-Au_1Cu_3 DSNs listing their sizes and size distributions directly after synthesis (left), after 3 months (middle), and after 9 months (right).

Like the Au_1Cu_1 DSNs, these Au_1Cu_3 DSNs also proved to be stable over 9 months when stored in solution (Figure 3.19). The sizes of the two different DSNs were also very similar throughout the duration of this experiment and the Cu again showed to be effective at preventing the Au in the NPs from agglomerating extensively.

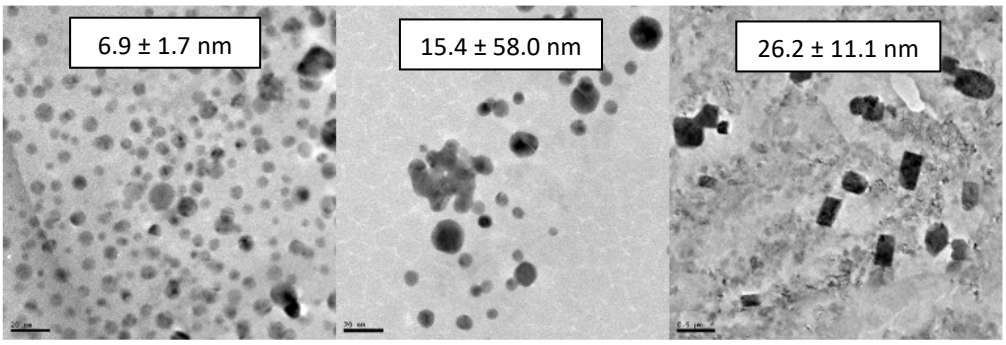

Figure 3.20 HR-TEM images of the M1-Cu DSNs listing their sizes and size distributions directly after synthesis (left), after 3 months (middle), and after 9 months (right).

Initially the Cu DSNs showed to be very promising with regards to NP stability. However, HR-TEM analysis after 3 and 9 months showed that, similarly to the DSNs with high Au content, the monometallic Cu DSNs were also prone to extensive agglomeration (Figure 3.20).

The following table and graph (Table 3.4; Figure 3.21) represent the NP sizes observed after the three different analyses with HR-TEM performed directly after synthesis, after 3 months, and after 9 months.

Table 3.4 Summary of the M1-Au_mCu_n NP sizes at various time points.

DSN	Initial DSN size (nm)	DSN size after 3 mo. (nm)	DSN size after 9 mo. (nm)
Au	17.9 ± 1.5	89.8 ± 35.5	127.2 ± 34.6
Au_3Cu_1	14.5 ± 2.4	14.3 ± 2.1	54.1 ± 27.5
Au_1Cu_1	7.2 ± 1.8	7.3 ± 1.6	8.1 ± 2.1
Au_1Cu_3	10.5 ± 2.1	9.3 ± 1.4	9.1 ± 2.2
Cu	6.9 ± 1.7	15.4 ± 58.0	26.2 ± 11.1

This study showed that the monometallic **M1**-Au and **M1**-Cu DSNs have a tendency to agglomerate in solution when prepared with and stabilised by the DAB G3 PPI dendrimer micelle. The tendency of these to agglomerate, however, overcomes the stabilizing effect of the dendrimer micelle and hence the average NP sizes and size distributions increased significantly as the time duration increased. The Au NPs showed the greatest increase in size and thus the lowest stability and highest tendency to agglomerate.

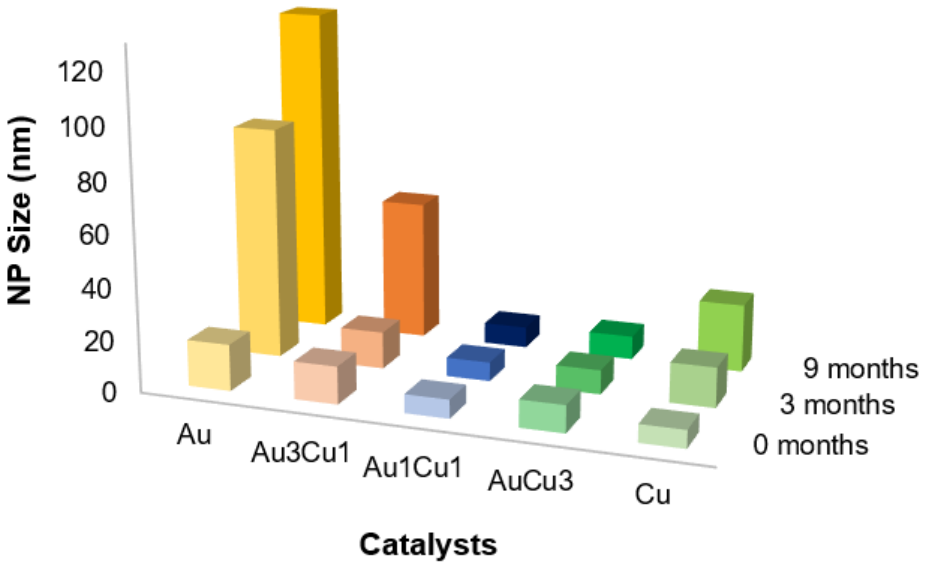

Figure 3.21 Graphical summary of the effect of time on the sizes of the M1-Au_mCu_n DSNs.

The same trend observed for the **M1**-Au DSNs was also evident with the **M1**-Cu DSNs, but not to the same degree. They tend to remain much smaller than the Au DSNs as seen throughout the different stages of this experiment.

The bimetallic DSNs (Au_3Cu_1, Au_1Cu_1, and Au_1Cu_3) are more stable in solution when prepared with and stabilized by the dendrimer micelles. Their sizes remained constant without any significant changes throughout the first 3 months. The next 6 months generally showed this same trend with the exception of the Au_3Cu_1 DSNs. Having undergone extensive agglomeration, these NPs became much larger, changing from 14.3 ± 2.1 nm to 54.1 ± 27.5 nm. These large changes in both the average NP size and size distribution was probably induced by the high Au content of the NP as seen to be the case with the monometallic Au NPs.

The Au_1Cu_1 DSNs appeared to be particularly stable, since they were the smallest throughout the various stages of the experiment and their sizes barely changed at all. The same can be said about the Au_1Cu_3 DSNs. This shows that a higher Cu content causes the NPs to be smaller and more stable as is seen in the comparison between the monometallic Au and Cu DSNs where the Au NPs agglomerated extensively and much more than the Cu NPs.

We attempted to optimise the synthesis method of all five different NPs that we were aiming to prepare: **M1**-Au, **M1**-Au_3Cu_1, **M1**-Au_1Cu_1, **M1**-Au_1Cu_3, and **M1**-Cu DSNs. This alteration was done by using more of the reducing agent (at the same concentration as earlier), $NaBH_4$, in the reduction step of the method. Analysis of these different DSNs by means of UV-Vis spectroscopy showed distinctive LMCT bands in the range of 300 – 326 nm based on the amounts of Au(III) and Cu(II) species present.

In Figure 3.22, various LMCT bands were observed for the Au(III) and Cu(II) ions coordinated to the amine groups in the dendrimer micelle interior. Afterwards, these solutions were reduced with $NaBH_4$ in a dropwise fashion and subsequently analysed with UV-Vis (Figure 3.23). The values of the LMCT and SPR peaks are listed in Table 3.5.

The average sizes and size distributions of the mono- and bimetallic DSNs were investigated by means of HR-TEM analysis. Figure 3.24 shows the TEM results for the five different **M1** DSNs. The monometallic **M1**-Au DSNs were found to have the largest average diameter size and was also the most polydisperse of the DSNs analyzed (22.0 ± 5.3 nm). On the other hand, the monometallic **M1**-Cu DSNs displayed the smallest average diameter size with a low degree of polydispersity (3.5 ± 1.1 nm). The bimetallic DSNs showed varying degrees of average size and size distribution. The **M1**-Au_1Cu_1 DSNs were very large on average, although still fairly monodisperse (19.0 ± 3.5 nm), the **M1**-Au_1Cu_3 DSNs were relatively small and nearly identical to the monometallic **M1**-Cu DSNs (3.6 ± 1.3 nm), and the **M1**-Au_3Cu_1 DSNs were of a relatively moderate size (6.7 ± 3.7 nm).

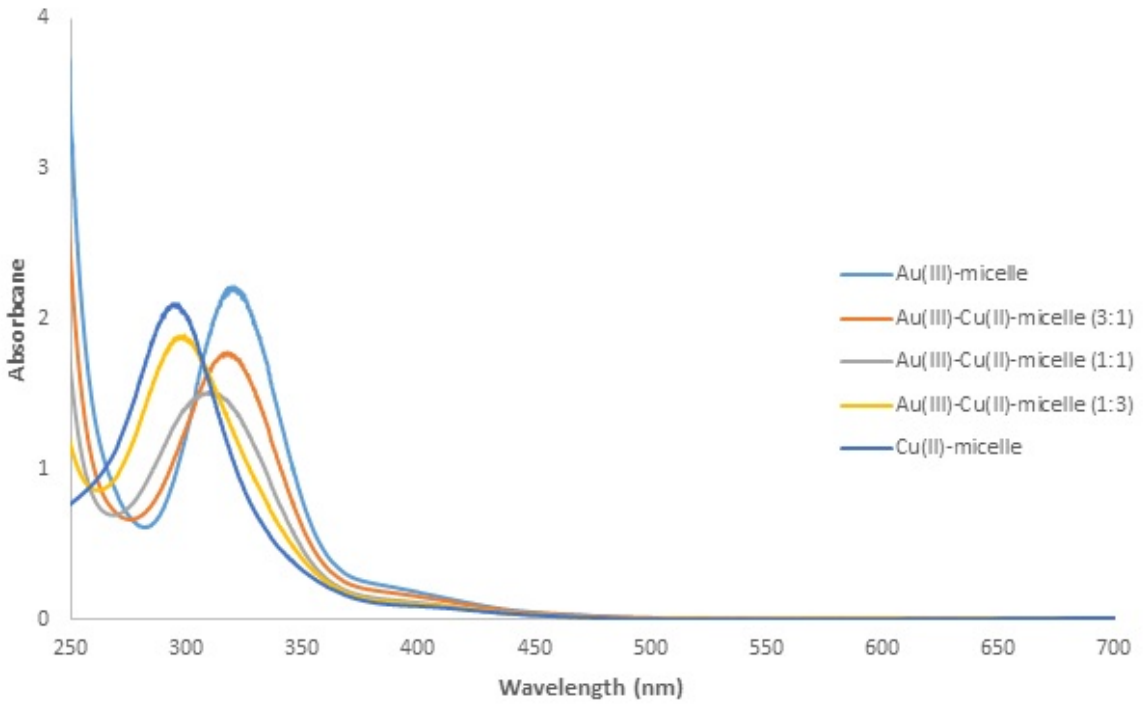

Figure 3.22 Overlaid UV-Vis spectra of the appropriate metal salt and M1 dendritic micelle solutions used to prepare the Au, Au_3Cu_1, Au_1Cu_1, Au_1Cu_3, and Cu DSNs.

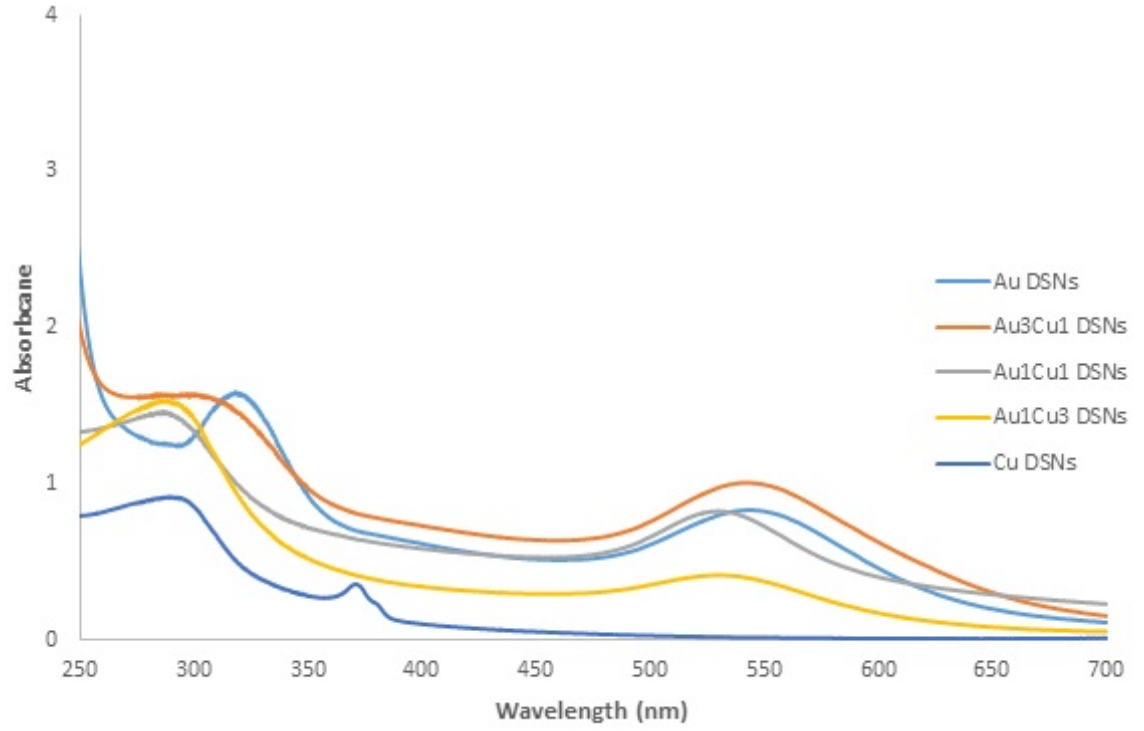

Figure 3.23 Overlaid UV-Vis spectra of the Au, Au_3Cu_1, Au_1Cu_1, Au_1Cu_3, and Cu DSNs prepared with the M1 dendritic micelle.

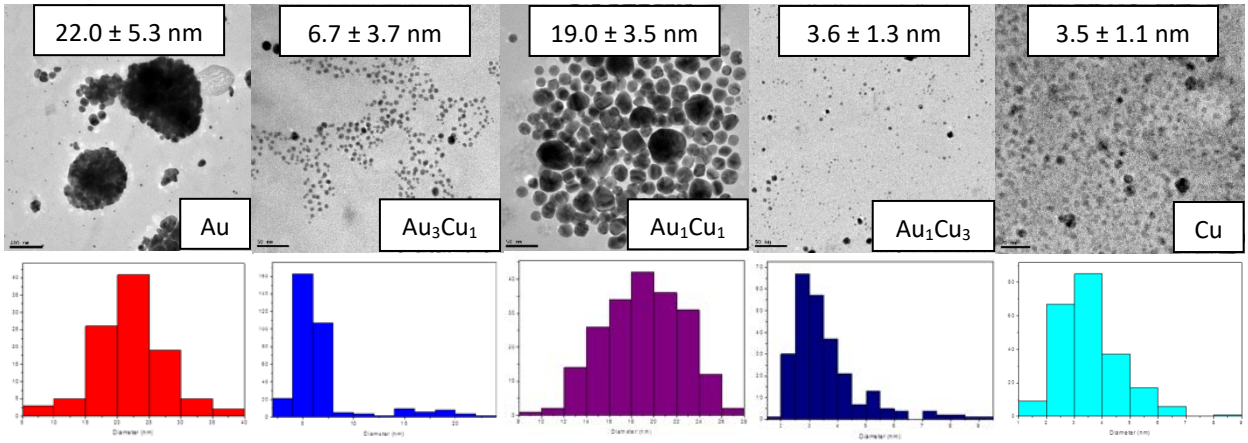

Figure 3.24 HR-TEM images and histograms of the M1- Au, Au_3Cu_1, Au_1Cu_1, Au_1Cu_3, and Cu DSNs listing their sizes and size distributions.

The HR-TEM results showed that the sizes of these NPs differed significantly in size and size distribution when compared to the different method attempted before that (Table 3.4). The sizes were also not similar to the expected values based on the metal composition of the different types of NPs, hence we decided to return to the method used when preparing the last set of NPs. This was done in an attempt to replicate those previous results so that NPs with sizes as close as possible to what was obtained before could be obtained again.

The subsequent steps of the NP synthesis were analysed with UV-Vis spectroscopy. This indicated distinctive LMCT bands in the range of 300 – 325 nm based on the amounts of Au(III) and Cu(II) species present. The masking and overlap of these absorbance peaks were clearly observed and were very similar to the UV-Vis spectra shown in the last instance of when the mono- and bimetallic DSNs were prepared with this method (Table 3.5).

Table 3.5 LMCT bands and SPR peaks for UV-Vis spectra of mono- and bimetallic DSNs of dendrimer micelles M1.

DSN	Au LMCT (nm)	Cu LMCT (nm)	SPR (nm)	DSN size (nm)
M1-Au	322	-	546	22.0 ± 5.3
M1-Au_3Cu_1	319	-	545	6.7 ± 3.7
M1-Au_1Cu_1	312	-	531	19.0 ± 3.5
M1-Au_1Cu_3	-	299	535	3.6 ± 1.3
M1-Cu	-	297	-	19.0 ± 3.5

In Figure 3.25, an LMCT band was observed at 325 nm for the **M1**-Au DSNs. This represents an absorbance by the Au(III). After reduction with $NaBH_4$, a single, broad SPR peak appears at 532 nm which indicates the formation of NPs larger than 2 nm in diameter. The **M1**-Au_1Cu_1 DSNs UV-Vis spectrum in Figure 3.25 shows a similar absorbance spectrum as seen in Figure 3.22, but a noticeable difference is that a shoulder is present on the broad absorbance at 304 nm. This latter absorbance arises due to the presence of the Au(III) species and the shoulder at 304 nm is the LMCT band of the Cu(II). Upon reduction with $NaBH_4$, a single, broad SPR peak was seen at 533 nm.

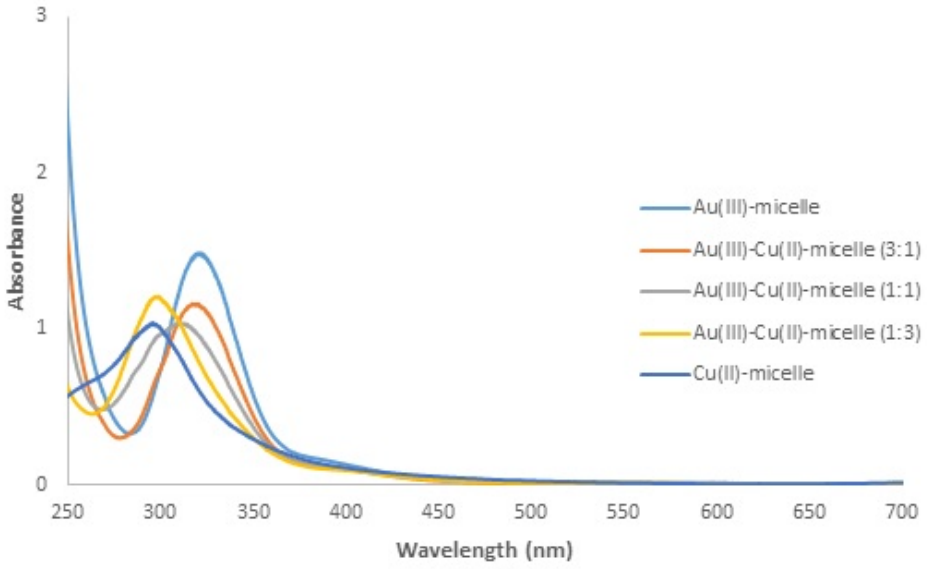

Figure 3.25 Overlaid UV-Vis spectra of the appropriate metal salt and M1 dendritic micelle solutions used to prepare the Au, Au_3Cu_1, Au_1Cu_1, Au_1Cu_3, and Cu DSNs.

The UV-Vis spectrum of the **M1**-Au_1Cu_3 DSNs in Figure 3.25 shows a clear LMCT band at 301 nm. The significantly higher concentration of the Cu(II) over the Au(III) causes this difference so that only this one LMCT band caused by the Cu(II) is visible. After this mixture of Au(III) and Cu(II) was reduced, an SPR peak was observed at 547 nm. This absorbance, however, is much weaker than what was seen with the **M1**-Au_3Cu_1 and **M1**-Au_1Cu_1 DSNs. This occurs as a result of the high Cu content of the DSNs.

In the UV-Vis analysis of the synthetic process used for the **M1**-Cu DSNs in Figure 3.25, a single LMCT band was present at 300 nm as a result of the Cu(II). After reduction with

$NaBH_4$, no SPR peak was observed, which suggests that the Cu DSNs that formed were small enough not to cause such a SPR peak upon UV-Vis analysis.

The UV-Vis spectrum observed in Figure 3.26 shows the absorbance spectrum of the **M1**-Au_3Cu_1 DSNs. Here we can observe an LMCT band at 320 nm which is ab LMCT absorbance band of the Au(III) species. Although the Cu(II) is also present, it is in a significantly lower concentration than the Au(III) and is masked as a result. After reduction with $NaBH_4$, a single, broad SPR peak appears at 533 nm which signifies the formation of NPs larger than 2 nm in diameter.

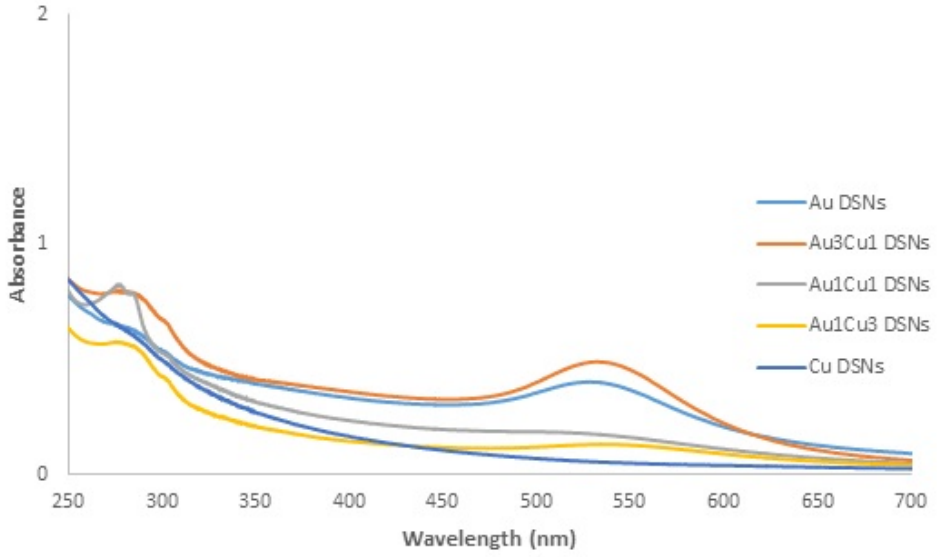

Figure 3.26 Overlaid UV-Vis spectra of the Au, Au_3Cu_1, Au_1Cu_1, Au_1Cu_3, and Cu DSNs prepared with the M1 dendritic micelle.

Table 3.6 LMCT bands and SPR peaks for UV-Vis spectra of mono- and bimetallic DSNs of dendrimer micelles M1.

DSN	Au LMCT (nm)	Cu LMCT (nm)	SPR (nm)	DSN size (nm)
M1-Au	325	-	532	18.6 ± 6.7
M1-Au_3Cu_1	320	-	533	10.7 ± 1.9
M1-Au_1Cu_1	312	304	533	12.7 ± 2.5
M1-Au_1Cu_3	-	301	547	9.8 ± 2.6
M1-Cu	-	300	-	8.2 ± 2.5

HR-TEM analysis was used to determine the average sizes and size distributions of the mono- and bimetallic NPs that were investigated. These HR-TEM results for these **M1** NP systems are shown in Figure 3.27. The monometallic **M1**-Au DSNs were found to have the largest average diameter size and were the most polydisperse of the NP systems analyzed (18.6 nm ± 6.7). The monometallic **M1**-Cu DSNs had the smallest average diameter size with a low degree of polydispersity (8.2 nm ± 2.5).

The bimetallic NPs showed similar average sizes and size distributions. The **M1**-Au_1Cu_1 DSNs were larger than the other bimetallic NPs on average (12.7 nm ± 2.5) and the **M1**-Au_3Cu_1 and Au_1Cu_3 DSNs were recorded to be 10.7 nm ± 1.9 and 9.8 nm ± 2.6, respectively. These sizes were similar to those observed in Table 3.4, whose results were obtained with the same method.

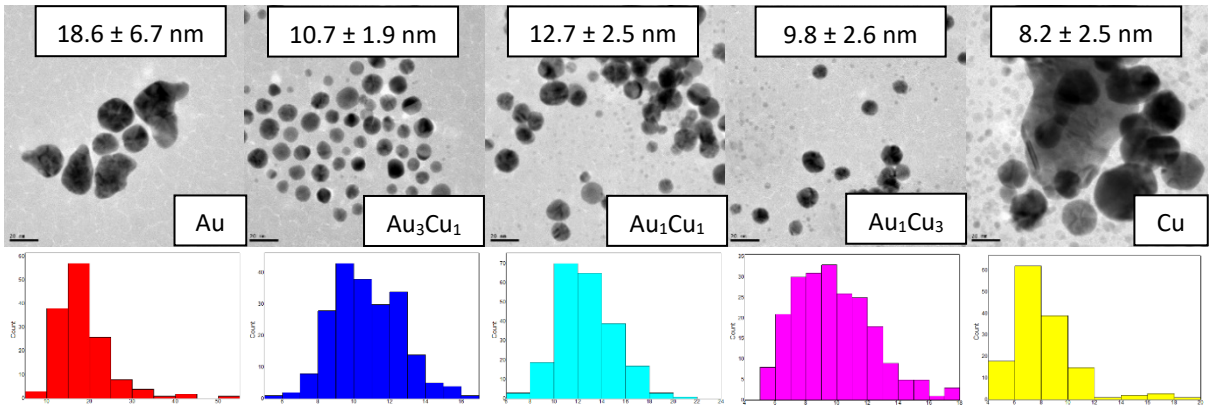

Figure 3.27 HR-TEM images and histograms of the M1- Au, Au_3Cu_1, Au_1Cu_1, Au_1Cu_3, and Cu DSNs listing their sizes and size distributions.

Table 3.7 Summary of the M1- Au, Au_3Cu_1, Au_1Cu_1, Au_1Cu_3, and Cu DSN sizes observed with HR-TEM (Figure 3.27) for the various mono- and bimetallic NPs.

DSN	DSN size (nm)
M1-Au	18.6 ± 6.7
M1-Au_3Cu_1	10.7 ± 1.9
M1-Au_1Cu_1	12.7 ± 2.5
M1-Au_1Cu_3	9.8 ± 2.6
M1-Cu	8.2 ± 2.5

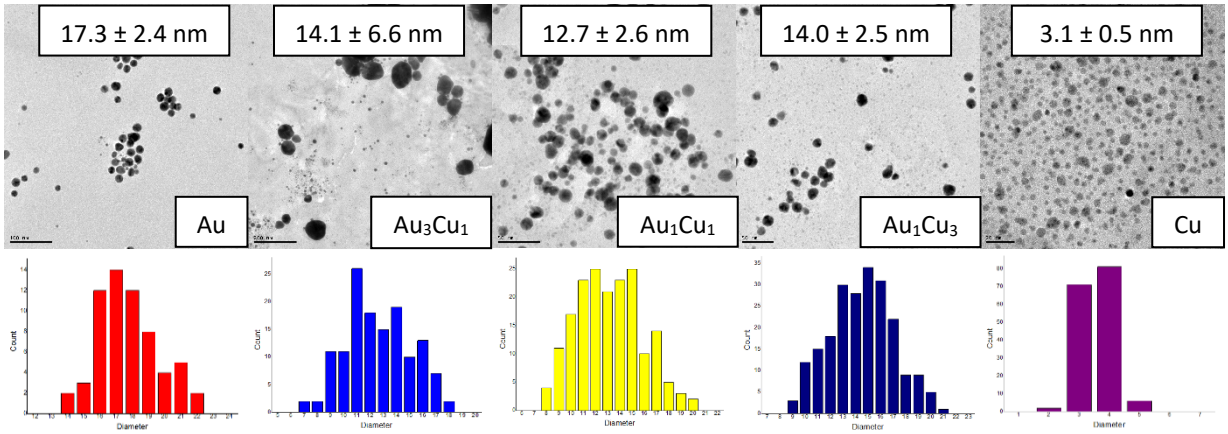

Figure 3.28 HR-TEM images and histograms of the M1- Au, Au_3Cu_1, Au_1Cu_1, Au_1Cu_3, and Cu DSNs listing their sizes and size distributions.

This same synthetic procedure was used in one more instance to determine whether the method is useful and can yield NPs of consistent, similar sizes. Again, the UV-Vis results were very similar to what was seen in other instances when the same method was used.

Table 3.8 Summary of the M1- Au, Au_3Cu_1, Au_1Cu_1, Au_1Cu_3, and Cu DSN sizes observed with HR-TEM (Figure 3.28) for the various mono- and bimetallic NPs.

DSN	DSN size (nm)
M1-Au	17.3 ± 2.4
M1-Au_3Cu_1	14.1 ± 6.6
M1-Au_1Cu_1	12.7 ± 2.6
M1-Au_1Cu_3	14.0 ± 2.5
M1-Cu	3.1 ± 0.5

Table 3.9 Summary of the M1 DSN sizes observed for the three instances in which the same synthetic procedure was utilised to determine the method's reproducibility (Tables 3.4, 3.7, and 3.8).

DSN	DSN size after 1st attempt (nm)	DSN size after 2nd attempt (nm)	NP size after 3rd attempt (nm)
M1-Au	17.9 ± 1.5	18.6 ± 6.7	17.3 ± 2.4
M1-Au_3Cu_1	14.5 ± 2.4	10.7 ± 1.9	14.1 ± 6.6
M1-Au_1Cu_1	7.2 ± 1.8	12.7 ± 2.5	12.7 ± 2.6
M1-Au_1Cu_3	10.5 ± 2.1	9.8 ± 2.6	14.0 ± 2.5
M1-Cu	6.9 ± 1.7	8.2 ± 2.5	3.1 ± 0.5

3.3 Conclusions

The developed method to synthesise DSNs was successful for preparing mono- and bimetallic NPs and it also allowed us to obtain some degree of control over the sizes and size distributions of the NPs. The Au NPs showed the highest affinity to agglomerate and form large NPs as well as having the most polydisperse size distribution of all the NPs we synthesised. The Cu NPs were the smallest with the most monodisperse size distribution. The sizes of the bimetallic NPs were between those of the monometallic Au and Cu NPs due to their unique bimetallic compositions.

The bimetallic NPs proved to be the most stable over extended periods, generally showing little change in size. The opposite was observed for the monometallic Au and Cu NPs since the extensive agglomeration that occurred for these NPs caused them to become much larger over time.

To summarize the above results, the Au NPs showed the highest degree of agglomeration and polydispersity, suggesting that these NPs are unstable despite the stabilization and optimizations carried out. This is clear in Figure 3.16, where there is a significant increase in the NP size over a period of 9 months. The Cu NPs were the smallest and most monodisperse of the NPs, showing a 3-fold increase in size over time (Figure 3.20). As expected, the bimetallic NPs sizes were found to vary between those of the monometallic NPs, depending on the metal composition. Interestingly, the bimetallic NPs, Au_1Cu_1 and Au_1Cu_3, were found to be the most stable, showing very little variation in size over time, even up to 9 months.

This was an interesting observation – metal NPs could potentially be used as stabilizers in bimetallic NPs systems. As stated in the introduction, bimetallic NPs are usually exploited for their potential to enhance catalytic activity and selectivity by the unique properties that arise from their bimetallic nature. However, these results show that the bimetallic nature lends more stability to the NPs, which will lead to enhanced catalyst life-time. Hence, metal NPs of one metal could be used to stabilize those of another metal in the same way that more conventional stabilizers, such as ligands and dendrimers, would. In this case, by looking at the stability of the monometallic NPs, it is observed that the Cu NPs are more stable than the Au NPs, hence, in the bimetallic NPs, the Cu NPs likely stabilize the Au NPs. Consequently, the higher the Cu content in the bimetallic NPs, the higher the stability. Furthermore, the monometallic NPs are

not as stable as the bimetallic NPs. This confirms that the stability is a property of the bimetallic nature and not solely due to the more stable nature of Cu NPs, relative to Au NPs. These results are very promising for industry application, where long term stability is sought after. More importantly, such stability may facilitate recycling of the catalyst.

3.4 Experimental

3.4.1 Materials and methods

All reactions were performed under ambient conditions, unless otherwise stated. All commercially available reagents were used as received. Solvents were dried by refluxing over the appropriate drying agents followed by distillation prior to use and all other reagents were employed as obtained. NMR (^{1}H: 300 and 400 MHz; ^{13}C: 75 and 100 MHz) spectra were recorded on Varian VNMRS 300 MHz; Varian Unity Inova 400 MHz spectrometers and chemical shifts were reported in ppm, referenced to the residual protons of the deuterated solvents. Tetramethyl silane (TMS) was employed as internal standard. Chemical shifts (δ) and coupling constants (*J*) were reported in ppm and Hertz (Hz), respectively. The data in bracket is as follows: multiplicity, coupling constants. The following abbreviations were used to describe multiplicity of signals: s = singlet, d = doublet, t = triplet, m = multiplet and dd = doublet of doublets. FT-IR spectroscopic analysis was performed on a Thermo Nicolet AVATAR 330 instrument. Spectra were recorded neat (ATR) unless otherwise specified. UV/Vis spectroscopic analysis was performed on a GBC UV/Vis 920 instrument. TEM analysis was performed on a FEI Tecnai G^2 Field Emission Gun (FEG) TEM operating at 200 kV and having a 2.5 Å point-to-point resolution, 1.02 Å line resolution and 1.4 Å information limit. GC analysis was performed on a Varian 3900 instrument with an Agilent Technologies 50 m × 0.21 mm × 0.5 μm column, using p-xylene as reference.

3.4.2 General procedure for the preparation of dendrimer micelles, **M1** – **M3**

The synthesis of C15 (**M1**), C11 (**M2**) and C5 (**M3**) was performed by the previously reported method by Meijer *et al*. [22]

3.4.2.2 Synthesis of mono- and bimetallic DENs with dendrimer micelles, **M2**.

3.4.2.2.1 **M2**-Au DSNs

The method, as described above for M1-Au DSNs, was employed with C_{11} dendrimer micelle (**M2**, 0.0401 g, 0.00920 mmol). UV-Vis spectroscopy was employed to monitor the reduction reaction. Before reduction: λ_{max} = 323 and 240 nm (LMCT). After reduction: λ_{max} = 555 nm (SPR peak).

3.4.2.2.2 **M2**-Cu DSNs

The method, as described above for M1-Cu DSNs, was employed with C_{11} dendrimer micelle (**M2**, 0.0399 g, 0.00916 mmol). UV-Vis spectroscopy was employed to monitor the reduction reaction. Before reduction: λ_{max} = 283 nm (LMCT). After reduction: λ_{max} = 577 nm (SPR peak).

3.4.2.2.3 **M2**-Au_3Cu_1 DSNs

The method, as described above for M1-Au_3Cu_1 DSNs, was employed with C_{11} dendrimer micelle (**M2**, 0.0391 g, 0.00897 mmol). UV/Vis spectroscopy was employed to monitor the reduction reaction. Before reduction: λ_{max} = 324 and 240 nm (LMCT to Au; LMCT to Cu not observed). After reduction: λ_{max} = 577 and 303 nm.

3.4.2.3 Synthesis of mono- and bimetallic DENs with dendrimer micelles, **M3**.

3.4.2.3.1 **M3**-Au DSNs

The method, as described above for M1-Au DSNs, was employed with C_5 dendrimer micelle (**M3**, 0.0296 g, 0.00915 mmol). UV-Vis spectroscopy was employed to monitor the reduction reaction. Before reduction: λ_{max} = 324 and 240 nm (LMCT). After reduction: λ_{max} = 552 nm (SPR peak).

3.4.2.3.2 **M3**-Cu DSNs

The method, as described above for M1-Cu DSNs, was employed with C_5 dendrimer micelle (**M3**, 0.0291 g, 0.00899 mmol). UV-Vis spectroscopy was employed to monitor the reduction reaction. Before reduction: λ_{max} = 276 nm (LMCT). After reduction: No λ_{max} observed.

3.4.2.3.3 **M3**-Au_3Cu_1 DSNs

The method, as described above for M1-Au_3Cu_1 DSNs, was employed with C_5 dendrimer micelle (**M3**, 0.0294 g, 0.00908 mmol). UV-Vis spectroscopy was employed to monitor the reduction reaction. Before reduction: λ_{max} = 330 and 240 nm (LMCT to Au; LMCT to Cu not observed). After reduction: λ_{max} = 560 nm.

3.4.2.4 Optimized synthesis of mono- and bimetallic DENs with dendrimer micelle, **M1**.

C_{15} dendrimer micelle (**M1**, 0.0502 g, 0.00916 mmol) was stirred in chloroform (100 mL) for 30 minutes. Next, the metal salt(s) ($HAuCl_4$ (0 – 171 mg; 0 - 0.504 mmol) and/or $CuCl_2$ (0 – 67.7 mg; 0 – 0504 mmol)) in methanol (0.3 mL) were added dropwise to the stirring micelle solution under an inert atmosphere to form a bright yellow solution. The solution was stirred for 1 hour. After which a $NaBH_4$ (0.065g, 1.73 mmol) solution was prepared in methanol (5 mL). The $NABH_4$ solution was added dropwise to the stirring yellow solution, resulting in a colour change to either dark purple or brown, depending on the metal ratio.

3.5 References

1. Knecht, M. R., Weir, M. G., Frenkel, A. I. & Crooks, R. M. Structural Rearrangement of Bimetallic Alloy PdAu Nanoparticles within Dendrimer Templates to Yield Core/Shell Configurations. *Chem. Mater.* **20,** 1019–1028 (2008).

2. Scott, R. W. J., Wilson, O. M. & Crooks, R. M. Synthesis, Characterization, and Applications of Dendrimer-Encapsulated Nanoparticles. *J. Phys. Chem. B* **109,** 692–704 (2005).

3. Crooks, R. M., Zhao, M., Sun, L., Chechik, V. & Yeung, L. K. Dendrimer-Encapsulated Metal Nanoparticles: Synthesis, Characterization, and Applications to Catalysis. *Acc. Chem. Res.* **34,** 181–190 (2001).

4. Balogh, L. *et al.* Formation of Silver and Gold Dendrimer Nanocomposites. *J. Nanopart. Res.* **1,** 353–368 (1999).

5. Niu, Y. & Crooks, R. M. Preparation of Dendrimer-Encapsulated Metal Nanoparticles Using Organic Solvents. *Chem. Mater.* **15,** 3463–3467 (2003).

6. Newkome, G. R. & Shreiner, C. D. Poly(amidoamine), polypropylenimine, and related dendrimers and dendrons possessing different 1 → 2 branching motifs: An overview of the divergent procedures. *Polymer (Guildf).* **49,** 1–173 (2008).

7. Qin, Y. *et al.* Size control over spherical silver nanoparticles by ascorbic acid reduction. *Colloids Surfaces A* **372,** 172–176 (2010).

8. Pyatenko, A., Yamaguchi, M. & Suzuki, M. Laser Photolysis of Silver Colloid Prepared by Citric Acid Reduction Method. *J. Phys. Chem. B* **109,** 21608–21611 (2005).

9. Myers, S. V. *et al.* Dendrimer-encapsulated nanoparticles: New synthetic and characterization methods and catalytic applications. *Chem. Sci.* **2,** 1632–1646 (2011).

10. Pal, U., Sanchez Ramirez, J. F., Liu, H. B., Medina, a. & Ascencio, J. a. Synthesis and structure determination of bimetallic Au/Cu nanoparticles. *Appl. Phys. A Mater. Sci. Process.* **79,** 79–84 (2004).

11. Cloete, J., Mapolie, S. F. & Malgas-Enus, R. Facile synthesis and characterization of PTA stabilized hydrophilic Au55 nanoparticles via a DEN-MPC method. *Polyhedron*

102, 469–478 (2015).

12. Peng, X., Pan, Q. & Rempel, G. L. Bimetallic dendrimer-encapsulated nanoparticles as catalysts: a review of the research advances. *Chem. Soc. Rev.* **37,** 1619–1628 (2008).

13. Boisselier, E., Salmon, L., Ruiz, J. & Astruc, D. How to very efficiently functionalize gold nanoparticles by ‘click’ chemistry. *Chem. Commun.* 5788–5790 (2008).

14. Andrés, R., de Jesús, E. & Flores, J. C. Catalysts based on palladium dendrimers. *New J. Chem.* **31,** 1161–1191 (2007).

15. Mackay, A. L. A dense non-crystallographic packing of equal spheres. *Acta Crystallogr.* **15,** 916 (1962).

16. Lewis, L. N. Chemical Catalysis by Colloids and Clusters. *Chem. Rev.* **93,** 2693–2730 (1993).

17. Schmid, G. *Clusters and Colloids: From Theory to Applications*. *Clusters and Colloids: From Theory to Applications* (2007). doi:10.1002/9783527616077

18. Zhao, M. & Crooks, R. M. Homogeneous hydrogenation catalysis with monodisperse, dendrimer-encapsulated Pd and Pt nanoparticles. *Angew. Chemie - Int. Ed.* **38,** 364–366 (1999).

19. Zhao, M. Molecule-Sized Gates Based on Surface-Confined Dendrimers. *Angew. Chemie - Int. Ed.* **36,** 2596–2598 (1997).

20. Wells, M. & Crooks, R. M. Interactions between Organized, Surface-Confined Monolayers and Vapor-Phase Probe Molecules. 10. Preparation and Properties of Chemically Sensitive Dendrimer Surfaces. *J. Am. Chem. Soc.* **118,** 3988–3989 (1996).

21. Sujitha, M. & Kannan, S. Green synthesis of gold nanoparticles using Citrus fruits (Citrus limon, Citrus reticulata and Citrus sinensis) aqueous extract and its characterization. *Spectrochim Acta A* **102,** 15–23

22. Stevelmans, S. *et al.* Synthesis, Characterization, and Guest-Host Properties of Inverted Unimolecular Dendritic Micelles. *J. Am. Chem. Soc.* **118,** 7398–7399 (1996).

CHAPTER 4

Solvent-free oxidation of styrene with mono- and bimetallic dendrimer-stabilised nanoparticles.

4.1 Introduction

After a method of synthesis that was able to yield mono- and bimetallic DENs of sufficient average sizes and size distributions was found, we proceeded to utilise this method for the synthesis of dendrimer stabilised nanoparticles (DSNs).

Once DENs has been synthesised they can be used for a host of different applications – especially within catalysis. DENs have exhibited enormous potential as catalysts, because they are able to combine the advantages of both homogeneous and heterogeneous catalysis. [1] This unique property of DENs has caused some to regard catalysis to be their primary application. Even though they can possess traits of both homogeneous and heterogeneous catalysts, they tend to be distinguished as homogeneous catalysts when dissolved in solution and heterogeneous catalysts when immobilised on a solid support. [2]

Heterogeneous catalysts are mainly used in industry because of their stability and also their ability to be separated from their products. However, their activity and selectivity is not as good as that obtained when using homogeneous catalysts. [1,3,4] The decreased activity that is often observed with heterogeneous DENs catalysts results from the reduced accessibility of the substrate to the NP surface due to the steric interference of the supports such as silica or cross-linked polymers. [5,6]

DENs are also a promising prospect for use as homogeneous catalysts, which should result in increased activity and selectivity. Apart from the advantages that will be obtained as a result of the homogeneous catalysis, DENs are also able to be separated from the reaction products by means of ultrafiltration, thereby granting them the advantages of both homo- and heterogeneous catalysts. [1,4] Furthermore, the hydrophobic nature of the dendrimer micelle will

allow it to be soluble in the substrate monomer that will be used for catalysis. Because of this advantage, we can attempt to perform solvent-free catalysis.

Having more than one metal present on the surface of a NP generally enhances the selectivity and activity of metal-assisted catalytic reactions. It is believed that the activity is increased in such cases because the metal which is more electronegative will cause the other metal atoms to become more electron deficient, thereby increasing the interaction of this electron-deficient metal with the electron-rich double bond of an olefin. [7,8]

It has been suggested in literature that one approach to consider for increasing the activity and improving the selectivity of catalytic Au-Cu NPs is to utilize them as alloys. [9,10] The reasoning behind this suggestion is that it is believed that the bimetallic alloy will allow the binding strength of catalytic intermediates to be tuned. Enhanced reaction kinetics are believed to arise as a result of this. Dendrimer encapsulated NPs and other similar nanoreactors are believed to be an ideal platform for analyzing the interactions between the substrate and the catalytic NP as well as the reaction kinetics. [10,11]

Even though the surface configuration of the NP (monometallic, alloy, core-shell, etc.) influences several parameters during catalysis, appropriate synthetic procedures can result in NPs with different sizes and morphologies. These kinds of NPs with such varying sizes and morphologies inevitably lead to a wide range of compositions, sizes and shapes can be investigated. This will allow in-depth investigations to be conducted so that we may develop a deeper understanding of how these catalysts perform by controlling their active sites. [12]

Because NPs inherently have high surface-to-volume and surface-to-mass ratios, they are often preferred to be used in instances where high mass activity is desired. [12,13] As a result of this, bimetallic Au-Cu NPs are used in order to investigate their capabilities as catalysts and we should also be able to quantitatively compare the activity and selectivity of such bimetallic NPs as a function of their metal composition. [11]

When altering the composition of bimetallic Au–Cu NPs, the degree to which intermediates are stabilised on these NP surfaces change and as a result, different catalysis products could be obtained. Efficient catalyst loading will also be able to contribute to significant enhancements in the catalyst's mass activity and additional information obtained through such quantitative comparisons will assist in the development of design principles for high-performance catalysts. [9,11]

The activities of bimetallic NPs, including the Au-Cu bimetallic types, are believed to be the result of two separate factors. Firstly, the electronic effect based on metal composition which affects the binding of intermediates and secondly, the geometric effect influenced by the arrangement of atoms on the NP surface. [14]

The selective oxidation of organic and olefinic compounds has attracted significant attention. For instance, the oxidation is performed with a metal catalyst and an oxidizing agent such as hydrogen peroxide (H_2O_2). [15–18] Known experimental results have indicated that certain parameters are vital in order to control the selectivity of oxidation reactions. These require due consideration when attempting such reactions or designing a catalyst. [19] Firstly, the substrate has to be able to access the active site of the catalyst. This applies to various types of catalysts, irrespective of which type of support or template is being utilised. Secondly, the acidity of the catalyst surface or active site. The presence of acidic compounds can cause the substrate and its intermediates to undergo undesired side reactions and decomposition. Thirdly, the hydrophobicity or hydrophilicity of the catalyst surface or active site. The differences in the polarities between hydrophobic or hydrophilic can often be the cause of differences in the behaviour of catalysts. [20,21] For example, organic substrates would experience limited access to such hydrophilic sites and as a result would undermine other considerations that have been effected in the catalyst design process. Finally, the environment of the catalyst also affects the results of oxidation. It has been reported that higher catalyst activities and more controlled selectivities can be obtained only when the catalyst is well and evenly dispersed throughout the mixture. [22,23]

The oxidation of styrene across the olefinic side chain has become an important focus point for both commercial and academic goals since it is used for the synthesis of styrene oxide and phenylacetaldehyde – two important products that are produced in this oxidation procedure. Hydrogen peroxide has also been widely investigated for its use as an oxidant in the oxidation of organic substrates. The root for this focus is founded in environmental factors, because water is the only by-product formed during these catalytic oxidation reactions. The reaction catalyst and reaction conditions also affect which oxidation products are formed when hydrogen peroxide is used to oxidize the olefinic side chain of the styrene. For instance, it has been reported that benzaldehyde is the main product when homogeneous metal catalysts are used. [24] In another instance, when the Wacker process was utilised with palladium catalysts, acetophenone was found to be the main product while other researchers have reported the epoxide and 1, 2-diol as the main products with different sets of reaction conditions. [24,25]

The use of heterogeneous catalysts in styrene oxidation, also showed that different products were being formed based on the metal used as catalyst. Iron and cobalt complexes have showed the promotion of oxidative C=C cleavage to form benzaldehyde and titanium with hydrogen peroxide in an organic solvent promotes the selectivity towards phenylacetaldehyde. [26–29] The formation of the phenylacetaldehyde is believed to be the result of the in-situ acid-catalysed rearrangement of styrene oxide which initially forms. [30]

Researchers have also found that the use of various protic and aprotic solvents for the catalytic oxidation of styrene has a significant effect on various parameters of the catalysis, such as by-product formation, conversion, and the reaction kinetics. [19,31] What they found was that the greatest activity was obtained with acetonitrile in all cases. They believe that this arises due to the electrophilicity of the catalytic surface and concluded that, in the presence of an aprotic solvent such as acetonitrile, a cyclic species is formed with the metal in which water is the ligand. The lower donor properties of the water, compared to alcohols, allows it to possess a greater electrophilic character and this consequently allows it to have a higher intrinsic activity when oxidising olefins. [32]

Their study also found a trend in the influence of the solvents on the styrene oxidation. They concluded that these solvents' decreasing electrophilicity and increasing steric hindrance, as a result of the molecule's size, were the main factors causing the observed trend in reactivity. As the size of the solvent molecules increase, the formation of the catalytic intermediates and the approach of the oxidant and catalyst become increasingly hindered. [19,32] However, if we can successfully do solvent-free catalysis, this specific drawback should easily be eliminated. Beyond this advantage, solvent-free catalysis will should also simplify the experimental catalytic procedure by removing the step in which the solvent is separated from the reaction mixture. Furthermore, these reactions are also green, since no solvent has to be discarded after the catalytic process.

4.2 Results and Discussion

The DSNs that were synthesised and reported in Chapter 3 (Figure 4.1) were utilised as catalysts in the solvent-free oxidation of styrene. Different sets of experiments were carried out by changing variables to optimize the reaction. All reactions were carried out in duplicate and the average values are reported with standard deviation.

Table 4.1 List of prepared DSNs reported in Chapter 3 and their sizes.

DSN	DSN size (nm)
M1-Au	17.9 ± 1.5
M1-Au_3Cu_1	14.5 ± 2.4
M1-Au_1Cu_1	7.2 ± 1.8
M1-Au_1Cu_3	10.5 ± 2.1
M1-Cu	6.9 ± 1.7

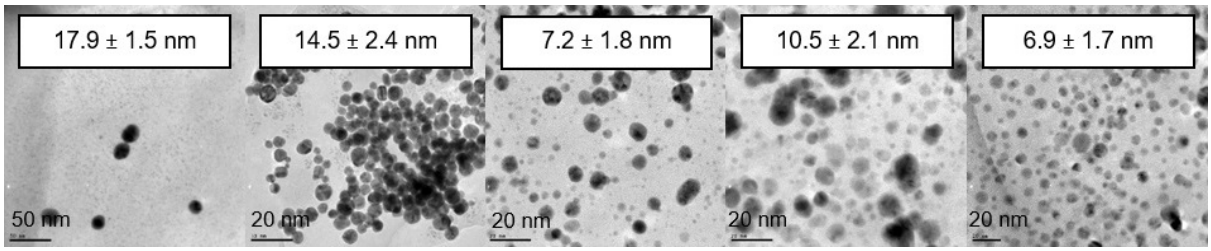

Figure 4.1 HR-TEM images for the monometallic M1-Au (left), M1-Cu (right), and bimetallic M1-Au_3Cu_1 (centre left), M1-Au_1Cu_1 (centre), and M1-Au_1Cu_3 (centre-right) DSNs prepared on the first attempt using the new, reproducible method.

The first variable we investigated was metal loading. The metal loading of the catalyst was altered, ranging from 0.025 mmol to 0.1 mmol. In all of these reactions, benzaldehyde and styrene oxide were found to be the major products. The conversions and selectivities of these reactions are summarised in Table 4.2 and Figure 4.2. After the reaction time of 16 h had expired, the Au_1Cu_1 DSNs showed the highest conversion and the Cu DSNs the lowest when the metal loading was set at 0.025 mmol. The Au_3Cu_1 and Au_1Cu_3 DSNs showed conversions that were between those of the monometallic Au and Cu DSNs. Furthermore a trend appeared based on the metal composition of the DSNs. If the DSNs have a higher proportion of Au its conversion will be greater than when the DSNs have a higher proportion of Cu. This trend was also observed when the metal loadings were set to 0.05 and 0.01 mmol.

It was mentioned earlier that the major products that formed during the oxidation of styrene were benzaldehyde and styrene oxide. Of these two major products, the amount of benzaldehyde that formed during the reaction was much more than the styrene oxide (Table 4.2). For the reactions in which the metal loadings were set to 0.025 and 0.050 mmol, the Au_1Cu_1 DSNs formed the highest percentage of styrene oxide. These reactions showed that the highest conversions were obtained when the metal loading of 0.050 mmol was used. Therefore reactions were carried out using a 0.050 mmol metal loading.

Table 4.2 Catalysis results with varied metal loading, where major oxidation products were benzaldehyde and styrene oxide.

DSN	Loading (mmol)	Conversion (%)	Selectivity (Benzaldehyde:Styrene oxide)
M1-Au		51.9 ± 4.90	
M1-Au_3Cu_1		44.2 ± 0.350	
M1-Au_1Cu_1	0.025	53.7 ± 3.90	Benzaldehyde >> SO
M1-Au_1Cu_3		46.5 ± 1.30	
M1-Cu		42.0 ± 4.95	
M1-Au		57.9 ± 0.200	
M1-Au_3Cu_1		57.1 ± 0.300	
M1-Au_1Cu_1	0.050	54.3 ± 3.10	Benzaldehyde >> SO
M1-Au_1Cu_3		52.3 ± 2.40	
M1-Cu		46.6 ± 0.800	
M1-Au		51.7 ± 2.05	
M1-Au_3Cu_1		43.7 ± 1.15	
M1-Au_1Cu_1	0.10	46.3 ± 4.00	Benzaldehyde >> SO
M1-Au_1Cu_3		48.2 ± 0.900	
M1-Cu		43.1 ± 1.35	

*Conditions: Temperature = 70 °C, time = 16 hrs, substrate = styrene (3 mL) and oxidant = 30 % H_2O_2 (4.5 mL).

Since it has been reported that using different oxidants for styrene oxidation can produce varying products, we changed the reaction to use tert-butyl hydroperoxide (TBHP) as an oxidant in the place of hydrogen peroxide (H_2O_2). These results are listed in Table 4.3 and Figure 4.3. These reactions showed increased activity of 9.5 % – 13.7 % when TBHP was used as the oxidant in the process of styrene oxidation. It is believed that this significant change in conversion when using different oxidants occurs as a result of the H_2O_2 decomposing during catalysis. [19,33]

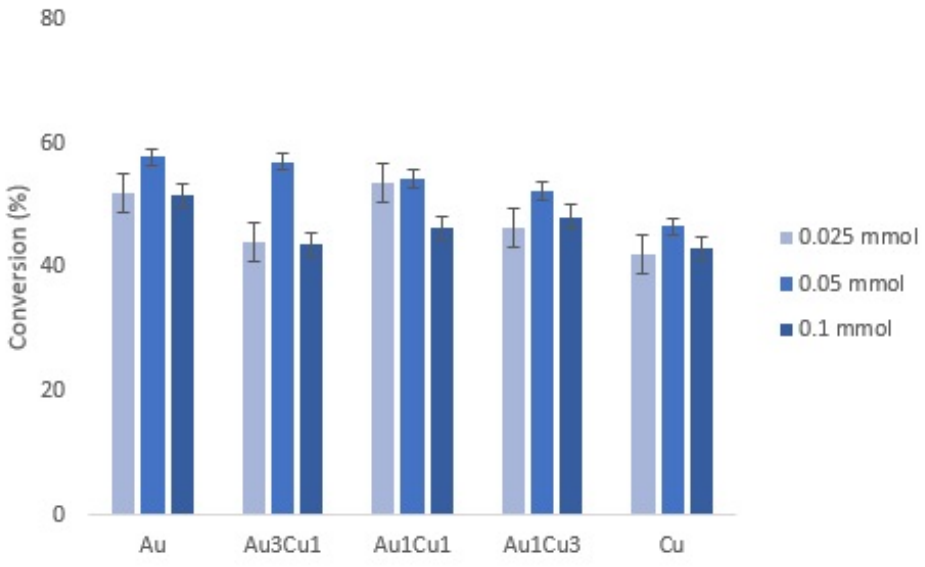

Figure 4.2 Catalysis results from Table 4.2 comparing varied metal loadings.

Table 4.3 Catalysis results with TBHP as oxidant and 0.050 mmol catalyst loading.

NPs	Conversion (%)
Au	67.4 ± 3.10
Au_3Cu_1	67.1 ± 2.25
Au_1Cu_1	66.2 ± 3.10
Au_1Cu_3	64.1 ± 0.800
Cu	60.3 ± 2.50

*Conditions: Temperature = 70 °C, time = 16 hrs, metal loading = 0.050 mmol; substrate = styrene (3 mL) and oxidant = 70 % TBHP (1.27 mL).

Since higher conversions were obtained with TBHP than H_2O_2 with 0.005 mmol catalyst loading, TBHP was employed as the oxidant when the reaction times were changed for subsequent reactions. The reaction times were varied from 1 h – 16 h in order to investigate its effect on the reaction. These results are listed in Table 4.4.

The data presented in Table 4.4 and Figure 4.4 show that an increase in the reaction time corresponds with an increase in the catalyst conversion, however, as the time increases beyond 8 h the percentage increase in conversion plateaus. After 1 hour, all the NPs displayed very similar conversions, however, it appears as though the previously observed trend is

repeated where the catalyst activity is higher for NPs with a higher Au content and lower for NPs with a higher Cu content. When the reaction time is extended from 1 h to 3 h, a significant increase in activity can be observed, increasing to a range of 50.4 % to 58.9 %. As it has been observed before, this trend which correlates the NP metal composition and conversion emerges more clearly with these results. After 8 h, the conversion increases again to the range of 59.7 % to 64.9 % and the trend previously observed is still clear – the higher Au content corresponds to higher conversions. However, after the reaction was done over a period of 8 h, the Au_1Cu_1 DSNs showed the highest conversion. Eventually, after 16 h, the conversions have increased to a range from 60.3 % to 67.4 % and the trend correlating metal composition to conversion is still clear. Therefore it can be stated that the catalyst activity increases as the Au content increases and decreases with increasing Cu content.

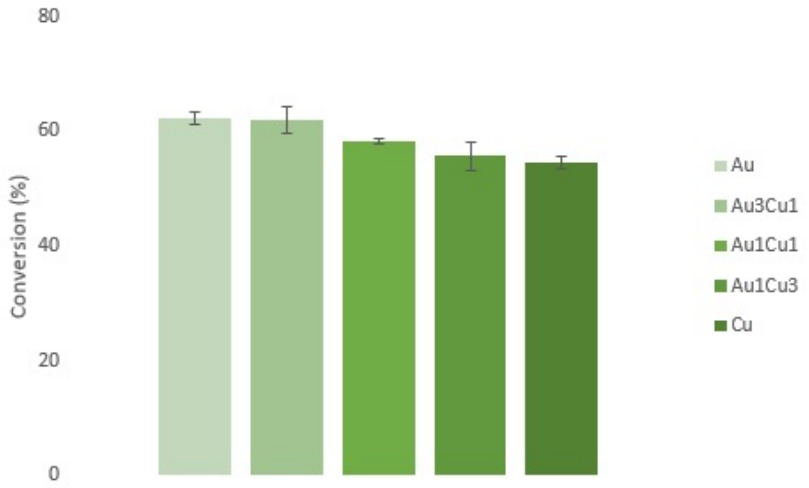

Figure 4.3 Catalysis results from Table 4.3 with TBHP as oxidant.

Finally, the catalyst selectivity with TBHP was evaluated after 1 hour and 3 hours, since significant changes were observed in the catalyst activity at these time points. The reaction conditions were kept the same as the previous experiments. The selectivities after 1 h and 3 h are shown in Figures 4.5 and 4.6 respectively.

When TBHP was used as the oxidant in the catalytic oxidation of styrene, the selectivity changed with regard to the reactions where H_2O_2 was utilised. In the reactions where H_2O_2 was used, the formation of benzaldehyde was favoured over that of styrene oxide, whereas the reactions with TBHP favoured the formation of styrene oxide. From literature, it has been suggested that the formation of benzaldehyde occurs due to oxidative cleavage while the

formation of styrene oxide is to be expected when styrene is oxidised. Thus it appears as though the choice of oxidant may influence which type of oxidation reaction will be favoured.[19]

Table 4.4 Catalysis results with TBHP as oxidant and varied time durations.

NP	Time (hrs)	Conversion (%)
Au		46.3 ± 2.10
Au_3Cu_1		47.2 ± 1.70
Au_1Cu_1	1	44.8 ± 0.900
Au_1Cu_3		44.6 ± 2.10
Cu		43.4 ± 1.10
Au		57.6 ± 1.40
Au_3Cu_1		58.9 ± 2.15
Au_1Cu_1	3	54.3 ± 2.50
Au_1Cu_3		50.5 ± 2.90
Cu		50.4 ± 1.70
Au		64.2 ± 2.90
Au_3Cu_1		63.1 ± 1.70
Au_1Cu_1	8	64.9 ± 1.20
Au_1Cu_3		62.8 ± 2.00
Cu		59.7 ± 2.20
Au		67.4 ± 3.10
Au_3Cu_1		67.1 ± 2.25
Au_1Cu_1	16	66.2 ± 3.10
Au_1Cu_3		64.1 ± 0.800
Cu		60.3 ± 2.50

*Conditions: Temperature = 70 °C, metal loading = 0.050 mmol; substrate = styrene (3 mL) and oxidant = 70 % TBHP (1.27 mL).

From our experimental results, we observed that after 1 h the selectivity for benzaldehyde is similar (< 0.2 g) for all five different DSNs that we prepared, whereas the styrene oxide formation increased (from 0.25 g to 0.48 g) with an increase in the Cu content of the DSNs. After only 3 h, this trend changed significantly, however. The formation of styrene

oxide is still generally favoured over that of benzaldehyde, but the quantity of benzaldehyde formed increased significantly from 0.1 g to 0.26 g. This indicates that when TBHP is utilised as the oxidant, the styrene oxide is formed before the benzaldehyde and subsequently more benzaldehyde is formed as the reaction time is increased.

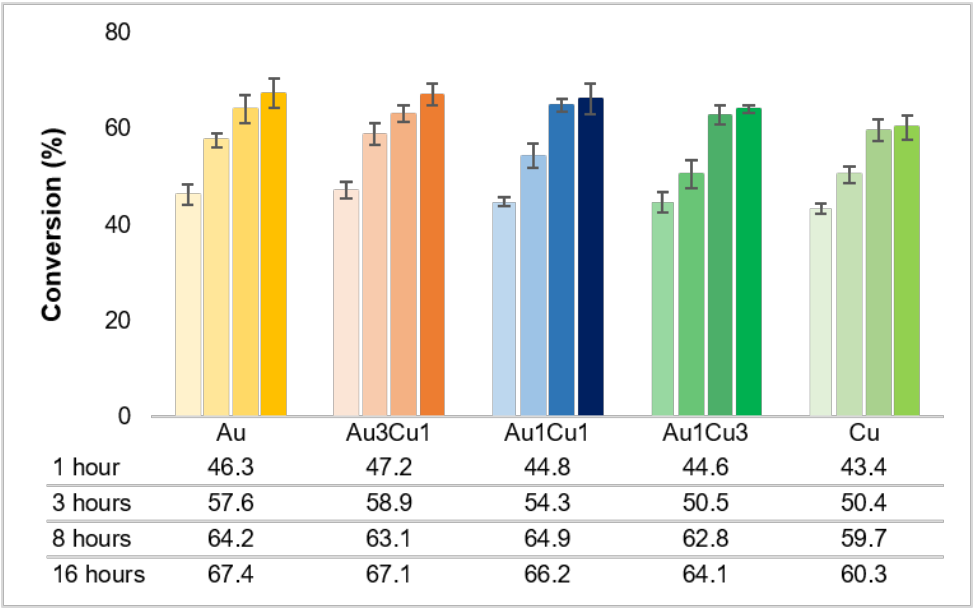

	Au	Au3Cu1	Au1Cu1	Au1Cu3	Cu
1 hour	46.3	47.2	44.8	44.6	43.4
3 hours	57.6	58.9	54.3	50.5	50.4
8 hours	64.2	63.1	64.9	62.8	59.7
16 hours	67.4	67.1	66.2	64.1	60.3

Figure 4.4 Change in M1-Au_mCu_n catalyst activity over time (1, 3, 8, and 16 h).

For the reactions containing H_2O_2, benzaldehyde formation was favoured over styrene oxide, whilst the TBHP containing reactions favoured the formation of styrene oxide. From the literature, it is suggested that the formation of benzaldehyde points to either a direct oxidative cleavage reaction via a radical mechanism or over-oxidation of styrene. [19] It was observed that after 1 hour, the selectivity for benzaldehyde is similar (< 30 %) for all the NPs, whilst the styrene oxide formation was around (70 – 80 %) for all catalysts. Notably, after 3 h, the trend has changed. Overall, the formation of styrene oxide is still favoured over benzaldehyde, but the quantity of benzaldehyde formed has increased. For all the Au containing catalysts, the selectivity for styrene oxide has decreased, while the selectivity of benzaldehyde formation has increased. This indicates that with TBHP as oxidant, styrene oxide is produced before benzaldehyde and more of the aldehyde is produced as the reaction time increases. This may point to over-oxidation of the styrene oxide to the aldehyde.

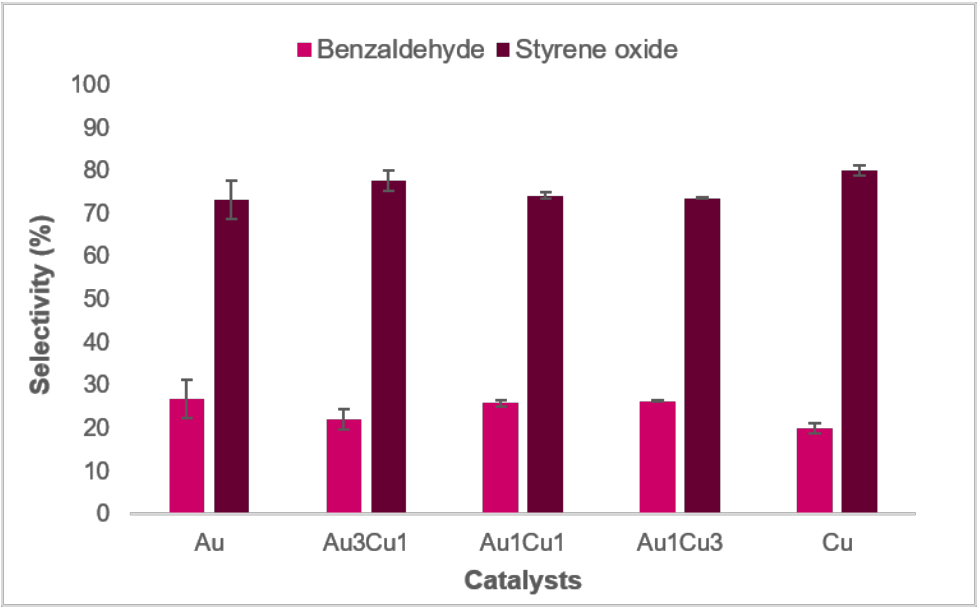

Figure 4.5 Selectivities of benzaldehyde and styrene oxide showing the amount of each product formed after 1 h with TBHP.

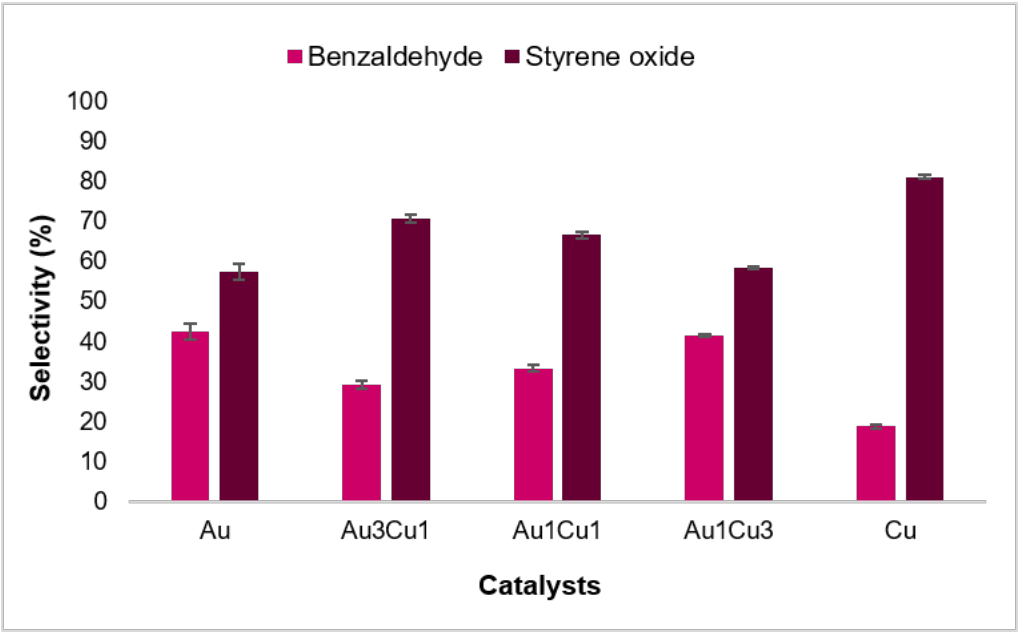

Figure 4.6 Selectivities of benzaldehyde and styrene oxide showing the amount of each product formed after 3 h with TBHP.

4.3 Conclusions

The general trend observed from the results described in this chapter showed that monometallic Au NPs exhibit the greatest conversions as catalysts. Conversely, the Cu NPs have consistently showed the lowest conversions. The conversions of the bimetallic NPs

exhibited a similar trend based on what was observed for the two different types of monometallic NPs. The bimetallic NPs with the most Au content, Au_3Cu_1, exhibited greater conversions followed by the Au_1Cu_1 and Au_1Cu_3 NPs, respectively.

The results that were obtained from the styrene oxidation indicated that conversions observed are not due to the size of the NPs that act as the catalysts, but rather that it is mostly influenced by the metal composition of the NPs: a higher conversion will be observed when more Au than Cu is present in the NP.

The various NPs also showed slight differences in terms of their selectivities. All NP systems favoured the formation of benzaldehyde whenever H_2O_2 was used as the oxidant. The other major oxidation product, styrene oxide, although being formed in significantly lower quantities than the benzaldehyde, showed to be more favoured in the presence of monometallic copper catalysts. Conversely, very little styrene oxide was formed when the monometallic Au NPs were used. When TBHP was used as the oxidant rather than H_2O_2, a different trend was observed for the catalyst selectivities. In this case the styrene oxide was the major product over the benzaldehyde.

4.4 Experimental

4.4.1 Materials and methods

All reactions were performed under ambient conditions, unless otherwise stated. All commercially available reagents were used as received. Solvents were dried by refluxing over the appropriate drying agents followed by distillation prior to use and all other reagents were employed as received. GC analysis was performed on a Varian 3900 instrument with an Agilent Technologies 50 m × 0.21 mm × 0.5 μm column, using p-xylene as reference.

4.4.2 Catalysis

For the catalytic reactions, 100 % metal loading was assumed, since no further workup was performed on the reaction mixture.

4.4.3 General reaction procedure

The required amount of catalyst was sampled from the DSN solution (0.025, 0.05, and 0.1 mmol) and the solvent was evaporated. The substrate, styrene (3 ml, 26.2 mmol), was added followed by the oxidant – either H_2O_2 (30 %, 4.5 ml) or TBHP (70 %, 1.27 ml). Finally, the reaction was set to reflux at 70 °C for the set time (1, 3, 8 and 16 hrs). After the allotted time had elapsed, the organic layer was extracted and filtered. The filtrate was analysed by GC-FID, using p-xylene as internal standard, to determine styrene conversion and selectivity.

4.5 References

1. Peng, X., Pan, Q. & Rempel, G. L. Bimetallic dendrimer-encapsulated nanoparticles as catalysts: a review of the research advances. *Chem. Soc. Rev.* **37,** 1619–1628 (2008).

2. Scott, R. W. J., Datye, A. K. & Crooks, R. M. Bimetallic Palladium-Platinum Dendrimer-Encapsulated Catalysts. *J. Am. Chem. Soc.* **125,** 3708–3709 (2003).

3. Myers, S. V. *et al.* Dendrimer-encapsulated nanoparticles: New synthetic and characterization methods and catalytic applications. *Chem. Sci.* **2,** 1632–1646 (2011).

4. Niu, Y. & Crooks, R. M. Preparation of Dendrimer-Encapsulated Metal Nanoparticles Using Organic Solvents. *Chem. Mater.* **15,** 3463–3467 (2003).

5. Inoue, K. Functional dendrimers, hyperbranched and star polymers. *Prog. Polym. Sci.* **25,** 453–571 (2000).

6. Niu, Y. & Crooks, R. M. Dendrimer-encapsulated metal nanoparticles and their applications to catalysis. *C. R. Chim.* **6,** 1049–1059 (2003).

7. Scott, R. W. J., Wilson, O. M., Oh, S. K., Kenik, E. A. & Crooks, R. M. Bimetallic Palladium-Gold Dendrimer-Encapsulated Catalysts. *J. Am. Chem. Soc.* **126,** 15583–15591 (2004).

8. Toshima, N. & Yonezawa, T. Bimetallic nanoparticles - novel materials for chemical and physical applications. *New J. Chem.* **22,** 1179–1201 (1998).

9. Peterson, A. & Nørskov, J. Activity descriptors for CO2 electroreduction to methane on transition-metal catalysts. *J. Phys. Chem. Lett.* **3,** 251–258 (2012).

10. Hansen, H., Varley, J., Peterson, A. & Nørskov, J. Understanding trends in the electrocatalytic activity of metals and enzymes for CO2 reduction to CO. *J. Phys. Chem. Lett.* **4,** 388–392 (2013).

11. Kim, D., Resasco, J., Yu, Y., Asiri, A. & Yang, P. Synergistic geometric and electronic effects for electrochemical reduction of carbon dioxide using Au-Cu bimetallic nanoparticles. *Nat. Commun.* 4948 (2014).

12. Moshfegh, A. Nanoparticle catalysts. *J. Phys. D. Appl. Phys.* **42,** 233001 (2009).

13. Zhu, W. *et al.* Monodisperse Au nanoparticles for selective electrocatalytic reduction of

CO2 to CO. *J. Am. Chem. Soc.* **135,** 16833–16836 (2013).

14. Nørskov, J. *et al.* Trends in the exchange current for hydrogen evolution. *J. Electrochem. Soc.* **152,** 23–26 (2005).

15. Arends, I., Sheldon, R., Wallau, M. & Schuchardt, U. Oxidative Transformations of Organic Compounds Mediated by Redox Molecular Sieves. *Angew. Chem. Int. Ed.* **36,** 1144–1163 (1997).

16. Clerici, M. & Ingallina, P. Epoxidation of Lower Olefins with Hydrogen Peroxide and Titanium Silicalite. *J. Catal.* **140,** 71–83 (1993).

17. Notari, B. Microporous Crystalline Titanium Silicates. *Adv. Catal.* **41,** 253–334 (1996).

18. van der Waal, J., Rigutto, M. & van Bekkum, H. Zeolite titanium beta as a selective catalyst in the epoxidation of bulky alkenes. *Appl. Catal. A* **167,** 331–342 (1998).

19. Hulea, V. & Dumitriu, E. Styrene oxidation with H_2O_2 over Ti-containing molecular sieves with MFI, BEA, and MCM-41 topologies. *App. Cat. A.* **277,** 99–106 (2004).

20. Blasco, T. *et al.* Unseeded synthesis of Al-free Ti-β zeolite in fluoride medium: a hydrophobic selective oxidation catalyst. *J. Chem. Soc. Chem. Comm.* 2367–2368 (1996).

21. Kochkar, H. & Figueras, F. Synthesis of Hydrophobic TiO_2-SiO_2 Mixed Oxides for the Epoxidation of Cyclohexene. *J. Catal.* **171,** 420–430 (1997).

22. Khouw, C., Dartt, C., Labinger, J. & Davis, M. Studies on the Catalytic-Oxidation of Alkanes and Alkenes by Titanium Silicates. *J. Catal.* **149,** 195–205 (1994).

23. Hutter, R., Mallat, T. & Baiker, A. Titania Silica Mixed Oxides: II. Catalytic Behavior in Olefin Epoxidation. *J. Catal.* **153,** 177–189 (1995).

24. Barak, G. & Sasson, J. Dual-function phase-transfer catalysis in the metal-assisted oxidation by hydrogen peroxide of styrene to benzaldehyde or acetophenone. *J. Chem. Soc., Soc. Commun.* 1266–1267 (1987).

25. Al-Ajlouni, A. & Espenson, J. Epoxidation of Styrenes by Hydrogen Peroxide As Catalyzed by Methylrhenium Trioxide. *J. Am. Chem. Soc.* **117,** 9243–9250 (1995).

26. Ma, N., Yue, Y., Hua, W. & Gao, Z. Selective oxidation of styrene over nanosized spinel-type $Mg_xFe_3{-}xO_4$ complex oxide catalysts. *Appl. Catal. A* **251,** 39–47 (2003).

27. Parvulescu, V., Constantin, C. & Su, B. Liquid phase oxidation of aromatic hydrocarbons using highly ordered Nb and NbCo-MCM-41 nanoreactors. *J. Mol. Catal. A Chem.* **202,** 171–178 (2003).

28. Neri, C. & Buonomo, F. *Eur. Pat.* **102,** 97 (1984).

29. Xia, Q., Wang, G., Chao, G., Zheng, L. & Ying, M. *Chin, J. Mol. Catal.* **8,** 313 (1994).

30. Zhuang, J. *et al.* Effect of acidity in TS-1 zeolites on product distribution of the styrene oxidation reaction. *Appl. Catal. A* **258,** 1–6 (2004).

31. Hulea, V. *et al.* Cyclopentene oxidation with H_2O_2 over Ti-containing zeolites. *Appl. Catal. A* **170,** 169–175 (1998).

32. Corma, A., Esteva, P. & Martinez, A. Solvent Effects during the Oxidation of Olefins and Alcohols with Hydrogen Peroxide on Ti-Beta Catalyst: The Influence of the Hydrophilicity-Hydrophobicity of the Zeolite. *J. Catal.* **161,** 11–19 (1996).

33. Sharma, S., Sinha, S. & Chand, S. Polymer Anchored Catalysts for Oxidation of Styrene Using TBHP and Molecular Oxygen. *Ind. Eng. Chem. Res.* **51,** 8806–8814.

CHAPTER 5

Summary and Conclusions

5.1 Synthesis

The synthetic aims of this project were to prepare dendrimer micelles which would subsequently be used to encapsulate metallic NPs. Dendrimers' unique ability to encapsulate NPs allow them to be utilized in a variety of applications, of which we placed our focus on catalysis. [1,2] This aim was achieved by modifying commercially-available DAB G3-PPI dendrimers by introducing alkyl chains to the dendrimers' peripheries. Doing this allowed us to alter the hydrophilic dendrimer in order to make its peripheries hydrophobic. This enabled us to prepare dendrimer micelles with the unique property of possessing a hydrophilic interior and hydrophobic peripheries. This dual nature of the dendrimer micelles' solubility allowed us to exploit the advantage of solubility-driven encapsulation of metallic NPs. Since the synthesis of the NPs was done with an organic solvent to dissolve the dendrimer micelle, any hydrophobic, metal salt precursors that were subsequently added would associate with the hydrophobic interior of the dendrimer micelle. [3]

Subsequent analysis was done by means of FT-IR, ^{1}H NMR, ^{13}C NMR, UV-Vis, and GC techniques. These enabled us to confirm that we had indeed prepared the desired dendrimer micelles. Three different dendrimer micelles were prepared. All of these three required the DAB G3-PPI dendrimer, but different alkyl chains were added in each instance: a C_{15} chain which was the longest (**M1**), a C_{11} chain (**M2**), and a C_5 chain which was the shortest (**M3**). These three different dendrimer micelles were tested as templates for metallic NPs.

Dendrimer micelles with varying alkyl chain lengths (M1-M3) were successfully synthesized and employed as both templates and stabilizers for DSNs of monometallic Au, Cu and bimetallic Au_mCu_n NPs. HR-TEM analysis showed that the alkyl chain length on the periphery of the dendrimer micelle influences NP size, viz. the longer the chain, the higher the degree of stabilization and hence, the smaller and more monodisperse the metal NPs.

Having identified M1, with the C_{15} alkyl chain, as the most effective dendrimer micelle for stabilizing the metal NPs, the long-term stability of the prepared DSNs was evaluated. It was found that the bimetallic DSNs are more stable over extended periods compared to the monometallic DSNs, which showed agglomeration. This was likely due to a stabilizing effect of the Cu NPs on the Au NPs and the nature of the bimetallic NPs.

For the Au DSNs, it was observed that the NPs increased in size as the dendrimer micelle chain length was shortened. This finding was consistent with what was expected based on the stabilizing effect that the peripheral alkyl chains would have on the NPs. The tendency of the longest dendrimer micelle chain lengths to form some of the smallest NPs is due to the better stabilization of these longer chains of the DSNs because of the greater steric radius provided by these longer peripheral alkyl chains. The sizes of the Cu DSNs remained largely similar throughout the range of dendrimer micelle chain lengths, yet showed a larger average NP size for the C_5 chain considering the size distribution of all these three different Cu DSNs. The average sizes of the bimetallic Au_3Cu_1 DSNs showed very similar sizes considering the average sizes as well as the size distributions.

The NPs sizes that we observed for the NPs mentioned in the previous paragraph were not consistent with what we expected for the DENs which we initially set out to achieve. If we were to have been successful in this endeavour the DENs would only be an approximate size of 2 nm, however, the NPs were much larger than this. Due to the NPs sizes that we obtained, we were able to conclude that we had rather prepared DSNs instead of DENs.

After we had initially prepared these three different monometallic Au and Cu DSNs and bimetallic Au_3Cu_1 DSNs, we also attempted to prepare NPs with different Au:Cu ratios, namely Au_1Cu_1 and Au_1Cu_3 DSNs. At first we were able to successfully synthesize and characterize these DSNs, but we saw a need to improve this synthetic method used to prepare the NPs, because the sizes of the DSNs with the same metallic compositions would differ significantly each time they were prepared.

In order to optimise this method, we shifted our focus to the second of these synthetic steps: the chemical reduction. We attempted to do this by setting out to find a procedure that is both repeatable and able to give us more control over the metal reduction. This was done by testing the effects of the concentration, volume, and addition of the $NaBH_4$. We chose to focus on these parameters rather than test other reducing agents, because the dendrimer micelles that

we use already account for stabilising effects. Using other reducing agents would consequently affect the overall stabilising effect. [4,5]

After we had developed a new method with which we could prepare mono- and bimetallic DSNs with different metal ratios, we set out to evaluate and compare the stabilities of these various DSNs. We had found that the monometallic Au DSNs were the most unstable and most prone to agglomeration despite optimising the synthetic method and the dendrimer micelle's stabilising effect. The monometallic Cu DSNs, however, were the smallest. In the instances of the three different bimetallic NPs, the sizes differed based on their metal compositions.

After keeping these mono- and bimetallic DSNs in solution for nine months, we found that bimetallic DSNs were very stable and generally showed little change in size and dispersity over such an extended time. This showed that the composition of metallic NPs affects the stability of the NP clusters. Bimetallic NPs have commonly been used to enhance the activity and selectivity of each of the metals, however, in our experiment, the results showed that the bimetallic nature of the NPs is very well suited to enhance the stability of these NPs. This is believed to be advantageous, since it should allow for a longer catalyst lifetime. This finding also opens up possibilities to use a bimetallic approach for enhanced stabilisation effects, as opposed to more conventional methods that require ligands, dendrimers, etc. Since our results showed the Cu DSNs are much more stable than the Au DSNs, it is believed that the Cu atoms in the bimetallic NPs stabilise the Au and prevent them from agglomerating.

5.2 Catalysis

The first parameter that was tested in the oxidation of styrene was the metal loading of the catalyst. Three different metal loadings were tested: 0.025, 0.050, and 0.10 mmol. For each of the five mono- and bimetallic DSNs that were evaluated as catalysts, the 0.050 mmol consistently yielded the highest conversions. In the cases of the Au, Au_3Cu_1, and Au_1Cu_1 DSNs, the 0.025 mmol loading showed the second-highest conversions, followed by the 0.10 mmol loading. However, with the Au_1Cu_3 and Cu DSNs, the 0.10 mmol loading had the second-highest conversions after the 0.050 mmol loading, followed by the 0.025 mmol loading.

Since the 0.050 mmol loading showed the highest conversions, this parameter was used for future oxidation reactions.

When the metal loading was tested, H_2O_2 was used as the oxidant, but TBHP was also utilised. Using TBHP as oxidant led to significantly higher conversions and also affected the selectivity of the styrene oxidation. Due to the higher conversions obtained with TBHP, it was utilised for further reactions instead of H_2O_2.

After the metal loading and oxidant parameters had been optimised, styrene oxidation was tested over different time periods: namely 1, 3, 8, and 16 h. These reactions consistently showed increases between all the time intervals, but the conversions consistently increased as the time increased. The biggest changes were observed between 1 and 3 h, while the smallest changes were observed between 8 and 16 h.

Throughout the course of testing the five different mono- and bimetallic DSNs as catalysts in the oxidation of styrene, we noticed that the general trend was that the DSNs with a greater proportion of Au exhibited greater conversions. These conversions, however, would tend to decrease slightly as the majority of Au in the NPs were gradually substituted with Cu. Hence, the Au DSNs generally converted the most of the substrate, followed by the Au_3Cu_1, Au_1Cu_1, Au_1Cu_3, and Cu DSNs, respectively. Furthermore, the bimetallic DSNs showed a similar trend in that the bimetallic DSNs with the highest Au content (Au_3Cu_1) exhibited the highest conversion, but not as high as the monometallic Au DSNs. Since the Au NPs were the largest and the Cu NPs were the smallest, it was concluded that conversion of styrene was not dependent on the NP size, but rather the metal content. The rationale behind this was that NP size-dependent catalysis would show the highest conversion for the smallest NPs, however, the results obtained showed the highest conversion for the larger Au NPs, whilst the small Cu NPs showed the lowest conversion. Additionally, the selectivity of the DSNs was found to vary depending on the oxidant employed. In the case of H_2O_2, benzaldehyde formation was favoured over the formation of styrene oxide, whilst the converse was true when TBHP was employed as the oxidant. Of the two oxidants, TBHP produced the highest activity and favoured formation of the desired product – styrene oxide.

From this work we established that a good compromise between stability and activity can be reached by employing bimetallic DSNs, where NPs of one metal provide catalytic activity and NPs of another metal serve as stabilizers. Furthermore, the exploitation of the dendrimer stabilizer in bimetallic DSN allows for further tailoring of the catalyst solubility, so

that green, solvent-free catalysis may be performed. Thus, bimetallic DSNs represent a class of attractive, green, industrially-applicable catalysts.

5.3 Future aims

The work that we have been able to complete in this project has by no means been a completed investigation and many areas that we have started to investigate can still be expanded. Firstly, since one of our initial aims was to synthesize DENs, higher-generation dendrimers should be utilised so that their effect on the NP synthesis can be investigated. Since these high-order generation dendrimers have already been reported to be effective in the successful preparation of various DENs, it would suggest that it might be effective for our ends.[1,3,6]

The bimetallic NPs that we focused on were all of the alloy type, since they were prepared according to the co-complexation method. This was also confirmed by analysis with UV-Vis spectroscopy and TEM-EDS. Further investigation should also focus on bimetallic NPs of the core-shell type prepared with a sequential reduction method, since these might possess properties different to those of the alloys.

Besides the analytical techniques that were already utilised, different techniques should be considered and explored. One area that could possibly be focused on and explored are X-ray absorption techniques such as Extended X-Ray Absorption Fine Structure (EXAFS) or X-ray Absorption Near Edge Structure (XANES). These techniques should be able to help determine the atomic environments of the various metallic atoms that make up each NP and would thus be helpful to determine the composition of the NPs.

Different substrates could also be used for the catalytic oxidation in which we utilise the NPs. This project only focused on styrene, but other terminal alkenes such as 1-octene and 1-heptene should also be utilised. Styrene derivatives varying in their steric and electronic properties could also be evaluated. This should help us to gain a better understanding of the oxidation process and how it affects the conversion rates and product selectivity.

Since the catalysts' selectivities are also affected by the choice of oxidant, various other oxidants such as O_2 should also be used in an attempt to determine how this affects the conversion and selectivity.

5.4 References

1. Myers, S. V. *et al.* Dendrimer-encapsulated nanoparticles: New synthetic and characterization methods and catalytic applications. *Chem. Sci.* **2,** 1632–1646 (2011).
2. Peng, X., Pan, Q. & Rempel, G. L. Bimetallic dendrimer-encapsulated nanoparticles as catalysts: a review of the research advances. *Chem. Soc. Rev.* **37,** 1619–1628 (2008).
3. Niu, Y. & Crooks, R. M. Dendrimer-encapsulated metal nanoparticles and their applications to catalysis. *C. R. Chim.* **6,** 1049–1059 (2003).
4. Qin, Y. *et al.* Size control over spherical silver nanoparticles by ascorbic acid reduction. *Colloids Surfaces A* **372,** 172–176 (2010).
5. Pyatenko, A., Yamaguchi, M. & Suzuki, M. Laser Photolysis of Silver Colloid Prepared by Citric Acid Reduction Method. *J. Phys. Chem. B* **109,** 21608–21611 (2005).
6. Scott, R. W. J., Wilson, O. M. & Crooks, R. M. Synthesis, Characterization, and Applications of Dendrimer-Encapsulated Nanoparticles. *J. Phys. Chem. B* **109,** 692–704 (2005).